Influence of vibrations on the electronic properties of DNA

Zur Erlangung des akademischen Grades eines

DOKTORS DER NATURWISSENSCHAFTEN

von der Fakultät für Physik der
Universität Karlsruhe (TH)

genehmigte

DISSERTATION

von

Dipl.-Phys. Benjamin Schmidt
aus Neumünster

Tag der mündlichen Prüfung: 11.07.2008
Referent: Prof. Dr. Gerd Schön
Koreferent: Prof. Dr. Juan-Carlos Cuevas

Deutsche Zusammenfassung

Die vorliegende Arbeit befasst sich mit dem elektronischen Transport durch kurze DNA Moleküle, wobei insbesondere untersucht wurde, welchen Einfluss Vibrationen der Basenpaare haben. Experimentelle und theoretische Arbeiten der letzten Jahre haben gezeigt, dass Vibrationen eine wichtige Rolle beim elektronischen Transport durch DNA spielen. Wie diese Rolle genau aussieht, wird allerdings zur Zeit noch kontrovers diskutiert. Insbesondere ist nicht eindeutig geklärt, ob sich Polaronen in DNA bilden, da nur einige Experimente mit Polaronenbildung zu erklären sind. In anderen Experimenten wurden hingegen relativ hohe Ströme gemessen, die sich eher mit einer (quasi-) kohärenten Beschreibung des Transport erklären lassen. Deshalb haben wir den elektronischen Transport durch DNA genau in diesen beiden Grenzfällen untersucht. Wir beschreiben dabei DNA Moleküle durch ein minimales *tight-binding* Modell, wobei jedes DNA Basenpaar mit einem *tight-binding* Platz identifiziert wird. Die Parameter für dieses Modell haben wir Experimenten und/oder *ab initio* Rechnungen entnommmen.

Im ersten Abschnitt haben wir die quasi-kohärente Transportsituation untersucht. In diesem Limit führt die Kopplung an Vibrationen zu inelastischen Beiträgen zum Strom, welcher zumindest teilweise seinen kohärenten Charakter behält. Für die Beschreibung dieser Situation haben wir einen Bewegungsgleichungsansatz (*equation-of-motion*) für die elektronische Ein-Teilchen Green-Funktion der DNA gewählt, welcher die Vibrationseffekte berücksichtigt, die durch lokale *und* nicht-lokale Elektronen-Vibrationskopplung entstehen. Um die starke Kopplung der Elektronen und Vibrationen beschreiben zu können, entfernen wir durch eine unitäre Transformation genau diesen Kopplungsterm aus dem Hamiltonoperator. Diese Prozedur erlaubt es uns, die Reihe von Green-Funktionen höherer Ordnung abzubrechen, welche sich aus der Bewegungsgleichung ergibt. Physikalisch lässt sich das Abbrechen der Reihe für eine schwache nicht-lokale Elektronen-Vibrationskopplung begründen. Da wir motiviert durch experimentelle Ergebnisse annehmen, dass das chemische Potential von DNA, welche an metallische Elektroden gekoppelt ist, in der Energielücke zwischen höchstem besetzten und niedrigstem unbesetzten Molekülorbital (HOMO und LUMO) liegt, zeigt die I-V Kennlinie ein für Halbleiter charakteristisches Verhalten.

In dieser Arbeit haben wir gezeigt, dass die Zustandsdichte von homogenen DNA Sequenzen bandartig ist, wobei aufgrund der geringen Größe des Systems die einzelnen elektronische Resonanzen sichtbar sind. Zusätzlich dazu erkennt man "Vibrations"-Resonanzen, die sich im Abstand von ganzzahligen Vielfachen der betrachteten Vibrationsenergie oberhalb und unterhalb der entsprechenden elektronischen Resonanz befinden. Je weiter die "Vibrations"-Resonanzen dabei von den dazugehörigen elektronischen Resonanzen entfernt sind, desto geringer ist ihr spektrales Gewicht in der Zustandsdichte. Aufgrund der nicht-lokalen Kopplung der Elektronen und Vibrationen weist die Zustandsdichte eine große Asymmetrie auf, die sich aber dennoch nur unwesentlich auf

den Strom auswirkt. Der Transport durch homogene DNA Moleküle wird durch elastische, quasi-ballistische Beiträge dominiert. Für endliche Spannung und Raumtemperatur bewirkt die Streuung von Elektronen an Vibrationen eine Verminderung des Stromes um ca 30% im Vergleich zum vibrationslosen Fall. Andererseits führt die Kopplung an Vibrationen bei niedrigen Temperaturen zu einer Erhöhung des Leitwertes um mehrere Größenordnung. Das liegt daran, dass es zur Bildung von "Vibrations"-Resonanzen in der Energielücke kommt, die eine von Null verschieden Transmission haben.

Die Zustandsdichte von inhomogenen DNA Sequenzen ist aufgrund von Anderson Lokalisierung stark fragmentiert, wobei es genau wie bei homogenen Sequenzen neben den elektronischen Resonanzen zusätzliche "Vibrations"-Resonanzen gibt. Der elektronische Transport durch derartige DNA Moleküle basiert fast vollständig auf inelastischen Effekten, da Energie für die Überwindung von Potentialbarrieren benötigt wird, welche sich aus der inhomogenen Sequenz ergeben. Diese Energie wird von den Vibrationen der Basenpaare bereitgestellt. Beispielhaft haben wir die Sequenz 5'-CAT TAA TGC TAT GCA GAA AAT CTT AT-3' untersucht. Die I-V Kennlinie dieser Sequenz weist drei Stufen auf, welche sich mit den Energien bestimmter, entweder reiner oder gemischter, Guanin- und Adeninzustände in Verbindung bringen lassen. Diese Zuständen befinden sich in der Zustandsdichte bei Energien $E - E_{\mathrm{F}} = -0.3\,\mathrm{eV}$, -0.7 eV und -0.95 eV. Wir konnten zeigen, dass im Gegensatz zu homogenen Sequenzen die I-V Kennlinie der inhomogenen DNA Moleküle durch die nicht-lokale Vibrationskopplung qualitativ modifiziert wird. Insbesondere führt die nicht-lokale Kopplung bei der von uns untersuchten Modellsequenz zu einer Halbierung der Transmission für die Zustände bei $E - E_{\mathrm{F}} = -0.7\,\mathrm{eV}$.

Erstaunlicherweise ergab sich bei unseren Untersuchungen, dass der Strom durch inhomogene DNA Sequenzen nicht-monoton von der Kopplung an die Elektroden (Γ) abhängt. Für eine feste Spannung erreicht der Strom ein Maximum, wenn Γ ungefähr gleich dem Imaginärteil der Vibrations-Selbstenergie $\Sigma_{\mathrm{vib}} \approx 0.01\,\mathrm{eV}$ ist. Dieses Ergebnis zeigt, dass es nicht unbedingt besser ist, die Kopplung an die Elektroden zu maximieren, und dass eine systematische (experimentelle) Untersuchung der Elektrodenkopplung notwendig ist.

Im zweiten Teil der Arbeit haben wir uns mit inkohärentem Polaron-Hüpftransport durch kurze DNA Moleküle beschäftigt, die an metallische Elektroden gekoppelt sind. Polaronen bilden sich in DNA durch eine starke Kopplung der elektronischen Freiheitsgrade an die Vibrationen der DNA Basenpaare. Wir nehmen in unserem Modell dabei an, dass die einzelnen Basenpaare unabhängig voneinander schwingen können. Um die Situation starker Kopplung beschreiben zu können, führen wir eine unitäre Transformation des Hamiltonoperators durch. Dies ermöglicht eine perturbative Beschreibung des untersuchten Problems in neuen Parametern, die sich aus der Transformation ergeben. Diese Parameter sind die Hüpf- (t_{ij}/Δ) und Tunnelintegrale ($t_i^{\mathrm{L/R}}/\Delta$), welche durch die Bindungsenergie der Polaronen Δ normalisiert wurden. Experimentelle Untersuchungen haben für diese Bindungsenergien folgende Werte gefunden: für Guanin $\Delta_{\mathrm{G}} = 0.47\,\mathrm{eV}$ und für Adenin $\Delta_{\mathrm{A}} = 0.18\,\mathrm{eV}$. Um physikalisch interessante Größen wie den Strom zu berechen, beschreiben wir das System durch eine Ratengleichung für die Besetzungszahl der einzelnen DNA Basen. Die Raten wurden anhand von Fermis Goldener Regel berechnet und beschreiben inkohärente Hüpfprozesse in der DNA unter der Berücksichtigung der Anregung oder Absorption von Basenpaar-Schwingungen.

Für alle DNA Moleküle erhalten wir halbleitende I-V Kennlinien, welche für homogene und symmetrische Sequenzen symmetrisch sind. Einige inhomogene Sequenzen allerdings zeigen stark gleichrichtendes Verhalten. Der Grund dafür liegt in den Transportengpässen durch Potentialstufen in der Sequenz, die nur unter Absorption von Vibrationsenergie überwunden werden können, d. h. die Raten für derartige Hüpfprozesse sind sehr gering. Je nach Stromflussrichtung liegen die Engpässe an anderen Stellen und sind mal mehr oder weniger "eng", so dass sich für positive und negative Spannung unterschiedliche Ströme ergeben. Außerdem konnten wir zeigen, dass die Schwellspannung, bei welcher der Stromfluss einsetzt, empfindlich von der DNA Sequenz anhängt. Bei homogenen Sequenzen entspricht die Schwellspannung gerade der lokalen Energie der betrachten DNA Basen. Bei inhomogenen Sequenzen hingegen hängt die Schwellspannung nicht direkt von einer internen Energieskala ab, wobei die Spannungen allerdings zwischen den Werten der homogenen Sequenzen liegen. Die Schwellspannung der inhomogenen Sequenzen ist dabei durch die nicht-triviale Ladungsverschiebung bei endlicher Spannung bestimmt. Der Stromanstieg der I-V Kennlinie weicht außdem von der Form einer Fermi Funktion ab. Diese Veränderung ist bei der Sequenz GAAAAAAG am ausgeprägtes, welche ein sehr breites Maximum im differentiellen Leitwert aufweist. Bei anderen Sequenzen, die mehr als eine einzelne Guanin Base an beiden Enden haben, ist die Verbreiterung des Maximums nur sehr gering. Die Ladungsverschiebungen werden durch die Darstellung des lokalen chemischen Potentials Φ_i visualisiert. Dieses zeigt anschaulich, wie die angelegte Spannung über die Länge des DNA Molekül abfällt. Wie man erwarten würde, fällt die meiste Spannung an den Schnittstellen zu den Elektroden und an der Transportengpässen im Inneren der DNA ab.

Wie für Polaronen Hüpfen zu erwarten ist, konnten wir zeigen, dass der Strom für eine homogene DNA Sequenz thermisch aktiviert ist und eine Temperaturabhängigkeit hat, die einem Arrhenius-Gesetz folgt. Dieses Ergebnis ist in Übereinstimmung mit einigen Experimenten der letzten Jahre. Die von uns berechnete Aktivierungsenergie E_a hängt von der angelegten Spannung ab und nähert sich für Spannungen oberhalb der Schwellspannung dem Wert $E_a = \Delta/2$ an, welcher für Polaronen im Festkörper gilt.

Im letzten Teil dieser Arbeit haben wir eine allgemeine Beschreibung für Polaronentransport in mesoskopischen Systemen entwickelt, die eine Kopplung an metallische Elektroden berücksichtigt. Diese Beschreibung ist nicht auf DNA Moleküle beschränkt. Der von uns gewählte Ansatz basiert auf einer diagrammatischen Echtzeit-Entwicklung der Ein-Teilchen-Dichtematrix entlang der Keldysh-Kontour. Unter Miteinbeziehung von Nicht-Diagonalelementen der Ein-Teilchen-Dichtematrix können auch Kohärenzeffekt in der Beschreibung von Polaronentransport berücksichtigt werden. Außerdem ergibt sich aus der diagrammatische Entwicklung, dass Divergenzen durch resonantes Tunneln, die im vorherigen Abschnitt aufgrund phänomenologischer Argumente vernachlässigt wurden, nicht mehr auftreten. Vielmehr führt die Möglichkeit von resonantem Tunneln zu Korrelationseffekten zwischen den Besetzungen von unterschiedlichen Basenpaaren.

Wir wenden diesen Formalismus auf Hüpftransport von Polaronen durch DNA an. Für starke Kopplung zwischen Elektronen und Vibrationen und hohe Temperaturen können Kohärenzeffekte vernachlässigt werden, so dass für eine korrekte Beschreibung die Diagonalelemente der Dichtematrix ausreichend sind. Im Gegensatz zum vorherigen Abschnitt berücksichtigen wir jetzt Korrelationen zwischen den Besetzungen und untersuchen, wann

Korrelationen auftreten und welche Änderungen in den Transporteigenschaften sie hervorrufen. Wie wir gezeigt haben, spielen Korrelationen nur für die Transporteigenschaften von inhomogenen DNA Sequenzen ein Rolle, wobei sie dabei im Allgemeinen zu einer Verminderung des Stroms um bis zu einer Größenordnung führen. Das interessantes Ergebnis ist jedoch, dass Korrelationen bei einigen DNA Sequenzen zu einer neuen Energieskala führen können, die sich in einem zweiten Maximum im differentiellen Leitwert niederschlägt. Diese neue Energieskala ergibt sich durch Korrelationen einzelner DNA Basen, welche von anderen Basen umgeben sind, die eine andere lokale Energie besitzen, z. B. das Guanin in der Sequenz AAAAGAAA. Für angelegte Spannungen, bei denen die relativen Korrelationen (Eq. 6.15) anfangen, stark von Null abzuweichen, bilden sich die zweiten Maxima im differentiellen Leitwert aus. Die Spannungen, bei denen dies geschieht, liegen oberhalb der Schwellspannung, aber auch hier ist die genaue Position stark abhängig von der betrachteten Sequenz.

Es zeigt sich, dass Korrelationen von einzelnen Basen an den Schnittstellen mit den Elektroden (z. B. GAAAAAAG) stark von der Kopplung an die Elektroden abhängen. Für verminderte Kopplung Γ ergeben sich schwächere Korrelationen und auch die entsprechenden zweiten Maxima im differentiellen Leitwert sind stark verkleinert. Korrelationen von einzelnen Basen in der Mitte von Sequenzen (z. B. AAAAGAAA) sind hingegen nicht von Γ abhängig und damit ändern sich auch die zweiten Maxima im differentiellen Leitwert nicht. Diese Verhalten ändert sich allerdings, wenn es zusätzliche isolierte Basen an den Schnittstellen zu den Elektroden gibt (z. B. GAATGAC). In diesem Fall vermindern sich auch die Korrelationen, die mit der Base im Inneren der Sequenz verknüpft sind, wenn die Kopplung an die Elektroden verringert wird. Wir habe außerdem gezeigt, dass Korrelationen zwischen nächsten Nachbarn am größten sind, da die Korrelationen exponentiell mit dem Abstand abnehmen.

Abschließend ist zusammenzufassen, dass Vibrationen zu sehr unterschiedliche Effekten im elektronischen Transport führen können, abhängig von der Stärke und dem Charakter der Kopplung. Wir hoffen, dass die vorliegende Arbeit dabei hilft, die Ergebnisse aus Transportexperimenten an DNA Molekülen besser zu interpretieren und zu einem tieferen Verständnis der dabei relevanten Physik beiträgt.

Contents

"I knew all the rules, but the rules did not know me..."

Eddie Vedder

1. Introduction

Since the invention of the transistor in 1948 the technological improvements in structuring silicon have lead to increasing integration densities of computer chips, accompanied by an increase in computational power. Where the first microprocessor in the 1970s held only about 2 000 transistors, today over 100 million CMOS (complementary metal oxide semiconductor) transistors fit on a single commercially available computer chip. This gain in computational power is answered by the introduction of ever more demanding applications, driving the development of the next generation of integrated electronics with even higher transistor densities.

The increase in integration density was so far mainly achieved by miniaturization of the gate length of the CMOS transistors. The current sizes are in the range of some tens to a hundred nanometers. It is clear that this trend cannot go on forever, as eventually further downscaling of the CMOS technology will reach the atomic limit. But even before that, for dimensions of a few nanometers, leakage currents due to quantum mechanical tunneling will render todays transistor design useless. Additional problems arise due to an increase in dissipated heat and growing capacitances between the components.

A way out of the dilemma is the use of novel materials that function in spite of or even because of quantum mechanics. Molecular electronics is one of the alternatives under investigation today. The conceptual advantages of molecules are their size in the order of a few nanometers and the possibility to parallelly synthesize moles of them by chemistry. In contrast, the cost and the technological difficulties of structuring silicon microscopically by ever more advanced methods are the limiting factors of todays electronics technology. The idea to use single organic molecules as diodes was first introduced by Aviram and Ratner in 1975 [1], but at that time the idea was just a theoretical hypothesis far from actual accomplishment. Only with the development of the scanning probe techniques in 1980s instruments for the investigation and manipulation at the atomic and molecular scale became available.

With the right 'tools' at hand researchers from different disciplines (physics, chemistry and biology) started the quest for molecules that could be used as components in integrated circuits. In the last decade this field has attracted an increasing interest as the ability to manufacture nanoscale contacts has improved considerably.

The three main concepts used today for producing such contacts are the break-junction technique [2, 3] and the scanning probe techniques, namely STM (scanning tunneling microscope) [4] and conducting AFM (atomic field microscope) [5]. To form a break junction at first a free standing thin metal constriction is produced by standard electron beam techniques. When bending the underlying substrate by pushing a rod against it, the constriction is stretched until it finally opens. Due to the setup geometry, pushing the rod against the substrate by a few micron will only change the size of the gap in the constriction by a few Ångstrøm. Thus, this technique allows a fairly controlled way

of producing nanoscale contacts. The central part of STM and AFM are atomically sharp tips. The position of these tips is controlled by either piezo actuator (STM) or by sensitive cantilever structures (AFM). The distance of the STM tip to the conducting sample is adjusted by measuring the magnitude of the tunneling current between tip and sample, whereas the deflection of the AFM cantilever is controlled by monitoring a laser beam reflected by it.

Using the above and other techniques, many different types of molecules have to date been investigated by researchers to study their capabilities for future electronics, e. g. carbon nanotubes [6–8] organic or biological molecules [9–12]. DNA (Deoxyribonucleic acid) is one of these molecules. The advantages of DNA are its 'recognition' and 'self-assembly' properties and the fact that it can be chemically synthesized in any length and sequence desired, i. e. tailor-made to fit specific needs. Recognition describes the property of a molecule to selectively bind only to a defined other molecule or substrate, whereas self-assembly is the capability of molecules to form greater super-molecules under the appropriate conditions without external aid. These properties allow the constructing of, for example, two- or even three-dimensional networks with DNA (e. g. [13, 14]), without complicated lithographic procedures, which facilitates the incorporation into conventional electronic components. These properties also make DNA molecules interesting as scaffolds for the construction of networks from many different materials, e. g. nano particles [15] or metallic wires [16]. Other molecules lacking this property would have to be incorporated into electronic circuits by more complicated means, diminishing somewhat the advantage over conventional integrated electronics.

It should be noted that the interest in electronic transport properties of DNA lies not only in molecular electronics, but also in the role that charge migration plays in the repair of oxidative damage (mutation) in DNA [17]. Rajski and coworkers argued that some proteins acting as transmitter and receiver might constantly test the soundness of the DNA by sending charges between them. A mutation of the DNA situated between transmitter and receiver would interrupt the charge migration, thus allowing for its detection and eventually its repair [18]. So, general research on transport properties of DNA can also help to understand the mechanisms of oxidative damage and its repair. Another aspect of the electronic properties of DNA has only emerged recently, namely the possibility of determining the sequence of DNA by electronic means [19]. A fast method to determine the DNA sequence would change todays medicine, as a detailed genetic map of a patient, showing e. g. genetic mutations, would allow specific personalized treatment. The current sequencing techniques are far to slow for such a task, since the procedure involves various time consuming chemical steps, including fragmentation of the DNA into smallest pieces. These steps are necessary, as only for very short DNA sections the sequence can be determined in reasonable time and accuracy. Electronic sequencing techniques could allow for a determination of the DNA sequence without prior fragmentation [20].

To find suitable candidates for integrated circuits, one has to fathom the response of the (DNA) molecule to an applied bias. As for all nano-scale systems the transport properties of molecules differ sometimes strongly from the macroscopic ones we are accustomed to. For example, a macroscopic wire has a resistance increasing proportionally with its length in accordance with Ohm's law, whereas the typical resistance e. g. of an atomic gold wire

is $R = 12.8\,\mathrm{k}\Omega$ independent of its length [21, 22] as long as it is shorter than the electron mean free path. In fact, the resistance is not intrinsic to the gold wire, but it is due to the interface between macroscopic electrode and nanoscopic wire. In a simple picture, the electrons coming from the leads have to 'squeeze' into the small wire, thereby experiencing a resistance. This means that the 'injection' of electrons into nanoscale system in many cases strongly influences the transport characteristics. Therefore it is crucial how the system, e. g. the molecule, is connected to the electrodes. Furthermore, experimental and theoretical investigation indicate that the actual atomic contact geometry might strongly influence the conduction properties of the molecule [19, 23]. This poses major problems on the interpretation of experimental results, as the exact contact geometries produced e. g. by the break-junction technique is not known.

There are two possibilities how a molecule can bind to a metallic electrode: through a covalent bond or via van-der-Waals type interaction (physisorption). Often molecules are functionalized with thiol linkers (mainly a sulphur atom) which form strong covalent bonds to noble metals, especially gold. Due to the strong bond, thiol linkers allow for a quite stable configuration of electrodes and molecule, but whether these linkers form good transport junctions is debatable. Theoretical calculations indicate that the overlap of the electronic states responsible for transport in the electrode and the molecule is rather poor, if a thiol linker setup is used [24].

One can imagine that macroscopic metallic electrodes coupled to a nanometer-sized molecule will alter the properties of the molecule. Effectively, (partial) charging and charge rearrangement on the molecule, accompanied by structural reorganization, might occur. The chemical potential inside the molecule will be determined by the metal and it usually lies in the gap between highest occupied and lowest unoccupied molecular orbital (HOMO and LUMO), but often closer to the HOMO than to the LUMO [25]. For a physical understanding of transport through molecules detailed knowledge of the nature and influence of the contacts is needed.

For small molecules the coupling to the electrodes is dominant, but for longer molecules (e. g. DNA), where the electron spends a considerable amount of time on the molecules itself, its intrinsic properties become more and more relevant. For these systems interactions with vibrations are important. Organic and biological molecules are usually quite soft and at room temperature many vibrational modes can be exited. At room temperature DNA experiences strong molecular vibration of the base pairs, with a root-mean-square displacement as high as 10% of the lattice constant [26]. So the transport properties of molecules, in particular DNA, cannot be understood without taking into account these vibrations. For example, the interaction with the vibration can strongly reduce the coherence length and change the transport from coherent tunneling or band-like transport to incoherent hopping.

For strong interaction with the vibration, a trapping of the charge by formation of a small polaron is possible. A polaron is a quasi-particle consisting of a charge and the surrounding lattice distortion. Many experiments on long-range charge transfer in DNA molecules have shown that holes can migrate along DNA covering quite large distances by polaron hopping [27]. Shorter distances are overcome mainly by quantum mechanical tunneling. Experiments of the physical community probing the conduction properties of DNA use setups that are closer to the situations in electronic circuits, i. e. DNA molecules

contacted to electrodes. These types of experiments have not lead to a clear picture of the physics involved in transport through DNA. The results range from insulating behavior to ohmic I-V characteristics, from absence of temperature dependence to strong temperature dependence. The major problem in developing a consistent description of transport through DNA is the lack of reproducibility of the experimental results. One reason for this is the aforementioned difficulty in producing reproducible contacts between (DNA) molecules and metallic electrodes. Also, experimentalists use many different approaches to study the transport characteristics of DNA, i. e. different setups (break junctions vs. STM-tips, freely suspended molecules vs. molecule lying on a substrate) or different sample types (single molecules vs. self-assembled monolayers). This, of course, makes a systematic interpretation of the results very difficult. Another point that should not remain unaddressed is the limited stability of molecules, which poses a major problem for long-term investigations on the same molecule and, unfortunately, eventually for their use in integrated circuits.

In this thesis, we investigate the electronic properties of DNA to shed more light on the question if and how DNA can allow for charge transport. We focus mainly on the influence that vibrations have on the electronic properties. For this we will discuss the two limits mainly used to describe transport in DNA. The 'quasi'-coherent situation, where interactions with vibrations introduce inelastic effects, which allow for transport even in inhomogeneous DNA sequences. On the other hand interactions with vibrations can lead to self-localization of the electrons, changing transport to a sequence of incoherent hopping processes.

About this thesis

In Chapter 2 we will give a short introduction to DNA, discuss its structural and electronic properties and explain the basic concepts of charge transfer in DNA. In particular, we will explain the special electronic features of DNA arising from the primary and secondary structure, i. e. why DNA is directed and what implications that has for electronic transport. Various experiments are discussed, which probe the electronic properties of DNA either by chemically introducing a charge onto the DNA (charge transfer) or by contacting it to biased electrodes (charge transport). We explain what conclusions can be drawn from the results of these experiments and what question still remain unanswered. In particular, the effect of polaron formation in DNA is discussed.

A general introduction to the physics of polarons is given in chapter 3 starting historically with the concept of large polarons and then explaining the properties of small polarons, which are relevant for transport in DNA. A short discussion of the general approaches to transport phenomena in mesoscopic systems follows, explaining also the relevant time and energy scales. The tight-binding approximation is introduced which is used throughout this thesis.

In Chapter 4 we will discuss transport through DNA molecules coupled to biased leads with strong inelastic contributions due to interaction with vibrational modes of the DNA base pairs. In the considered situation the coupling to vibrations does not lead to polaron formation so at least partial coherence of transport is retained. We focus on the influence of an additional non-local (non-diagonal) electron vibration coupling on the transport

properties of homogeneous and inhomogeneous DNA sequences. We describe the DNA by a tight-binding model and calculate the physical quantities of interest by equation-of-motion theory. For a description of the nonequilibrium situation due to biasing of the system an approximative scheme is applied. Mathematical details of the calculations are found in Appendix B and C. We see that the inelastic contributions to the current in inhomogeneous DNA sequences are dominant. This is obvious, since for transport to occur, the electrons have to overcome potential barriers arising from the different energies of the DNA base pairs. This energy is provided by the base pair vibrations, which only allow transport in inhomogeneous sequences. Additionally a nonmonotonic dependence of the current on the coupling to the electrodes is found; i. e. , a stronger coupling to the electrodes (exceeding some threshold value) reduces the conductivity.

In the fifth Chapter we concentrate on the limit of incoherent polaron hopping transport, where the electrons are localized due to strong local interaction with vibrational modes of the DNA base pairs. This situation is described by a classical rate equation with rates obtained by golden rule arguments, valid for any applied bias. The resulting formulation is formally an extension of the so-called $P(E)$ theory. Due to the strong electron-vibration coupling a straightforward calculation of the golden rule rates based on this coupling is not possible. By performing a unitary transformation on the Hamiltonian the strong coupling term vanishes and a perturbative treatment becomes possible. We investigate how the characteristics of the current voltages curves change for different DNA sequences and how this is related to the chemical potential of the various base pairs. We observe rectifying behavior for inhomogeneous sequences and explain the origin of this effect. Finally, we study the temperature dependence of transport at different bias voltages and compare to experiments.

A generalization of the approach of the fifth chapter is presented in Chapter 6. We develop a real-time diagrammatic expansion of the single particle density matrix along the Keldysh contour, which is not restricted to DNA, but can be applied to arbitrary polaronic systems coupled to biased electrodes. This diagrammatic approach allows for the inclusion of non-diagonal elements of the single particle density matrix describing coherence effects and higher order processes. We will not consider these, but instead focus on the influence of correlations between occupations on different base pairs on the transport properties of DNA. We see that for inhomogeneous sequences these correlation give rise to changes in the current voltage profile as compared to the more simple approach in Chapter 5. We show that these changes are due to a new energy scale introduced into the system by the correlations.

Chapter 7 concludes our investigation on the influence of vibrational modes on the electronic transport properties of DNA. We compare the results from the two approaches presented in the fourth to sixth chapter and indicate how these could be distinguished in experiments. This might help to understand which physical effect underlies transport in DNA. A brief outlook is presented in the end. In the Appendices A, B, C, and E we present the mathematical details involved in the calculation for this thesis, which are not central for an understanding of our results. In Appendix D we sketch an extension of the approach discussed in the fourth chapter, which is formally valid for all applied biases.

Parts of this thesis have been published

- Chapter 4
  B. B. Schmidt, M. H. Hettler, and G. Schön
  Influence of vibrational modes on the electronic properties of DNA
  Physical Review B, **75**, 115125, (2007) and

  B. B. Schmidt, E. B. Starikov, M. H. Hettler, and W. Wenzel
  Vibrations in DNA: Their Influence on Transport
  Charge migration in DNA - Physics, Chemistry and Biology Perspectives, Springer 2007 (ISBN 354-072-493-1), pp. 249-262
  Proceedings of "Charge migration in DNA", Winnipeg, June 6-9, 2006.

- Chapter 5
  B. B. Schmidt, M. H. Hettler, and G. Schön
  Non-equilibrium polaron hopping transport through DNA
  Physical Review B,**77**, 165337 (2008).

2. Motivation: Charge transport in DNA

2.1. Structural and electronic properties

Deoxyribonucleic acid (DNA) is a long polymer fiber consisting of a chain of deoxyribonucleotides. A deoxyribonucleotide comprises a base, a sugar and a phosphate group. The central part is the sugar molecule deoxyribose (see Fig. 2.1), where the prefix 'deoxy' indicates that the sugar has an oxygen atom less than ribose. In Fig. 2.1 the 5 carbon atoms of the molecule are numbered 1' to 5', where the prime is used to distinguish them from carbon atoms of other parts of the DNA molecule. The labeling is helpful, since each carbon atom is specific in binding to the different entities building the DNA. The 1' carbon atom of the deoxyribose binds to one of four bases, guanine (G), cytosine

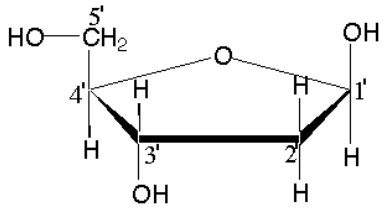

Figure 2.1: Schematic picture of a deoxyribose molecule. The various carbon atoms are numbered 1' through 5'. Picture taken from [28].

(C), adenine (A) or thymine (T). Two sugar-nucleotide entities are connected by a single phosphate group, which binds to the 3' carbon atom of one sugar and to the 5' carbon atom of another (see Fig. 2.2b). This chain of sugar-phosphate groups is called the DNA backbone, which is directed, having an unbound hydroxyl group (3') at one end and an unbound phosphate group (5') at the other. Whereas the backbone molecules are the same for every link of the DNA chain, the base connected to it (either A, G, T or C) underlies no restriction, rather the genetic code of life is encrypted in the specific sequence of these bases. Of course, in natural DNA as well adenine-thymine as guanine-cytosine base pairs are present in great number.

In 1953 James Watson and Francis Crick discovered the three dimensional structure of DNA by studying x-ray diffraction patterns of DNA fibers. They found that DNA forms the today well known double helix structure by combining two chains of deoxyribonucleotides, which run in opposite direction (see Fig. 2.2a). An important aspect in the formation of the double helix is that the two strands are complementary, i. e. a guanine base on one strand is always connected to a cytosine base on the other strand via three

hydrogen bonds, and an adenine base is always connected to a thymine base via two hydrogen bonds (see Fig. 2.2c). This property is essential for the self-reproduction of DNA, which is the basis of cell devision, since one strand is always the matrix for its complementary strand. The specific binding properties of two single DNA strands are the basis of the recognition properties of DNA. It is energetically favorable to combine two DNA strands and form the double helix structure as either two or three hydrogen bonds are formed per base pairs. In this structure the hydrophilic phosphate groups are on the outside of the double helix in direct contact with the water. In aqueous solution a single strand will therefore eventually bind to another complimentary strand (self-assembly).

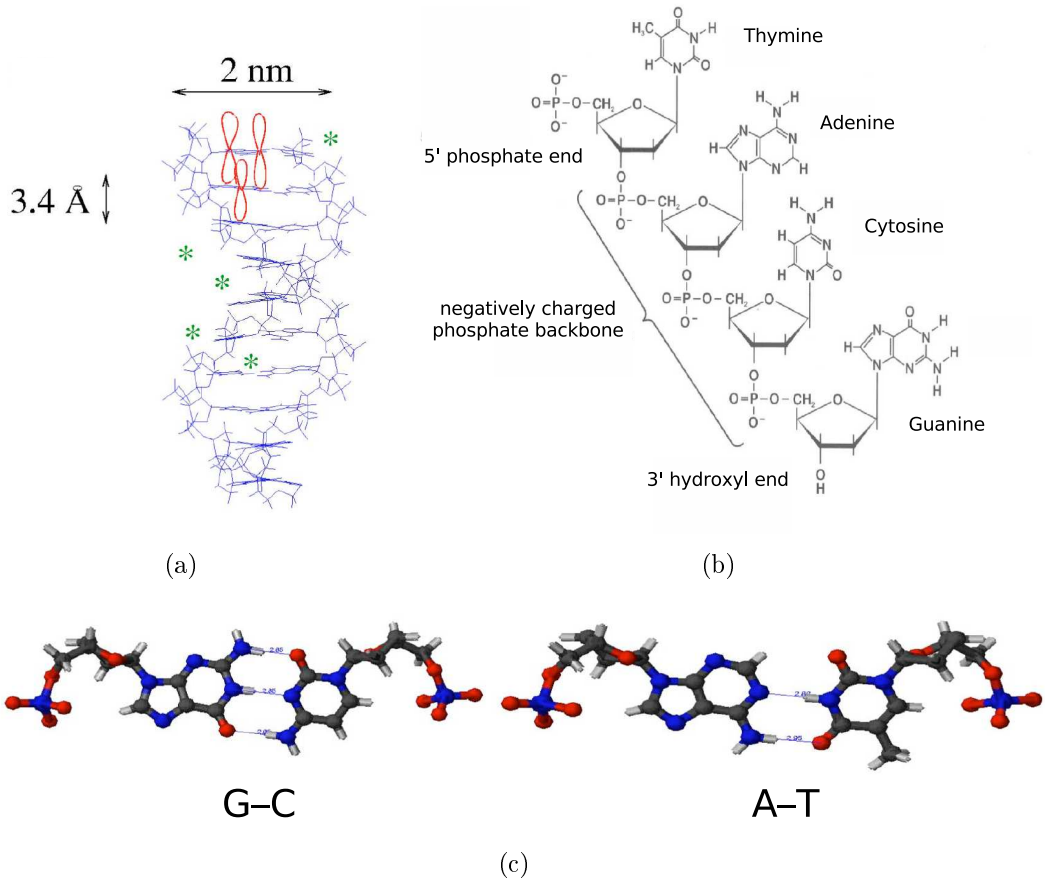

Figure 2.2: Molecular structure of DNA and its bases. (a) DNA double helix in a stick diagram with three π-orbitals and their overlap schematically depicted for the top two base pairs. (b) backbone structure of DNA and the four bases with the strand direction indicated by 3' and 5'. (c) the two Watson-Crick base pairs guanine-cytosine (G-C) and adenine-thymine (A-T) in an all atom ball-stick representation. Picture taken from [17].

Additionally to the primary structure given by the sequence of bases, the DNA also has a secondary structure, i. e. the specific structural form of the double helix. In natural, aqueous environment DNA is in the so called B-Form, where the distance between two subsequent base pairs is 3.4 Å and they enclose an angle of 36°. In this conformation

the bases of the two strands are aligned to each other and orthogonal to the DNA axis. In aqueous environment the negative charge of the phosphate groups is compensated by positively charged counter-ions (mainly sodium, potassium or magnesium). There are also other known secondary structures. Most common is the A-form that DNA assumes in dry environment. In the A-DNA two neighboring base pairs enclose an angle of 33.6° and are separated 2.3 Å.

In 1962 Eley and Spivey argued that the stack of π-orbitals formed by the DNA in its natural conformation could allow charge migration (see Fig. 2.2a) [29]. The reason for this assumption is the aromaticity of the DNA bases, i. e. the delocalization of the π-orbitals in the 'aromatic' ring structures of the bases (compare Fig. 2.2c). An overlap of these orbitals between neighboring bases could result in a delocalization of the orbitals over more than one base pair. The question of how well the electrons in homogeneous or inhomogeneous DNA molecules are delocalized is still a matter of debate, since the effect of DNA base dynamics and the environment might be crucial. The *ab initio* calculations by Artacho *et al.* [30] for homogeneous polyG-polyC DNA showed delocalization, however the resulting band-width was only about 40 meV. Other works also support the idea of partial electronic delocalization in homogeneous DNA molecules [31–33]. Experimentally Buchvarov and coworkers found evidence for electronic delocalization over 3 to 4 base pairs in some samples of homogeneous polyA-polyT DNA, which, they argued, was probably enhanced by nuclear rearrangement, i. e. lattice distortion [34].

In general, a DNA molecule is not a periodic, least of all homogeneous system. Since in inhomogeneous DNA molecules the electronic coupling between the orbitals of neighboring bases is small compared to the energy differences between these orbitals, one would expect such DNA sequences to be an insulator with Anderson localization. At room temperature natural DNA experiences strong molecular vibration of the base pairs, with a root-mean-square displacement as high as 10% of the lattice constant [26]. Therefore the properties of DNA cannot be understood without taking into account vibrations and interaction with the environment. As we will later show, also inhomogeneous sequences can support charge transport, assisted by lattice vibrations and environment.

Calculations have shown that the highest occupied molecular orbital (HOMO) of a DNA base pair resides on either guanine or adenine, whereas the lowest unoccupied molecular orbital (LUMO) resides on the other half of the base pair, i. e. either cytosine or thymine [30,32]. A measure for the energies of the HOMO, which are the most relevant for transport, are the ionization potential of the bases. For guanine it is $\epsilon_{\mathrm{G}} = 7.75\,\mathrm{eV}$ and for adenine $\epsilon_{\mathrm{A}} = 8.26\,\mathrm{eV}$. The gap between HOMO and LUMO is about 2 eV [30].

Senthilkumar *et al.* studied the hopping integrals t_{ij} for all possible combinations of neighboring base pairs [35]. They saw for example that the overlap between a guanine and an adenine is strongly dependent on their sequence, even if they are on the same strand. In a sequence 5'-GA-3' the hopping parameter is $t_{\mathrm{GA}} = -0.186\,\mathrm{eV}$, whereas for the reverse sequence 5'-AG-3' the hopping parameter is just $t_{\mathrm{AG}} = -0.013\,\mathrm{eV}$. The reason for this is the broken symmetry along the DNA axis due to the twisting of the DNA and the directedness of backbone. Note that this does not imply an non-hermitian Hamiltonian. Forward and backward hopping between A and G in a specific sequence of two base pairs are complex conjugates.

5'-XY-3'(all in eV)				
X\Y	G	C	A	T
G	0.119	0.046	-0.186	-0.048
C	-0.075	0.119	-0.037	-0.013
A	-0.013	-0.048	-0.038	0.122
T	-0.037	-0.186	0.148	-0.038

Table 2.1: Hopping integrals t_{ij} taken from Ref. [35] and adapted to our model. The notation 5'-XY-3' indicates the direction along the DNA strand (see, e. g. Fig. 2.2).

In this work, we will reduce the electronic complexity of DNA to a simple tight-binding model, which we introduce in chapter 4. In this model we consider one tight-binding site per base pair, i. e. we only model the HOMO and the coupling between the HOMOs of neighboring base pairs. We extract the parameters for the hopping integral t_{ij} from the results obtained by Senthilkumar *et al.* and adapt them to our simplified model. The resulting values for t_{ij} are given in Table 2.1.

2.2. Experiments

The question whether the prediction of Eley and Spivey (DNA being able to transport charge) can be confirmed, aroused and still arouses the attention of many researchers in chemistry, biology, and physics. The pioneering work in this field was done by Jacqueline Barton and her group, who measured the fluorescence of an organic chromophore. They found that the fluorescence is quenched, when the molecule was attached to a DNA molecule. They explained this quenching with the charge migrating along the DNA away from the excited molecule [36].

A typical charge transfer experiment was conducted by Giese and coworkers [37]. In this experiment a hole was injected into a guanine donor base (labeled G_{22} in Fig. 2.3) by photo-chemical means. After some time the DNA strands were chemically treated, so that the strands cleaved exactly at the guanine base pair that carried the hole. Using electrophoresis the number of DNA molecules of different lengths was determined. Since the DNA molecules were cleaved at the base pair that carried the hole, the length of such a DNA section was identical to the distance the hole had migrated. Therefore the relative number of DNA section with a certain length is equivalent to the ratio of holes that migrated the corresponding distance. Thus the number of holes that have reached the acceptor site (GGG) was determined. Typically, donor and acceptor are separated by a bridge of DNA bases, which in this case consist only of adenine. Figure 2.3 shows the logarithm of the yield ($P_{\mathrm{GGG}}/P_{\mathrm{G}}$) versus the number of intermediate adenine bases n measured in this experiment. The yield is the ratio of holes reaching the acceptor triple guanine compared to the number staying at the single donor guanine.

For short intermediate bridges ($n = 1, 2, 3$), i. e. few adenine bases, the slope of the straight line (logarithm of the yield versus number of bridge bases) in Fig. 2.3 is $\beta = 0.6\,\text{Å}^{-1}$. This strong distance dependence is characteristic for tunneling between the

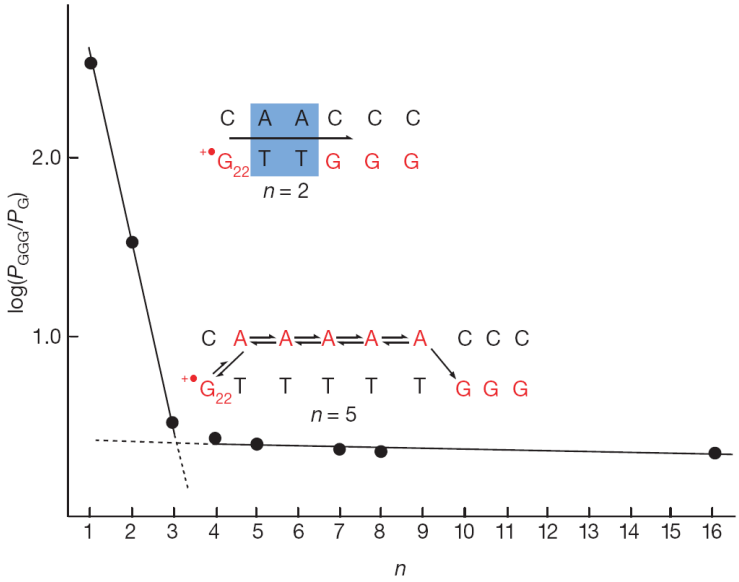

Figure 2.3: Logarithm of the Yield ($P_{\mathrm{GGG}}/P_{\mathrm{G}}$) against number of adenine bridge bases n, where P_{G} (P_{GGG}) is the number of holes at the donor (acceptor) site. The yield is a measure for the charge transfer efficiency. Clearly two regimes are visible. For short donor-acceptor distances ($n = 1, 2, 3$), i. e. in the tunneling limit the slope is $\beta = 0.6\,\text{Å}^{-1}$. For $n \geq 4$ the line is drawn to illustrate the weak distance dependence (hopping limit). The picture is taken from [37].

donor and the acceptor guanine through the potential barrier of the adenine base pairs. The tunneling rate decreases exponentially with the distance between the G-C base pairs and it becomes negligible if the two G-C base pairs are too far apart. For $n \geq 4$ the distance dependence becomes very weak, i. e. tunneling is no longer relevant. The interpretation is that the hole migrates via activated, incoherent hopping also using the adenine bases as 'stepping stones'.

These two mechanisms were verified by experiments of many groups. In particular, experiments on long-range equilibrium charge transfer along DNA show that the dominant transport mechanism is activated hopping of holes between the HOMOs of adjacent base pairs in the DNA stack [27,38–42]. In the simplest case the bridges separating the donor and acceptor guanine bases consist of a number of adenine bases (see Fig. 2.3), but more complicated bridges were investigated as well. All these experiments showed a weak distance dependence for bridges longer than a few base pairs, which is consistent with activated hopping transport.

The choice of using guanine bases as donor and acceptor molecules separated by various bridges which mainly consist of adenine bases is easily understood: from the ionization potential it is clear that the most stable position for a hole is the HOMO of a guanine base. As an acceptor a triple guanine (GGG) is chosen, that has a slightly higher ionization potential than the single guanine. So the triple guanine exerts a small 'thermodynamic force' on the hole. In the bridge of A-T base pairs the adenine is the most relevant since

its ionization potential is the closest to guanine. The idea is that in the hopping regime the hole will hop only between guanine and adenine bases even if they are on different strands of the double helix. In their experiments Joy *et al.* found clear indications for this behavior. They proved this by replacing bridge adenine bases with another molecule of similar structural, but different electronic properties [43].

For hopping transport to occur, the charge first has to undergo a localization. Several theoretical articles argue that holes are localized on single (guanine) bases either by solvation effects and/or structural reorganization [44–47]. The degree of localization is still a matter of debate [43], but many authors agree that conformational motion of the DNA is important for charge migration in DNA [48–51]. This localization can be interpreted as a polaron, which is a quasi-particle consisting of a charge and the surrounding lattice distortion (in the next chapter we will give a short introduction into this subject). Many authors have used the polaron hopping picture to model experimental results [52–54]. It is now the most promising candidate for the transport mechanism in charge transfer experiments. It should be noted that for the study of general sequences the competition between hopping and superexchange tunneling has to be accounted for [37, 55–57].

A measure for the degree of localization is the so called reorganization energy or polaron binding energy Δ, i. e. the energy gain through distortion of the lattice (or polarization of the solvent), when an additional charge is placed on a base pair. Olofsson and coworkers extracted reorganization energies (not accounting for solvation effects) from experiments and obtained values of $\Delta_A = 0.18\,\mathrm{eV}$ and $\Delta_G = 0.47\,\mathrm{eV}$ for adenine and guanine bases respectively [46]. The DFT calculation performed by them and also by another group [47] show values of the polaron binding energy of the same order of magnitude.

In contrast to the chemical community, where the ideas of tunneling and activated (polaron) hopping can explain the experimental findings and therefore the nature of charge transfer along DNA, the sometimes contradictory results in experiments of the physics community still give rise to controversial discussions. For the understanding of the electronic properties of DNA these latter experiments are indispensable, since the transfer of charges in electrochemical experiments is not sensitive to the details of the intrinsic electronic structure, i. e. whether DNA has a continuum of electronic states (electronic band) or discrete levels [58]. These characteristics can only be probed by non-equilibrium transport experiments.

To date there are only very few experiments in which the I-V characteristics of individual DNA molecules are measured(e. g. [16, 59–68]), mainly because of the difficulties to contact the DNA to metallic electrodes and to ensure that only single molecules are measured. The first experiment on a single DNA molecule was performed by Braun and coworkers in 1998 [16]. In this experiment the DNA of the bacteriophage lambda with 48 502 base pairs ($\approx 15\,\mu$m) was placed between two metal electrodes $12\,\mu$m apart using the recognition and self-assembly properties of DNA. For this purpose the electrodes where functionalized with single stranded segments of the used DNA molecules. The added DNA solution contained the complementary strands and therefore spontaneously attached to the functionalized electrodes (see Fig. 2.4(a)). The sample was dried and kept at ambient conditions during the measurements, which showed no current even up to a bias voltage of 10 V.

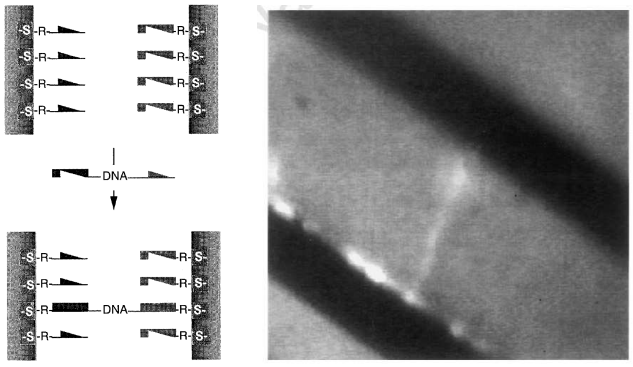

(a) (b)

Figure 2.4: (a) schematic drawing of how the λ-DNA molecules are contacted to the metal electrodes by self-assembly and recognition. (b) fluorescence image of the DNA (light diagonal line) bridging the gap between the electrodes (dark wide lines). The pictures are taken from [16].

A year later Fink *et al.* reported nearly ohmic behavior with currents of over 10 nA in transport measurements of bundles of few 'λ'-DNA molecules with lengths of some hundred nanometers contacted directly with a tungsten tip [59]. A possible explanation for this good conductivity is a likely doping due to imaging with a low-energy electron point source. The first experiment on single, short DNA molecules was performed by Porath and coworkers in 2000 [60]. Homogeneous DNA strands with 30 poly(dG)-poly(dC) base pairs (10.4 nm) in solution were electrostatically trapped between two lithographically etched Pt electrodes. After trapping, the sample was dried by a flow of nitrogen. The current measurements showed 'semi-conducting' behavior with currents slightly above 1 nA and thresholds between 0.5 and 1 eV. The measurements were performed at different temperatures, ranging from 4 K to room temperature and always showed similar characteristics, but with stronger variations between the samples in properties like the threshold for higher temperatures (see Fig. 2.5(a)).

Xu and coworkers followed a different path [64]. They performed all of their experiments at room temperature in buffer solution, driving a movable gold STM tip into a gold substrate and then pulling it away, constantly measuring the current. DNA molecules with thiol linkers from the solution could bridge the gap between STM tip and surface and form covalent bonds with the gold via the thiol groups. If an individual DNA molecule was found to be trapped, I-V characteristics were measured (see Fig. 2.5(b)). They saw nearly ohmic behavior with maximum currents of up to 150 nA for DNA molecules with sequence 5'-GCGCGCGC-3' and length of about 2.7 Å. Varying the number n of GC segments in the molecules (5'-$(GC)_n$-3') they saw a shallow 1/length dependence of the conductance, in agreement with hopping transport.

Newer experiments performed in the group of Danny Porath [65, 69], where single inhomogeneous DNA molecules of 26 base pairs were spanned between a gold substrate and a gold nanoparticle contacted by an AFM tip using thiol linkers, showed even higher currents of up to 220 nA at 2 V. The measurements were again performed at room temperature under ambient conditions. They reported higher conductivities in DNA molecules

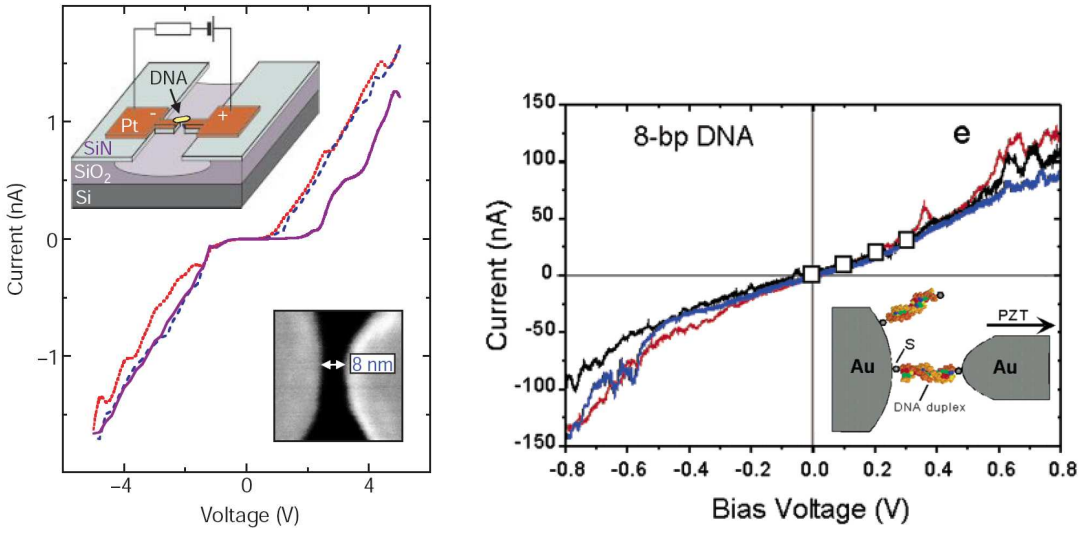

(a) (b)

Figure 2.5: Current-Voltage characteristics and experimental setups of two experiments. (a) three I-V curves measured on short homogeneous DNA strands with 30 poly(dG)-poly(dC) base pairs (10.4 nm), which were electrostatically trapped between two fixed Pt electrodes. Graph taken from [60]. (b) three I-V curves measured on DNA molecules with sequence 5'-GCGCGCGC-3', which were also electrostatically trapped between two gold electrode tips. Graph taken from [64].

with 26 base pairs with increasing number of G-C base pairs in the sequence. For a homogeneous sequence only comprising A-T base pairs they even found insulating behavior [69]. These latter findings were independently supported by experiments of Igbal and coworkers [70]. On the other hand an experiment with similar setup as in [69], where single DNA molecules (in this case functionalized with trimethylenethiol linkers) were spanned between a gold substrate and a gold STM tip, showed comparable currents for both homogeneous poly(dG)-poly(dC) and poly(dA)-poly(dT) DNA [67]. The currents though were quite small, only about 100 pA at 0.2 V.

In all of the above measurement (except the one by Braun and coworkers), the DNA molecules were suspended by the contacts, but otherwise free hanging. In a second group of experiments the DNA molecules were placed on a substrate and either lithographically fabricated electrodes and/or STM or metalized AFM tips were used for probing the transport characteristics. For longer DNA molecules all experiments showed insulating behavior of the DNA, whether they investigated λ-DNA of hundred nanometers [71] or a few micrometers [16, 72] or homogeneous poly(dG)-poly(dC) DNA molecules of lengths $L \geq 40$ nm [73]. An explanation for this behavior is, of course, the length of the molecules under consideration, but the interaction with the substrate might also promote the insulating behavior. Storm *et al.* showed that DNA molecules prepared on a substrate (SiO_2 or mica) were flattened out on the surface having only about one fourth of their natural height [73]. Other conformational changes of the DNA and the induction of defects due to interaction with a substrate are also conceivable.

On the other hand short DNA molecules prepared on substrates have repeatedly shown high conductivities and currents of up to a few nanoampere [74, 75]. In their experiment Shigematsu *et al.* prepared salmon sperm DNA on a SiO_2/Si substrate and fixed it by two carbon nanotube (CNT) probes of a pair of nanotweezers [75]. One of these CNTs was used as source and another CNT attached to an AFM tip was used as drain (see schematic drawing in Fig. 2.6(a)). The current for a fixed bias of $V_\mathrm{b} = 2\,\mathrm{V}$ was recorded as a function of the source-drain distance d_{CA} (see Fig. 2.6(b)). The resulting distance dependence fitted well with the relation

$$I \propto \sinh\left(\frac{eV_\mathrm{b}}{2k_\mathrm{B}T}\frac{a}{d_{CA}}\right) \tag{2.1}$$

for bulk polaron hopping [76], where a is the hopping distance. This indicates that polaron hopping is a probable mechanism for transport in DNA.

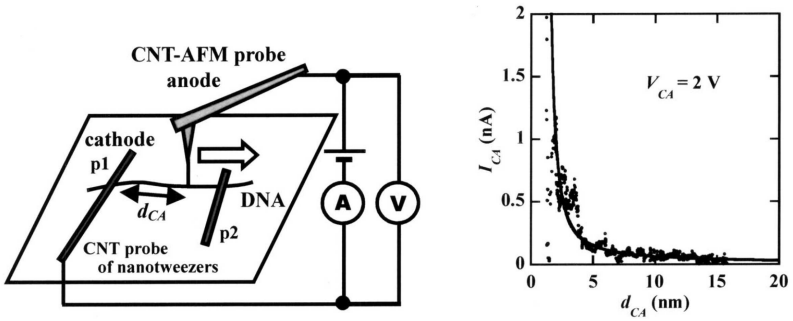

(a) (b)

Figure 2.6: (a) Schematic drawing of measurement setup used by Shigematsu *et al.*, where two carbon nanotube (CNT) probes fix the DNA molecule. One of these CNTs was used as source and another CNT attached to an AFM tip was used as drain. (b) Dependence of the current for $V_\mathrm{b} = 2\,\mathrm{V}$ on the source-drain distance d_{CA}. The black line shows a fit with equation 2.1. Pictures taken from [75].

Yoo *et al.* used the same formula (Eq. 2.1) to fit their results, but instead of the distance dependence they probed the temperature dependence of transport [62]. The results obtained by Roy *et al.* [68] also show a temperature dependence in agreement with the concept of polaron hopping. Other experiments show quite the contrary behavior, i. e. quasi temperature independent currents [60, 67]. For a detailed comparison of experiments see the reviews by Endres *et al.* [17] and Porath *et al.* [58].

In conclusion, some trends emerge from the experiments indicating that short DNA molecules can carry currents and longer molecules can not. The variance in the maximum currents are owed partially to the differing environmental parameters and the difficulty to reproducibly couple DNA to metallic electrodes. It seems that free hanging DNA molecules conduct better than DNA lying on a substrate. This, of course, would pose additional problems, when trying to use DNA in integrated circuits in future electronics. The physical reason for charge transport on the other hand is not clear. Experiments which show strong temperature dependence suggest polaron hopping transport, or at

least a strong interaction with vibrations. But this temperature dependence is not seen in other experiments. Furthermore, most experiments show 'semi-conducting' I-V characteristics, but other groups see ohmic behavior. Consequently, there is also no conclusive evidence about the intrinsic electronic properties of DNA.

For this work, we take the observations showing strong temperature dependence and the results of the chemical charge transfer experiments as the basis for our investigations, suggesting that vibrations and polarons play an important role also in non-equilibrium transport through DNA.

3. General concepts

3.1. Polarons

In this section we will shortly introduce the subject of polarons in general. We start with the concept of large polarons which were the first to be investigated historically. Later we will come to small polarons which are most likely present in DNA molecules.

3.1.1. Large Polarons

First investigations by Landau on self-trapping of electrons pioneered the work on polarons before the name even existed [77]. Landau and Pekar extended their research on electrons strongly coupled to a polar environment, which they described in a classical continuum model [78]. In this model a polaron is an electron or a hole surrounded by a charge cloud from the polar ionic environment, which is described by its static ϵ and classical high-frequency ϵ_∞ dielectric constants, whereas the polarization is modeled by a harmonic oscillator with frequency ω. Ionic crystals, in which the electron/hole interacts with optical phonons, seem to fulfill these requirements. The charge carrier wave function is modeled by a Gaussian distribution function with the mean squared deviation r_p. The effective environment description is valid only if the polaron size r_p is considerably larger than the lattice spacing a. When the particle moves, it drags the polarization with itself which affects its energy and effective mass. An important measure for the coupling strength is the Fröhlich coupling constant

$$\alpha = \frac{e^2}{4\pi\epsilon_0\hbar\kappa}\sqrt{\frac{m^*}{2\hbar\omega}} \; ; \text{with } \kappa^{-1} = \left(\epsilon_\infty^{-1} - \epsilon^{-1}\right).$$

The model by Pekar et al. [78] predicts a polaron radius $r_p = 1.51\kappa a_B$ where $a_B = \frac{4\pi\epsilon_0\hbar^2}{m^* e^2}$ is the Bohr radius. The ground state energy and the polaron mass are

$$\begin{aligned} E_0 &= -\,0.109\alpha^2\hbar\omega \\ M_P &\simeq 0.02\alpha^4 m^*, \end{aligned}$$

where m^* is the effective electron mass due to the electronic bands. The use of an effective environment is justified if $r_p \gg a$, i. e. $\alpha \ll \frac{\hbar}{2m^*\omega a^2}$. On the other hand, the phonon number has to be high to justify the classical approach. The phonon number is of the order $\frac{2E_0}{\hbar\omega}$, that is $\frac{2E_0}{\hbar\omega} \gg 1$. From this we deduce $\alpha^2 \gg 5$. The above two conditions are rarely fulfilled in reality [79,80].

A situation more often found in nature is that of weak-coupling large polarons with $\alpha < 1$ where due to small phonon number the quantization of the lattice vibrations has to

be taken into account. Fröhlich was the first to investigate this regime [81]. The so called Fröhlich Hamiltonian describes the linear interaction of a single electron in a solid with longitudinal optical (LO) phonons of frequency ω. As in the model by Pekar the electron is modeled as a free particle with effective mass m^* due to non-parabolic bands. The Hamiltonian was investigated by many others thereafter, but the most accurate results were obtained by Feynman, who used a variational approach based on path-integrals to solve the problem [82]. Up to second order in α the ground state energy and polaron mass are:

$$\begin{aligned} E_0 =& -\hbar\omega\left(\alpha + 0.0159\alpha^2\right) \\ M_p =& m^*\left(1 + \frac{\alpha}{6} + 0.0236\alpha^2\right). \end{aligned}$$

The Fröhlich model can describe the behavior of some semi-conductors and ionic crystals with an isotropic effective mass and their conduction band minimum at the Γ point. [79]

3.1.2. Small Polarons

In the 1950s a discussion started on how to explain the very low mobility μ in some materials. The classical band-like transport theory did not apply, so it was suggested that the low mobility might be explained by hopping transport of localized charge carriers [83]. A little later experiments by Heikes and Johnston showed that the mobility in NiO at high temperatures follows an activation law. They concluded that the ionic transport in NiO was due to phonon assisted hopping [84].

Holstein was the first to propose a mathematical model to concisely explain these phenomena [85]. He showed that due to strong electron-phonon interaction the electron can undergo 'self-trapping'. Thus transport is only possible when the electron and the lattice distortion move together. In this model the lattice distortion, i. e. the polaron size is confined to about one lattice spacing a; this approach is therefore called the 'small polaron' model. Holstein could show that at sufficiently low temperatures the transport was band-like with a strongly reduced band-width

$$\Delta E_P \propto \Delta E \exp\left(-\left(\frac{\lambda}{\hbar\omega}\right)^2 \coth\frac{\hbar\omega}{2k_BT}\right),$$

where ΔE is the original electronic band-width and λ is the electron-phonon coupling constant, which will be defined in Eq. 3.4. At temperatures higher than the Debye temperature the bands are too narrow and transport is a random walk of polaron hopping from site to site. The probability for such a hop follows an activation law $W_p \propto \exp\left(-E_a/k_BT\right)$, with the activation energy $E_a \sim \frac{\lambda^2}{2\hbar\omega}$.

An important step in the investigation of the small polaron was done by Lang and Firsov. Since the electron phonon coupling λ is large it is no use to do a perturbation theory in this parameter, so they introduced the so called polaron unitary transformation [86]. As a result of this transformation the electron is 'dressed' in a multiphonon cloud and other small parameters arise that can be used as a basis for a perturbative treatment or the use of the Kubo formula.

Nowadays the small polaron has attracted new interest as a candidate to explain the behavior of novel high-T_C superconductors but also in molecular electronics. We will use the concept of small polarons to investigate hopping transport in DNA. For an extensive introduction into the field of small polarons see books by Alexandrov [80, 83] and Böttger [76].

3.2. Transport in molecular systems

The electronic properties of a bulk conductor can be described by a set of continuous electronic bands. For a molecular system this is not true: the electronic states are usually not continuous but discrete levels and the transport can be strongly affected by quantum-mechanical effects due to the small size, the coupling to the contacts and the position of the Fermi energy. A crucial aspect is the interaction with vibration, since molecules are rather soft and flexible and vibrations are easily excited.

The transfer of an electron from a donor to an acceptor in a molecular system is therefore *driven* by the accompanying nuclear rearrangement in the molecule in the direction of minimal free energy. The rate k_{et} for such a transfer (quantum-mechanical tunneling) process is given by the Marcus theory [87, 88]

$$k_{et} = \frac{4\pi^2}{h} |t_{DA}|^2 \sqrt{4\pi\lambda k_B T} \exp\left[\frac{-(\delta E_{DA} - \lambda)^2}{4\lambda k_B T}\right],$$

where t_{DA} is the electronic coupling between donor and acceptor, which are separated by a energy gap δE_{DA}. λ is the reorganization energy, i. e. the energy describing the rearrangement of the atoms in the molecules in such a transfer process. The electronic coupling usually depends exponentially on the distance d between donor and acceptor $t_{DA} \propto \exp(-\beta d)$, since this is a usual tunneling event.

If the molecule is connected to two electrodes the situation changes; now the driving force for transport is the applied bias and we are no longer interested in a transient phenomenon like charge transfer, but in a steady state property of the system [88]. In this situation the electronic coupling strengths between donor, acceptor and the electrodes determine the transport [89]. If the coupling between donor and acceptor is good and their energies agree, charges become delocalized over the molecular system, which allows coherent transport. If the coupling to the vibrations is not too strong, the vibrations will lead to inelastic effects in the transport process, but the coherence of the transport is at least partially conserved. We call this regime 'quasi'-coherent. For small enough temperatures ($k_B T \ll \hbar\omega$) characteristic steps in the I-V curves arise, where the position of the steps agrees with the frequency ω of the vibrational mode that produces them. For strong coupling and high temperature, i. e. in the small polaron limit, the interaction with vibrations leads to a trapping of the charge and transport becomes a sequence of incoherent hopping processes. In this work we will study both regimes for the case of transport through DNA molecules.

Time and energy scales

The two limits of coherent and incoherent transport can also be described by respective time and energy scales. These time scales are the dwell time τ of the electron on the molecule and the dephasing time τ_ϕ, describing the time in which the electron loses its phase coherence due to interaction with the vibrations [88]. The dephasing time decreases with temperature and electron-vibration coupling strength. The ratio τ_ϕ/τ determines the dominant transport mechanism. For large ratio τ_ϕ/τ the electron moves very fast and its motion can be decoupled from the molecular motion by the Born-Oppenheimer approximation. The interaction with the vibrations is just a perturbation to the mainly coherent transport through the molecule. For small τ_ϕ/τ we have polaron formation and incoherent hopping transport. Transport is also governed by other internal energy scales of the system, which are the position of the molecular levels participating in the transport (HOMO (highest occupied molecular orbital) and LUMO (lowest unoccupied molecular orbital)), their relative position to the Fermi energy and the coupling to the electrodes. Of course, the temperature $k_\mathrm{B}T$ plays an important role in the occupation of electronic states.

One of the most important factors determining the current is the position of the chemical potential μ, describing the energy up to which the states are occupied. For an isolated molecule this is easily determined but for a molecules sandwiched between two metallic electrodes, which usually are by far bigger than the molecule, this task becomes difficult. The reason for this is the charging of the molecule due to charge transfer from the electrodes during the alignment of the chemical potential with the Fermi energy of the electrodes. In general this charge transfer is fractional, depending on the work function of the metal and the resulting chemical potential lies somewhere in the HOMO-LUMO gap [90]. Unless ab initio calculations or experiments obtain reliable values, the position of the chemical potential in the molecular system can be seen as a fitting parameter. Throughout this work we chose the chemical potential to be slightly above the HOMO states.

Transport in DNA

A molecular system like DNA consists of various parts/molecular orbitals, which can have different energies and coupling to each other. Of course, if it is homogeneous, all energies and couplings are the same. In the limit $\tau_\phi/\tau \gg 1$ such a homogeneous system gives rise to a band-like density of states (except for finite-size features) where electrons form Bloch-states which are delocalized over the entire molecule. Transport in such a system is mainly coherent and transmission probabilities are high and nearly independent of the length of the molecule. Interactions with vibration will lead to inelastic contributions to the current.

For inhomogeneous systems, the electrons undergo Anderson localization (depending on the degree of inhomogeneity) and the transmission, still being coherent, is suppressed and decreases exponentially with the length of the molecule. A coupling of the electronic degrees of freedom to vibrations can lead to a small but finite broadening of the levels. More importantly, the vibrational energy can allow the electrons to overcome potential

barriers, diminishing the localization in inhomogeneous samples and enabling transport. At least partial coherence of the transport is conserved.

In the opposite limit $\tau_\phi/\tau \ll 1$ small polarons are formed, which are localized on one or a few base pairs of the DNA, so the band picture is no longer applicable. The charge can hop between different base pairs, depending on the specific rates. The differences between homogeneous and inhomogeneous sequences are more subtle than for the coherent situation.

3.2.1. Theoretical methods

As argued in the introduction of this section, the current-voltage characteristics in nanoscale systems and molecules can differ strongly from the characteristics of bulk systems. The first important discovery in this field was done by Landauer in 1957 [21, 91]. He found that for systems smaller than the electron mean free path, i. e. in a ballistic conductor, transport can be described as a quantum mechanical scattering problem. The simple model system he studied consisted only of a scatterer (the molecule) sandwiched between two biased metallic leads. In the linear regime, i. e. for small bias, transport is characterized by the linear conductance g, which at zero temperature is proportional to the transmission T through the system

$$g = g_0 T(E_\mathrm{F})\,.$$

The proportionality factor $g_0 = 2e^2/h$ is the so called quantum of conductance of a perfect ballistic conductor with transmission $T = 1$. The transmission is calculated at the Fermi energy E_F of the leads, where the electrons are injected into the molecule.

The transmission function $T(E)$ can be obtained from the scattering matrix or, using the Fisher-Lee relation [92], directly from the retarded and advanced Green-functions $G^{\mathrm{ret/adv}}(E)$ of the molecule coupled to the electrodes

$$T(E) = 4\,\mathrm{tr}\left\{\Gamma_\mathrm{L}(E) G^\mathrm{ret}(E) \Gamma_\mathrm{R}(E) G^\mathrm{adv}(E)\right\}\,. \tag{3.1}$$

The Green function describe the density of states of the system and is given by

$$G^\mathrm{ret}(E) = \left[\left[G_0^\mathrm{ret}(E)\right]^{-1} + \Sigma_\mathrm{L}(E) + \Sigma_\mathrm{R}(E)\right]^{-1}\,,$$

where

$$G_0^\mathrm{ret}(E) = \left[E - H_\mathrm{mol} + i0^+\right]^{-1}$$

is the Green-function of the isolated molecule (for general definition of the Green function and relation between G^ret and G^adv see App. A). The Hamiltonian H_mol of the molecular or mesoscopic system is assumed to be known, which of course is a problem of its own. In the next section we will address this point. $\Sigma_{\mathrm{L/R}}(E)$ are the self-energies of the left/right electrode respectively. The electrode self-energies describe the energy contribution to the system/molecule due to the electrodes. In general this contribution is complex and describes a broadening of the electronic states, which is equivalent to a finite lifetime due to the possibility of electrons escaping from the molecule via the electrodes. The electrode

self-energies are determined by the spectral densities of the electrodes; for a flat density of states in the electrodes (wide band limit) they are given by $\Gamma_{\mathrm{L/R}}(E) = \mathrm{Im}\left(\Sigma_{\mathrm{L/R}}(E)\right)$. For the current at finite temperature one obtains

$$J = \frac{e}{4h}\int dE\,[f_{\mathrm{L}}(E) - f_{\mathrm{R}}(E)]\,T(E)\,, \tag{3.2}$$

where $f_{\mathrm{L/R}}(\epsilon)$ is the Fermi function in the left/right lead.

The Landauer formula and Fisher-Lee relation are only valid when there are no interactions on the molecule. This of course is not true if we include vibrations into our calculation. For the case of an interacting region between two electrodes Meir and Wingreen obtained a general formula for the current [93]

$$\begin{aligned} J = \frac{ie}{2h}\int dE\Big(&\mathrm{tr}\left\{[f_{\mathrm{L}}(E)\Gamma_{\mathrm{L}}(E) - f_{\mathrm{R}}(E)\Gamma_{\mathrm{R}}(E)]\left(G^{\mathrm{ret}}(E) - G^{\mathrm{adv}}(E)\right)\right\} \\ &+ \mathrm{tr}\left\{[\Gamma_{\mathrm{L}}(E) - \Gamma_{\mathrm{R}}(E)]\,G^{<}(E)\right\}\Big)\,, \end{aligned} \tag{3.3}$$

where $G^{</>}(E)$ are the 'lesser' and 'greater' Green functions of the molecule coupled to the electrodes. These Green functions describe the occupation of the system. In equilibrium these are connected to the retarded and advanced Green function ($G^{\mathrm{ret/adv}}$) by the fluctuation-dissipation relation (see App. A). In nonequilibrium these are independent quantities and have to be calculated separately. Therefore one has to use a formalism valid also out of equilibrium, like the Keldysh formalism [94], or one has to apply some approximative scheme. For the non-interacting case Eq. 3.3 reduces to the simple Landauer form (Eq. 3.2).

Meir and Wingreen derived their formula from a general expression for the current. From the continuity relation it is obvious that

$$J_{\mathrm{L}} = -e\frac{d}{dt}\langle N_{\mathrm{L}}\rangle = -\frac{ie}{\hbar}\langle[H, N_{\mathrm{L}}]\rangle\ ,$$

were N_{L} is the number of electrons in the left lead and H is the total Hamiltonian. Obviously for a steady-state situation the number of electrons on the molecule is constant, since all electrons that enter from the left leave to the right. The above two formulas are the basis of most transport calculation for DNA so far. Some also include interaction with vibrations or dephasing due to coupling to a reservoir [95–97].

Another approach for the calculation of transport quantities is the formulation of a master equation

$$\frac{d}{dt}P_{\mathrm{s}} = \sum_{\mathrm{s}'} P_{\mathrm{s}'}W_{\mathrm{s}',\mathrm{s}} - P_{\mathrm{s}}W_{\mathrm{s},\mathrm{s}'}$$

where P_{s} is the probability to be in some (charge) state s and $W_{\mathrm{s}',\mathrm{s}}$ is the rate for a transition from state s to s'. In steady state $\frac{d}{dt}P_{\mathrm{s}} = 0$. From this the current can be easily obtained

$$I = -e\left\{\sum_{\mathrm{s}'} P_{\mathrm{s}'}W^{\mathrm{L}}_{\mathrm{s}',\mathrm{s}} - P_{\mathrm{s}}W^{\mathrm{L}}_{\mathrm{s},\mathrm{s}'}\right\}\ .$$

Here the index L indicates that only rates are considered that describe transitions where the charge leaves to the left lead. Again some formalism has to be used that can describe nonequilibrium situations when a a finite bias is applied. In the most simple case the rates can be obtained from Fermi's golden rule, which assumes that the transition from an initial state i to final state f is induced by a perturbation H'. The transition rate is then given by

$$W = \frac{2\pi}{\hbar} \left|\langle f \left| H' \right| i \rangle\right|^2 \delta(E_i - E_f) \ ,$$

where initial and final states have the energy E_i and E_f, respectively. As one can see, the rate from Fermi's golden rule is second order in the perturbation. Master or rate equations are usually applied to describe the charge transfer in chemical experiments [98, 99], but they have also been successfully used to describe tunneling through microscopic contacts and in quantum dots (e. g. [100]).

Tight-binding description

In the previous subsection we have introduced several approaches for the calculation of observable quantities, in particular the current and the conductance. We assumed that the Hamiltonian, describing the system under consideration, was known. Of course, in general this is not the case. In particular, a solution to the full many-electron system is out of reach of todays computational power. Thus, if a microscopic description of the system is needed, an appropriate approximative scheme has to be applied.

The most common approximation in the description of complex systems is the so-called tight-binding (TB) approach. In 1929 Bloch introduced the basic ideas of the TB scheme, which approximates the many-electron wave function by a linear combination of single particle 'atomic' wave function [101]. Throughout the years, the TB model was successfully used, e. g. in band structure calculation of various solid state systems [102]. In particular, the tight-binding scheme is often used to model electronic properties in molecular systems and we will also resort to it throughout this thesis. As a further approximation, we will not consider atoms as elemental building blocks for our TB description but molecular orbitals that are extended over various atoms (for details see Chap. 2 and 4). The essential difficulty of this scheme lies in the appropriate choice of the TB parameters for the considered system.

By the nature of the approximation the TB model is in general discrete, performing a sum over all atoms that are included in the description. The Hamiltonian is then characterized by the atomic 'onsite' energies ϵ of the specific atoms/sites and the overlap of the various 'atomic' orbitals. In second quantization, where one no longer considers wave functions, but occupation numbers of states, the Hamiltonian in the tight-binding picture has the following form:

$$H_{\mathrm{el}} = \sum_i \epsilon_i a_i^\dagger a_i - \sum_{i,j} t_{ij} a_i^\dagger a_j \ .$$

Here ϵ_i is the onsite energy of site i and t_{ij} is the so called hopping integral which describes the overlap of wave functions between different sites i and j. The inclusion of interaction terms is formally straightforward.

Electron-vibration coupling

When studying interaction with vibrations or phonons, usually the deviation from the equilibrium position of the vibrating atoms or larger entities (DNA bases) is taken to be small. Thereby, non-linear effects are neglected and the interaction Hamiltonian becomes linear in the vibrational displacement. The resulting Hamiltonian for the vibration and the electron-vibration coupling are

$$H_{\text{vib}} = \sum_{\alpha} \hbar\omega_{\alpha} B_{\alpha}^{\dagger} B_{\alpha}$$
$$H_{\text{el-vib}} = \sum_{\alpha} \sum_{i,j} \lambda_{ij}^{\alpha} a_i^{\dagger} a_j \left(B_{\alpha}^{\dagger} + B_{\alpha} \right) \ ,$$

where α labels the vibrational mode and $B_{\alpha}^{\dagger} + B_{\alpha}$ is proportional to the vibrational displacement. The coupling matrix element is given by

$$\lambda_{ij}^{\alpha} = \sum_{n} C_{n\alpha} \sqrt{\frac{\hbar}{2M_n\omega_{\alpha}}} \langle i | \nabla_{R_n} H(\mathbf{R}) | j \rangle \ , \tag{3.4}$$

where M_n is the mass of the atom n with displacement coordinate R_n. The matrix element $C_{n\alpha}$ describes the transformation between atomic displacement and normal mode α and $H(\mathbf{R})$ is the electronic Hamiltonian for a given position of all atoms $\mathbf{R}$ [88].

The diagonal components of the interaction Hamiltonian ($i = j$) describe the polarization of the structure when the site is occupied by a charge, which is reflected in a change in onsite energy. Often calculations are restricted to just the diagonal components, which is justified for small overlap between neighboring states i and j. For many situations this approximation is not justified. As e. g. Starikov showed, the non-diagonal (from here on we will call them non-local) elements of some vibrational modes in DNA are of the same order as the diagonal elements [50]. The non-local elements describe the influence of vibrations on the probability for tunneling, which clearly changes if e. g. the distance between the two involved sites varies. This phenomenon can be described as vibration assisted tunneling. In this work we will discuss both diagonal (local) and non-local electron-vibration coupling for the quasi-coherent case, but restrict us to the local coupling for the situation of polaron hopping.

4. Quasi-coherent transport

4.1. Definition of the Problem

As discussed in chapter 2, several experiments and theoretical considerations in the past have stressed the importance of the environment and vibrations on the electron transfer [38, 52] and transport [62, 103]. But experiments alone cannot explain the physics underlying charge transport through DNA. For an detailed understanding and interpretation of the experimental results, modeling and theoretical calculations are indispensable.

Numerous recent theoretical articles addressed the electronic transport properties of DNA in a microscopic approach [67, 95–97, 104–110]. In these approaches the DNA is typically described within a tight-binding model for the electronic degrees of freedom with parameters either taken from ab-initio quantum chemistry simulations [35, 50, 111] or motivated by a fit to experiments [96]. The variance of qualitatively different tight-binding models is large, ranging from involved all-atomic representations to models where each base pair is represented by only a single orbital. However, the vibrations have been treated so far only within very simple models (if treated at all), where specifically only a local site independent electron-vibration coupling has been taken into account [95,96].

While these approaches are sufficient to describe the transition from elastic (quasi-ballistic) to inelastic (dissipative) transport they ignore the fact that the non-local electron-vibration coupling strength can be comparable in magnitude to the local one [50]. As the non-local electron-vibration coupling leads effectively to a vibration-assisted hopping, the proper inclusion of this coupling can be important for transport through DNA with inhomogeneous sequences. Starikov calculated the change in onsite energy ϵ_i and hopping integrals t_{ij} using a PM3 semi-empirical quantum chemistry package for various displacements of the DNA bases associated with certain vibrational modes of the DNA. He observed that certain vibrational modes not only strongly change the onsite energy, but also the hopping integrals, sometimes in the same order of magnitude [50].

In this chapter we formulate a minimum model for a DNA molecule coupled to left and right electrodes, where the base pairs are represented by single tight-binding orbitals, with energies differing for Guanine-Cytosine (GC) and Adenine-Thymine (AT) pairs, as motivated in section 2.1. Figure 4.1 shows a schematic drawing of the situation under consideration. The light blue rectangles to both sides represent left and right electrodes which are coupled to the first and last base. The coupling is characterized by the spectral densities $\Gamma_{\mathrm{L/R}}$. The DNA double-helix is unequivocally defined by the sequence of only a single strand, since the second one is complementary. We always consider the strand starting from left at the 5' end and running to the 3' end at the right, when describing a certain DNA sequence.

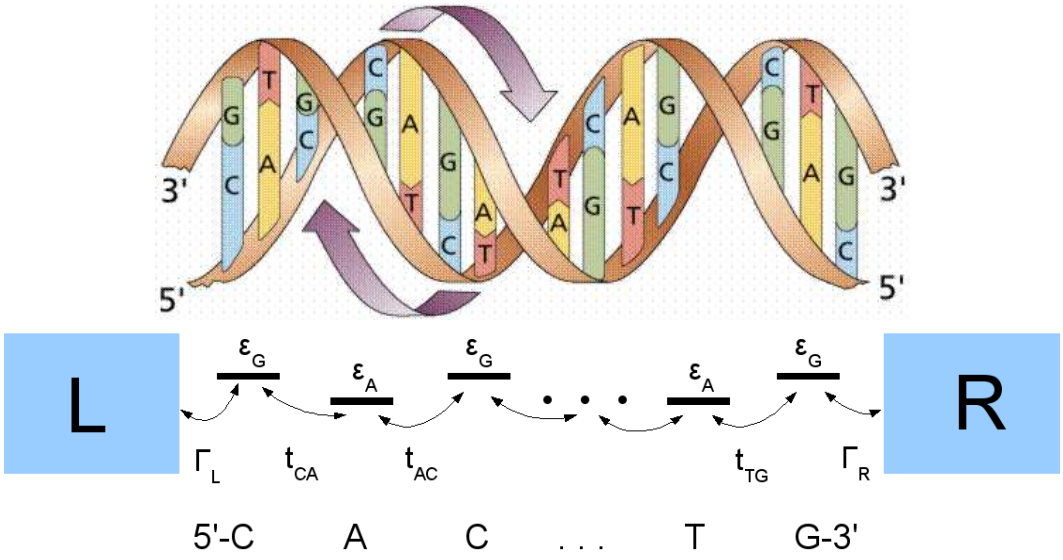

Figure 4.1: Schematic drawing of a DNA helix (taken from [112]) and the tight-binding model used to describe its electronic properties.

We adopt a situation of strong local electron-vibration interaction, where the vibrational modes are also coupled to the surrounding environment (water or buffer solution). This extension allows for dissipation of energy, leading to a continuous spectrum of the vibration with a broadened resonance. We assume that the excited vibration is extended over the whole DNA molecule. This does not allow small polaron formation (we will discuss this limit in the following chapters). Transport retains (at least partial) coherence, but there can be strong inelastic effects. We call this regime 'quasi'-coherent, to distinguish it from both a pure ballistic and the fully incoherent polaron hopping situation. An additional non-local coupling further changes the hopping between adjacent molecular orbitals/tight-binding sites and allows for vibration assisted tunneling.

4.2. Model and technique

In this section we explain, how DNA coupled to biased electrodes is modeled in the 'quasi'-coherent regime, as introduced before. We will then dwell on the techniques we used to obtain measurable quantities like the current.

4.2.1. Hamiltonian

From the discussion above, we arrive at the Hamiltonian $H = H_{\rm el} + H_{\rm vib} + H_{\rm el-vib} + H_{\rm L} + H_{\rm R} + H_{\rm T,L} + H_{\rm T,R} + H_{\rm bath}$ with

$$\begin{aligned} H_{\rm el} &= \sum_i \epsilon_i a_i^\dagger a_i - \sum_{<ij>} t_{ij} a_i^\dagger a_j \\ H_{\rm T,L} + H_{\rm T,R} &= \sum_{\nu,r,i} \left[t_i^r c_{\nu r}^\dagger a_i + t_i^{r*} a_i^\dagger c_{\nu r} \right] \\ H_{\rm vib} &= \sum_\alpha \omega_\alpha B_\alpha^\dagger B_\alpha \\ H_{\rm el-vib} &= \sum_\alpha \sum_i \lambda_0 \, a_i^\dagger a_i (B_\alpha + B_\alpha^\dagger) \\ &\quad + \sum_\alpha \sum_{<ij>} \lambda_{ij} \, a_i^\dagger a_j (B_\alpha + B_\alpha^\dagger) \, . \end{aligned} \tag{4.1}$$

The index $r = {\rm L, R}$ represents left and right electrode. The term $H_{\rm el}$ describes the electrons in the molecular chain with operators $a_i^\dagger, a_i$ in a single-orbital tight-binding representation with onsite energies ϵ_i of the base pairs and hopping t_{ij} between neighboring base pairs. As mentioned above, both onsite energies and hopping depend on the base pair sequence, e. g. the onsite energy of a Guanine-Cytosine base pair differs from the onsite energy of a Adenine-Thymine base pair. As explained in Sec. 2.1, for the hopping matrix elements t_{ij} we adopted the *ab initio* results, from Siebbeles *et al.* [35] denoted in table 2.1. For the onsite energies of guanine and adenine, we resort to the ionization potentials of these bases, i. e. $\epsilon_{\rm G} = 7.75\,{\rm eV}$ and $\epsilon_{\rm A} = 8.26\,{\rm eV}$, but actually only the differences between these two energies ($\epsilon_{\rm G} - \epsilon_{\rm A} = 0.51\,{\rm eV}$) and to the Fermi energy $E_{\rm F}$ matter.

The terms $H_{\rm L/R}$ refer to the left and right electrodes. They are modeled by non-interacting electrons, described by operators $c_{\nu\,{\rm L/R}}^\dagger, c_{\nu\,{\rm L/R}}$, with a flat density of states ρ_e (wide band limit). The chemical details of the coupling between the molecule and the electrodes are not the focus of this work. For our purposes it is fully characterized by $H_{\rm T,L} + H_{\rm T,R}$ with tunneling amplitudes assumed to be independent of the type of base pair i and the quantum numbers of the electrode states ν. The left lead is coupled only to the first base pair and the right electrode is coupled only to the last base pair. The coupling strength is then characterized by the parameter $\Gamma^{\rm L,R} = 2\pi\rho_e^{\rm L,R}|t^{\rm L,R}|^2$, which leads to a level broadening of the base pair orbitals coupled to the electrodes.

The vibrational degrees of freedom are described by $H_{\rm vib}$, with bosonic operators B_α and $B_\alpha^\dagger$ for the vibrational mode with frequency ω_α. $H_{\rm el-vib}$ couples the electrons on the molecule to the vibrational modes, where λ_0 and λ_{ij} are the strengths for the local and non-local electron-vibration coupling, respectively. Note that the vibration modes are extended over the entire DNA molecule and that the coupling of the modes to electrons is assumed independent of the base pairs involved. This retains a 'quasi'-coherent transport situation even in the strong coupling limit. The strength of the electron-vibration coupling for various vibrational modes has been computed in Ref. [50] for homogeneous

dimers and tetramers of AT and GC pairs. Here we consider also inhomogeneous sequences, for which the electron-vibration couplings are not known, but we assume that they differ not too much from the values for homogeneous sequences. As an exemplary mode we chose the 'stretch' mode (see Fig. 4.2) of Ref. [50], which shows relatively strong coupling to both electronic parameters for AT and GC base pairs. The values for the

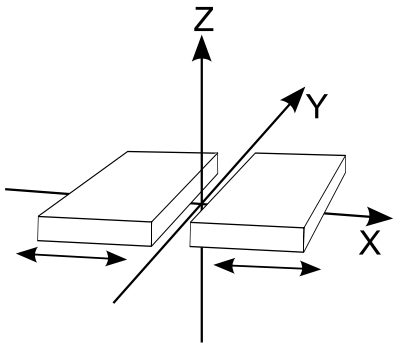

Figure 4.2: Schematic drawing of the vibrational stretch mode of two DNA bases. The DNA strand runs along the z-direction. Picture according to [50].

stretch mode obtained by Starikov for the vibrational frequencies ω and matrix elements in Eq. 3.4 are given by (using $g_{ij} = \langle i | \nabla_{R_n} H(\mathbf{R}) | j \rangle$)

$$\begin{array}{rclrcl} \hbar\omega_{\mathrm{AT}} & = & 0.011\,\mathrm{eV} & \hbar\omega_{\mathrm{GC}} & = & 0.016\,\mathrm{eV} \\ g_{ii}(\mathrm{AT}) & = & 0.1104\,\mathrm{eV/\AA} & g_{ii}(\mathrm{GC}) & = & \text{-}0.2349\,\mathrm{eV/\AA} \\ g_{ij}(\mathrm{AT}) & = & 0.0820\,\mathrm{eV/\AA} & g_{ij}(\mathrm{GC}) & = & \text{-}0.1779\,\mathrm{eV/\AA}\ . \end{array}$$

From this one can estimate the local and non-local electron-vibration coupling by assuming a reduced mass of 118.92 g/mol for the AT and 122.69 g/mol [50] for the GC base pairs

$$\begin{array}{rclrcl} \lambda_{ii}(\mathrm{AT}) & \approx & 0.004\,\mathrm{eV} & \lambda_{ii}(\mathrm{GC}) & \approx & \text{-}0.008\,\mathrm{eV} \\ \lambda_{ij}(\mathrm{AT}) & \approx & 0.003\,\mathrm{eV} & \lambda_{ij}(\mathrm{GC}) & \approx & \text{-}0.006\,\mathrm{eV}\ . \end{array}$$

We restrict the non-local coupling terms to nearest neighbors, $\lambda_{ij} = \lambda_1 \delta_{i,j=i\pm1}$ and for our model we take λ_0 and λ_1 as parameters, independent of the base pairs involved, for which we choose values in rough agreement with the above estimates, i. e. $\lambda_{0,1} \approx 1 - 10\,\mathrm{meV}$. This allows for a qualitative discussion of the effects that arise from the electron-vibration coupling in DNA.

The vibrations themselves are coupled to the environment, the microscopic details of which do not matter. We model it by a harmonic oscillator bath H_{bath} whose relevant properties are summarized by its linear ('Ohmic') power spectrum (or spectral function) up to a high-frequency cut-off ω_c [113]. The cut-off is necessary for convergent results and is physically equivalent to the Debye frequency in a solid state system. The coupling of the vibrations to the bath changes the vibrations spectra from discrete (Einstein) modes to continuous spectra with a peak around the vibrational frequency. This can be shown explicitly when calculating the polarization of the vibration (the vibrational self-energy due to coupling to the bath) [114]. Physically, the coupling to a bath allows for dissipation

of electronic and vibrational energy. This dissipation is crucial for the stability of the molecule in a situation where inelastic contributions to the current dissipate a substantial amount of power on the molecule itself.

We only consider a single vibrational mode when performing the numerical calculations, since we are mainly interested in the physics involved when including non-local electron-vibration coupling. The vibrational mode with resonance frequency ω_0 coupled to the bath is then described by a spectral density

$$\begin{aligned} D_i(\omega) =& -i \int dt e^{i\omega t}\theta(t) \left\langle \left\{ B^\dagger(t) + B(t), B^\dagger + B \right\} \right\rangle \\ =& \frac{1}{\pi} \left(\frac{\eta_i(\omega)}{(\omega-\omega_i)^2 + \eta_i(\omega)^2} - \frac{\eta_i(\omega)}{(\omega+\omega_i)^2 + \eta_i(\omega)^2} \right) . \end{aligned} \tag{4.2}$$

with a frequency dependent broadening $\eta(\omega)$ which arises from the vibration-bath coupling. For the 'Ohmic' bath with weak vibration-bath coupling and cut-off ω_c we consider $\eta(\omega) = \eta_0\, \omega\, \theta(\omega_c - \omega)$, with $\eta_0 = 0.05\,\mathrm{eV}$. Mathematically the crossover from the discrete vibrational modes to a continuous spectrum of a single mode is done by substituting $\sum_\alpha \to \int d\omega D(\omega)$.

4.2.2. Lang-Firsov transformation

In order to treat the limit of strong local electron-vibration coupling we perform the Lang-Firsov unitary transformation [79, 86] on the Hamiltonian H. The transformation was developed for the description of small polarons (see Sec. 3.1). Since in this chapter we assume a global vibration, i. e. all base pairs 'vibrate' together in phase, we do not have small polaron formation, but still can describe inelastic effects arising from the strong coupling to the vibrations, which would not arise in a direct perturbative treatment in the electron-vibration coupling. The transformation is defined by the generator function S.

$$\tilde{H} = e^S H e^{-S} \; ; \; S = -\sum_{i\alpha} \frac{\lambda_0}{\omega_\alpha} a_i^\dagger a_i \left[B_\alpha - B_\alpha^\dagger \right] .$$

We introduce transformed electron and vibration operators according to

$$\begin{aligned} \tilde{a}_i &= a_i \chi \\ \tilde{B}_\alpha &= B_\alpha - \sum_i \frac{\lambda_0}{\omega_\alpha} a_i^\dagger a_i \\ \chi &= \exp\left[\sum_\alpha \frac{\lambda_0}{\omega_\alpha} (B_\alpha - B_\alpha^\dagger) \right] , \end{aligned}$$

where the operator χ incorporates the interaction with the vibrations and is crucial for the description of the inelastic effects. The new Hamiltonian reads (with $\chi\chi^\dagger = \chi^\dagger\chi = 1$)

$$\begin{aligned}\tilde{H} = &\sum_i (\epsilon_i - \Delta) a_i^\dagger a_i - \sum_{<ij>} t_{ij} a_i^\dagger a_j \\ &+ \sum_{r,\nu,i} \left[t_i^r c_{\nu r}^\dagger a_i \chi + t_i^{r*} a_i^\dagger \chi^\dagger c_{\nu r} \right] + H_{\mathrm{L}} + H_{\mathrm{R}} \\ &+ \sum_\alpha \omega_\alpha B_\alpha^\dagger B_\alpha + \sum_\alpha \sum_{<ij>} \lambda_{ij}\, a_i^\dagger a_j (B_\alpha + B_\alpha^\dagger) + \tilde{H}_{\mathrm{ee}} \,, \end{aligned} \tag{4.3}$$

where the Hamiltonian

$$\tilde{H}_{\mathrm{ee}} = - \sum_{<ij>} \sum_\alpha \frac{\lambda_0^2}{\omega_\alpha} a_i^\dagger a_i \cdot a_j^\dagger a_j - 2 \sum_{<ij>} \sum_k \sum_\alpha \frac{\lambda_{ij}\,\lambda_0}{\omega_\alpha} a_i^\dagger a_j \cdot a_k^\dagger a_k \tag{4.4}$$

describes an effective vibration mediated electron–electron interaction which will be neglected throughout this chapter. This is a reasonable approximation for the low charge carrier (hole) density in molecular systems [76].

The purpose of the Lang-Firsov transformation is to remove the local electron-vibration coupling term from the transformed Hamiltonian in exchange for the transformed operators and the so-called polaron shift

$$\Delta = \int d\omega D(\omega) \frac{\lambda_0^2}{\omega} \,.$$

The polaron shift or reorganization energy describes the lowering of the onsite energy of the electron due to the interaction with the vibration. Since we couple the electronic degrees of freedom to a global vibration, Δ is constant for all base pairs. The non-local electron-vibration coupling term, however, remains unchanged and has to be dealt with in a different way than the local term. There is an additional electron-vibration coupling due to the operator χ in the transformed tunnel Hamiltonian from the leads. In this study we neglect effects arising from this additional coupling. This is a valid approximation for $\Gamma^{\mathrm{L,R}} \gg \lambda_0$, the usual approximation taken in the literature [96, 114].

Green functions

In this section we consider the above Hamiltonian and use an approximative scheme to describe the situation of finite bias. A more rigorous treatment will be introduced in Appendix D.

For the calculation of physical quantities like current and density of states we use the Green function formalism as introduced in the previous chapter. We introduce the retarded electron Green function (see App. A).

$$G_{kl}^{\mathrm{ret}}(t) = -i\theta(t) \left\langle \left\{ a_k(t)\chi(t), a_l^\dagger \chi^\dagger \right\} \right\rangle \,, \tag{4.5}$$

where the thermal average is taken with respect to the transformed Hamiltonian $\tilde{H}$, which does not explicitly include the local electron-vibration interaction. By applying

the equation of motion (EOM) technique we can derive a self-consistent calculation scheme for $G^{\mathrm{ret}}_{kl}(t)$. The EOM technique for an interacting system generates correlation functions of higher order than initially considered, resulting in a hierarchy of equations that does not close in itself. Therefore, an appropriate truncation scheme needs to be applied. In our case, we close the hierarchy on the first possible level neglecting all higher order Green functions beyond the one defined above. In particular, our approximations are perturbative to first order in λ_1, restricting our study to relatively weak non-local electron-vibration coupling strengths.

Equation of motion

The equation of motion for an operator in the Heisenberg picture is given by

$$\frac{d}{dt}a_i(t) = i\left[H, a_i\right](t)\ .$$

From the above expression the behavior of the time evolution of the operator can be obtained. This is the basis of the equation of motion technique. Before applying it, we separate the retarded electron Green function into two parts,

$$\begin{aligned} G^{\mathrm{ret}}_{kl}(t) &= -i\theta(t)\left\langle\left\{a_k(t)\chi(t), a_l^\dagger\chi^\dagger\right\}\right\rangle \\ &= \underbrace{-i\theta(t)\left\langle a_k(t)\chi(t)a_l^\dagger\chi^\dagger\right\rangle}_{G^{(1)}_{kl}(t)} \underbrace{-i\theta(t)\left\langle a_l^\dagger\chi^\dagger a_k(t)\chi(t)\right\rangle}_{G^{(2)}_{kl}(t)}\ . \end{aligned}$$

This is useful, because for $G^{(1)}_{kl}(t)$ and $G^{(2)}_{kl}(t)$ self-consistency equations can be derived via the equation of motion technique (EOM), but the equation of motion applied to the retarded Green function itself leads to an equation containing not only the retarded Green function, i. e. a coupled equation.

The expressions of the commutator of all fermionic operators with the Hamiltonian (Eq. 4.3) can be found quite easily, whereas the explicit derivation of $\left[\tilde{H}, \chi\right]$ is more involved and therefore shown in App. B. With these, we obtain the following expression for the equation of motion of $G^{(1)}_{kl}(t)$,

$$\begin{aligned} &\sum_j \left[(i\frac{d}{dt} - \epsilon_k)\delta_{jk} + t_{kj}\right] G^{(1)}_{jl}(t) \\ &= \delta(t)\left\langle a_k a_l^\dagger\right\rangle + i\theta(t)\Delta\left\langle a_k(t)\chi(t)a_l^\dagger\chi^\dagger\right\rangle \\ &- i\theta(t)\Bigg\{\sum_{j\neq k,\alpha}\lambda_{kj}\left\langle a_j(t)\left[B_\alpha(t) + B_\alpha^\dagger(t)\right]\chi(t)a_l^\dagger\chi^\dagger\right\rangle \\ &+ \sum_\alpha \lambda_0\left[\left\langle a_k(t)B_\alpha(t)\chi(t)a_l^\dagger\chi^\dagger\right\rangle + \left\langle a_k(t)\chi(t)B_\alpha^\dagger(t)a_l^\dagger\chi^\dagger\right\rangle\right] \\ &+ \sum_\alpha\sum_{<ij>}\frac{2\,\lambda_{ij}\,\lambda_0}{\omega_\alpha}\left\langle a_k(t)a_i^\dagger(t)a_j(t)\chi(t)a_l^\dagger\chi^\dagger\right\rangle + \sum_{\nu,r} t_k^{r*}\left\langle c_\nu^r(t)a_l^\dagger\chi_l^\dagger\right\rangle\Bigg\} \end{aligned} \tag{4.6}$$

and a similar relation for $G^{(2)}_{kl}(t)$,

$$\begin{aligned}
&\sum_j \left[(i\frac{d}{dt} - \epsilon_k)\delta_{jk} + t_{kj} \right] G^{(2)}_{jl}(t) \\
&= \delta(t) \left\langle a_l^\dagger a_k \right\rangle + i\theta(t)\Delta \left\langle a_l^\dagger \chi^\dagger a_k(t)\chi(t) \right\rangle \\
&- i\theta(t) \Bigg\{ \sum_{j\neq k} \lambda_{kj} \left\langle a_l^\dagger \chi^\dagger a_j(t) \left[B(t) + B^\dagger(t) \right] \chi(t) \right\rangle \\
&+ \lambda_0 \left[\left\langle a_l^\dagger \chi^\dagger a_k(t) B(t) \chi(t) \right\rangle + \left\langle a_l^\dagger \chi^\dagger a_k(t) \chi(t) B^\dagger(t) \right\rangle \right] \\
&+ (t) \sum_{<ij>} \frac{2\,\lambda_{ij}\,\lambda_0}{\omega_0} \left\langle a_l^\dagger \chi^\dagger a_k(t) a_i^\dagger(t) a_j(t) \chi(t) \right\rangle + \sum_{\nu,r} t_k^{r*} \left\langle a_l^\dagger \chi^\dagger c_\nu^r(t) \right\rangle \Bigg\} . \qquad (4.7)
\end{aligned}$$

To determine expressions like $\left\langle a_j(t) B_\alpha(t) \chi(t) a_l^\dagger \chi^\dagger \right\rangle$ and similar higher order correlation functions one would have to compute the EOM for these, too. This leads to correlators of ever higher order, so we truncate the hierarchy and approximate them by assuming, e. g. for the expression

$$\left\langle a_j(t) B_\alpha(t) \chi(t) a_l^\dagger \chi^\dagger \right\rangle_{\tilde{H}} \approx F_\alpha(t) \left\langle a_j(t) \chi(t) a_l^\dagger \chi^\dagger \right\rangle_{\tilde{H}} . \qquad (4.8)$$

The explicit expression for the functions $F_\alpha(t)$ and their derivation for the various correlators in Eqs. 4.6 and 4.7 can be found in appendix B. The approximative scheme involves a factorization of vibrational and electronic operators in the correlation functions, which is exact for vanishing electron-vibration coupling. Since the strength of the electron-vibration coupling in $\tilde{H}$ is proportional to λ_1, this approximation is valid for not too large values of λ_1.

Expressions like $\left\langle a_l^\dagger \chi^\dagger a_k(t) a_i^\dagger(t) a_j(t) \chi(t) \right\rangle$ are treated in a mean-field like manner, where we neglect correlations arising from the effective interaction of charges on different bases due to non-local electron-vibration coupling:

$$\begin{aligned}
&\left\langle a_k(t) a_i^\dagger(t) a_j(t) \chi(t) a_l^\dagger \chi^\dagger \right\rangle \\
&\quad \approx \left\langle a_k(t) a_i^\dagger(t) \right\rangle \left\langle a_j(t) \chi(t) a_l^\dagger \chi^\dagger \right\rangle - \left\langle a_j(t) a_i^\dagger(t) \right\rangle \left\langle a_k(t) \chi(t) a_l^\dagger \chi^\dagger \right\rangle .
\end{aligned}$$

This approximation is based on the same principle as the neglect of $\tilde{H}_{\mathrm{ee}}$ in the transformed Hamiltonian, the small charge density in DNA.

The correlators $\left\langle c_\nu^r(t) a_l^\dagger \chi^\dagger \right\rangle$ and $\left\langle a_l^\dagger \chi^\dagger c_\nu^r(t) \right\rangle$ in Eq. 4.6 and 4.7, respectively, arise from the coupling to the electrodes and describe the according self-energy. The calculation of these expressions can be found in Appendix C.

After Fourier transformation and crossover to the continuous vibrational spectrum (see Eq. 4.2) we obtain

$$\begin{aligned}
&\sum_j \left[(E-\epsilon_k)\delta_{jk}+t_{kj}\right]\, G^{(1)}_{jl}(E) \\
&\quad = \left\langle a_k a_l^\dagger \right\rangle - \Delta G^{(1)}_{kl}(E) + \sum_j \Sigma^{\mathrm{ret,L}}_{kj} G^{(1)}_{jl}(E) + \sum_j \Sigma^{\mathrm{ret,R}}_{kj} G^{(1)}_{jl}(E) \\
&\quad + \int d\omega D(\omega) \Bigg\{ - \sum_{<ij>} \left\langle a_j a_i^\dagger \right\rangle \frac{2\lambda_{ij}\lambda_0}{\omega} G^{(1)}_{kl}(E) + \sum_{<ij>} \left\langle a_k a_i^\dagger \right\rangle \frac{2\lambda_{ij}\lambda_0}{\omega} G^{(1)}_{jl}(E) \\
&\quad + \frac{\lambda_0^2}{\omega} \left[\int dt e^{iEt} F_1(t,\omega)\, G^{(1)}_{kl}(t) \right] + \sum_{j\neq k} \frac{\lambda_{kj}\lambda_0}{\omega} \left[\int dt e^{iEt} \left[F_1(t,\omega)-1\right]\, G^{(1)}_{jl}(t) \right] \Bigg\}
\end{aligned} \tag{4.9}$$

and

$$\begin{aligned}
&\sum_j \left[(E-\epsilon_k)\delta_{jk}+t_{kj}\right]\, G^{(2)}_{jl}(E) \\
&\quad = \left\langle a_l^\dagger a_k \right\rangle - \Delta G^{(2)}_{kl}(E) + \sum_j \Sigma^{\mathrm{ret,L}}_{kj} G^{(2)}_{jl}(E) + \sum_j \Sigma^{\mathrm{ret,R}}_{kj} G^{(2)}_{jl}(E) \\
&\quad + \int d\omega D(\omega) \Bigg\{ - \sum_{<ij>} \left\langle a_j a_i^\dagger \right\rangle \frac{2\lambda_{ij}\lambda_0}{\omega} G^{(2)}_{kl}(E) + \sum_{<ij>} \left\langle a_k a_i^\dagger \right\rangle \frac{2\lambda_{ij}\lambda_0}{\omega} G^{(2)}_{jl}(E) \\
&\quad + \frac{\lambda_0^2}{\omega} \left[\int dt e^{iEt} F_2(t,\omega)\, G^{(2)}_{kl}(t) \right] + \sum_{j\neq k} \frac{\lambda_{kj}\lambda_0}{\omega} \left[\int dt e^{iEt} \left[F_2(t,\omega)-1\right]\, G^{(2)}_{jl}(t) \right] \Bigg\} ,
\end{aligned} \tag{4.10}$$

where the electron-vibration interaction is described by the two functions

$$\begin{aligned}
F_1(t,\omega) &= (N(\omega)+1)\, e^{-i\omega t} - N(\omega) e^{i\omega t} \\
F_2(t,\omega) &= N(\omega) e^{-i\omega t} - (N(\omega)+1)\, e^{i\omega t} ,
\end{aligned}$$

with the Bose function $N(\omega)$.

In the wide band limit the retarded right and left electrode self-energies are constant and purely imaginary,

$$\begin{aligned}
\Sigma^{\mathrm{ret,R}}_{jk} &= \sum_\nu t^{R*}_k g^{\mathrm{ret}}_{\nu R}(E) t^R_j = -i\Gamma^{\mathrm{R}} \delta_{jN}\delta_{kN} \\
\Sigma^{\mathrm{ret,L}}_{jk} &= \sum_\nu t^{L*}_k g^{\mathrm{ret}}_{\nu L}(E) t^L_j = -i\Gamma^{\mathrm{L}} \delta_{j1}\delta_{k1} .
\end{aligned}$$

We can now identify

$$(E-\epsilon_k)\delta_{jk} + t_{jk} + i0^+ = \left[G^{\mathrm{ret}}_0(E)\right]^{-1}_{jk} ,$$

where $G_0^{\mathrm{ret}}(E)$ is the retarded Green function for the isolated molecule without electron-vibration interaction. The validity of this equation can easily be seen by computing the equation of motion for $G^{\mathrm{ret}}(t)$ for the isolated molecule without electron-vibration coupling.

In the equations above, many factors of the kind $\left\langle a_k\, a_l^\dagger \right\rangle$ appear. The exact value for these is: $\left\langle a_k\, a_l^\dagger \right\rangle_{\tilde{H}} = \int \frac{dE}{2\pi i} G_{kl}^<(E)$. In order to have a decoupled system of equations we approximate these by $\left\langle a_k\, a_l^\dagger \right\rangle_{\tilde{H}} \approx \left\langle a_k\, a_l^\dagger \right\rangle_{\tilde{H}_{\mathrm{el}}}$, where $\tilde{H}_{\mathrm{el}}$ is the Hamiltonian for the isolated molecule (compare Eq. 4.3).

With all the above approximations we calculate the retarded Green function by iteration of the self-consistency equations Eq. 4.9 and 4.10. For a molecular DNA chain with N bases the density of states then reads

$$A(E) = -\frac{1}{\pi N} \sum_{i=1}^{N} \mathrm{Im}\left\{G_{ii}^{\mathrm{ret}}(E)\right\} .$$

We evaluate the current using the relation be Meir and Wingreen [93] as introduced in Section 3.2.

$$I = \frac{ie}{h} \int d\epsilon \Big(\mathrm{tr}\left\{ \left[f_{\mathrm{L}}(\epsilon)\Gamma^{\mathrm{L}} - f_{\mathrm{R}}(\epsilon)\Gamma^{\mathrm{R}} \right] \left(G^{\mathrm{ret}}(\epsilon) - G^{\mathrm{adv}}(\epsilon) \right) \right\} + \mathrm{tr}\left\{ \left[\Gamma^{\mathrm{L}} - \Gamma^{\mathrm{R}} \right] G^<(\epsilon) \right\} \Big) , \tag{4.11}$$

where $f_{\mathrm{L}}(\epsilon)$ and $f_{\mathrm{R}}(\epsilon)$ are the Fermi distributions in the left and right lead, respectively.

To compute the 'lesser' Green function $G^<(\epsilon)$, we use the relation [79] (see also App. A)

$$G^<(\epsilon) = G^{\mathrm{ret}}(\epsilon) \left[\Sigma^{\mathrm{L}<} + \Sigma^{\mathrm{R}<} + \Sigma_{\mathrm{vib}}^<(\epsilon) \right] G^{\mathrm{adv}}(\epsilon) .$$

While the lesser electrode self-energies, such as $\Sigma^{\mathrm{L}<}$, can be determined easily within the above approximation for any applied bias, we have to approximate the behavior of the lesser self-energy due to the vibrations $\Sigma_{\mathrm{vib}}^<$. Extending the fluctuation-dissipation relation of the equilibrium situation we write

$$\Sigma_{\mathrm{vib}}^<(\epsilon) = -f_{\mathrm{eff}}(\epsilon) \left[\Sigma_{\mathrm{vib}}^{\mathrm{ret}}(\epsilon) - \Sigma_{\mathrm{vib}}^{\mathrm{adv}}(\epsilon) \right] ,$$

with an effective electron distribution $f_{\mathrm{eff}} = [f_{\mathrm{L}}(\epsilon) + f_{\mathrm{R}}(\epsilon)]/2$. The expressions for $\Sigma_{\mathrm{vib}}^{\mathrm{ret}}, \Sigma_{\mathrm{vib}}^{\mathrm{adv}}$ are obtained from the retarded Green function (see App. A) calculated for a given bias as explained above. Combining all terms we obtain a concise expression for the current, which can be separated into 'elastic' and 'inelastic' parts as

$$I = \frac{2e}{h} \int d\epsilon \, \left[T_{\mathrm{el}}(\epsilon) + T_{\mathrm{inel}}(\epsilon) \right] \left[f_{\mathrm{L}}(\epsilon) - f_{\mathrm{R}}(\epsilon) \right] ,$$

where we identify the 'elastic' and 'inelastic' transmission functions [115, 116]

$$T_{\mathrm{el}}(\epsilon) = 2\,\mathrm{tr}\left\{ \Gamma^{\mathrm{R}} G^{\mathrm{ret}}(\epsilon) \Gamma^{\mathrm{L}} G^{\mathrm{adv}}(\epsilon) \right\} \tag{4.12}$$

$$T_{\mathrm{inel}}(\epsilon) = \frac{i}{4}\,\mathrm{tr}\{ (\Gamma^{\mathrm{R}} + \Gamma^{\mathrm{L}}) G^{\mathrm{ret}}(\epsilon) \left[\Sigma_{\mathrm{vib}}^{\mathrm{ret}}(\epsilon) - \Sigma_{\mathrm{vib}}^{\mathrm{adv}}(\epsilon) \right] G^{\mathrm{adv}}(\epsilon) \} . \tag{4.13}$$

Note that also the 'elastic' transmission depends on the effects of vibrations, since the self-consistent evaluation of the Green function is performed in the presence of vibrations and environment. The inelastic contribution can also be termed 'incoherent', as typically the electrons will leave the DNA at a lower energy than they enter it.

4.3. Results

In this section we analyze the effect of vibrations on the electronic properties of DNA, i.e., we determine the density of states, the transmission and the current. As explicit examples we consider homogeneous and inhomogeneous DNA sequences of 26 base pairs in the presence of a single vibrational mode as described in the previous section. For simplicity, we couple the left and right electrodes symmetrically to the DNA, so $\Gamma^{\mathrm{L}} = \Gamma^{\mathrm{R}} \equiv \Gamma$, and we choose $\Gamma = 0.1\,e\mathrm{V}$. We further assume that the bias voltage V_b drops symmetrically across both electrode-DNA interfaces.

4.3.1. Homogeneous Poly-(GC) DNA

For a homogeneous DNA consisting of 26 Guanine-Cytosine base pairs we obtain a band-like density of states displayed in Fig. 4.3. With the fairly small hopping element of $0.119\,e\mathrm{V}$ (see Tab. 2.1) for this finite system one can still resolve the peaks due to single electronic resonances, especially near the van-Hove-like pile up of states near the band edges. All states are delocalized over the entire system. The inset displays the elastic transmission, showing that the states have a high transmission of $T_{\mathrm{el}} \sim 0.5$, with the states at the upper band edge showing the highest values. Both density of states and elastic transmission show a strong asymmetry, which is a direct consequence of the non-local electron-vibration coupling in this model.

To further elucidate this connection we take a closer look at the upper and lower band edge of the density of states (see Fig. 4.4). Without electron-vibration coupling (solid curve) we see the electronic resonances of equal height, positioned at the energies corresponding to the 'Bloch'-like states of this finite size tight-binding chain. If we include only local electron-vibration coupling (dashed line), vibrational satellite states appear, and the spectral weight of the original electronic resonances decreases, consistent with the spectral sum rule. Note that the displayed vibration satellites are not satellites of the displayed electronic states, but emerge from other states at higher and lower energies. Indeed the difference in peak positions is not equal to $\hbar\omega_0$. Inclusion of the non-local coupling λ_1 shifts the original electronic resonance positions (dashed-dotted line). In the present example, with positive sign of λ_1, the resonances are shifted to the 'outside', corresponding to an effective increase in bandwidth; for the opposite sign of λ_1 the resonances shift to the 'inside'. Furthermore, a distinct asymmetry of the resonances is observed, i.e. the upper band edge states have a larger peak height than the lower band edge states. This asymmetry in the density of states comes with a corresponding asymmetry in the elastic transmission, see Fig. 4.3 for the overall view.

As shown in Fig. 4.5 the coupling to vibrations strongly increases the zero-bias conductance at low temperatures, whereas at high temperatures the conductance slightly

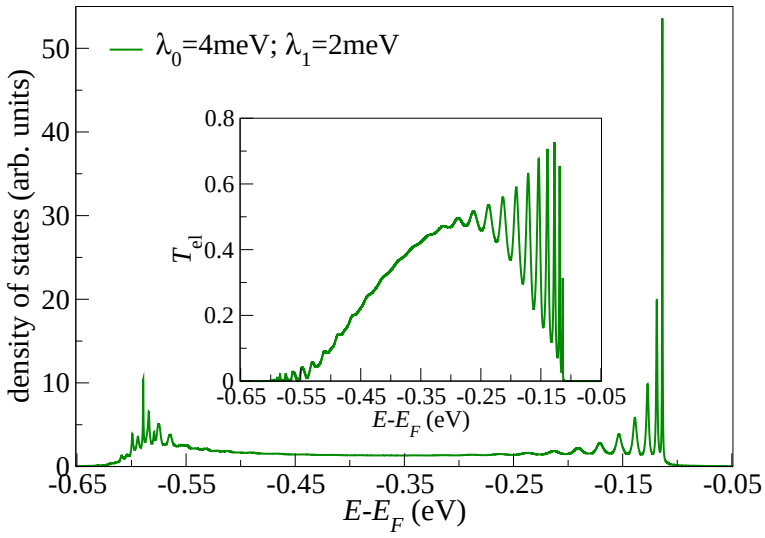

Figure 4.3: Density of states and transmission of Poly-(GC) with 26 base pairs and the following parameters: base pair onsite energy $\epsilon_G = -0.35\,eV$, Fermi energy $E_F = 0\,eV$, vibrational energy $\hbar\omega_0 = 0.01\,eV$, cutoff $\hbar\omega_c = 0.03\,eV$, linewidth $\Gamma = 0.1\,eV$ and room temperature $k_BT = 0.025\,eV$. The strong asymmetry of the curves with respect to the band center is a consequence of the non-local electron-vibration coupling λ_1.

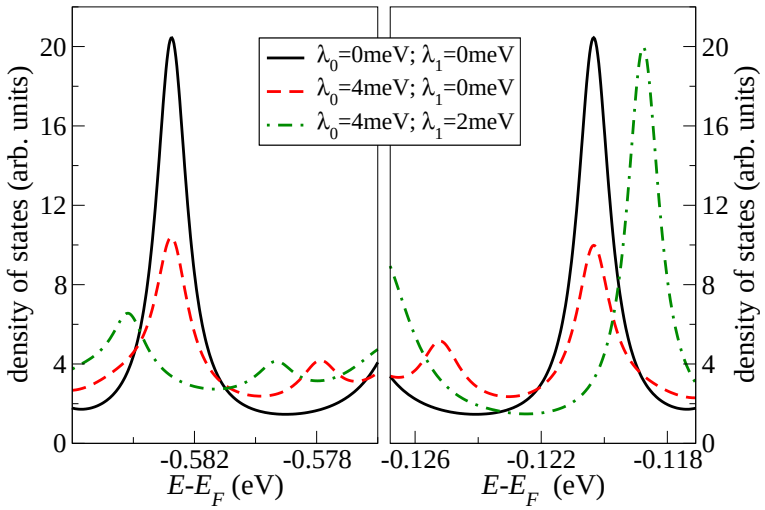

Figure 4.4: Density of states of Poly-(GC) with 26 base pairs and parameters as in Fig. 4.3. The solid line shows the purely electronic resonances. Inclusion of only a local electron-vibration coupling λ_0 reduces the weight at the original electronic resonance in favor of 'vibrational satellites' (dashed line). The addition of a non-local electron-vibration coupling λ_1 (dash-dotted line) introduces shifts of the resonance peaks to the 'outside' (changing the effective band width) as well as a strong asymmetry in the height of the resonances.

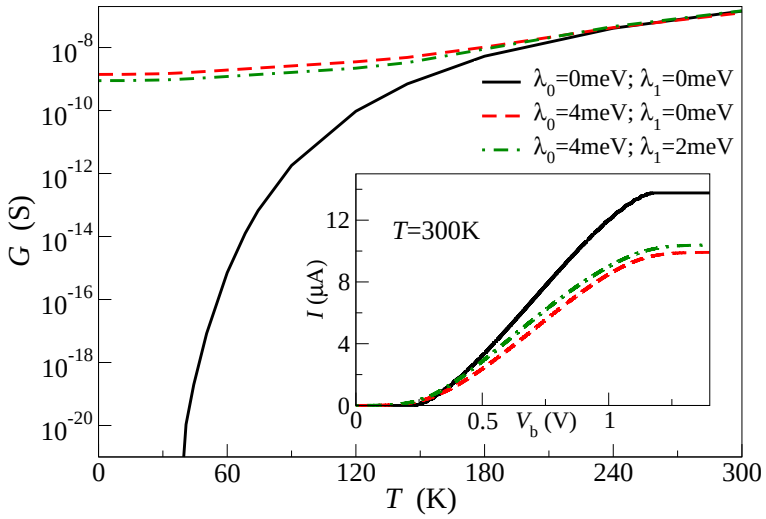

Figure 4.5: Zero-bias conductance and I-V-characteristics for Poly-(GC) with 26 base pairs and parameters as in Fig. 4.3. The inclusion of vibrations increases the zero-bias conductance at low temperatures ($k_{\mathrm{B}}T$ roughly below $\hbar\omega_0$) by several orders of magnitude. At room temperature, however, the zero bias conductance is slightly reduced. Inset: the I-V-characteristics shows a 'semiconducting' behavior at room temperature. The non-local electron-vibration coupling λ_1 increases both the non-linear conductance in the gap and around the threshold, leading to a slightly enhanced current.

decreases (dashed and dash-dotted line). This effect has been observed before, e.g. in Ref. [95]. At low temperatures, the conductance is increased since the density of states at the Fermi energy is effectively enhanced due to (broadened) vibrational 'satellite' resonances. The transport remains 'elastic', i.e. electrons enter and leave the DNA at the same energy (first contribution to the current Eq. 4.12). At sufficiently high temperatures, however, the back scattering of electrons due to vibrations reduces the conductance in comparison to situation without electron-vibration coupling (solid line).

The inset of Fig. 4.5 shows a typical I-V-characteristic for the system. A quasi-semiconducting behavior is observed, where the size of the conductance gap is determined by the energetic distance of the Fermi energy to the (closest) band edge. After crossing this threshold, the current increases roughly linear with the voltage until at larger bias it saturates when the right chemical potential drops below the lower transmission band edge. Small step-like wiggles due to the 'discrete' electronic states are visible at low temperature (not shown), but are smeared out at room temperature. The current is dominated by the elastic transmission, as expected for a homogeneous system.

The non-local coupling has a quantitative effect on the nature of the I-V-curve. The zero bias conductance as well as the non-linear conductance around the threshold are increased by close to a factor 1.2. This increase is directly related to the enhancement of the density of states and elastic transmission around the upper band edge (see Figs. 4.3 and 4.4).

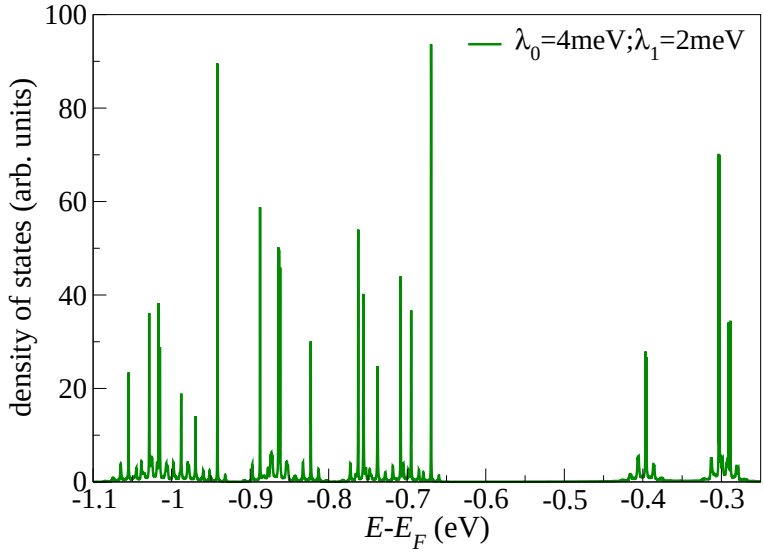

Figure 4.6: Density of states of an inhomogeneous DNA with sequence (5'-CAT TAA TGC TAT GCA GAA AAT CTT AG-3'). We chose the following parameters: GC onsite energy $\epsilon_G = -0.35\,eV$, AT onsite energy $\epsilon_A = -0.86\,eV$, Fermi energy $E_F = 0\,eV$, vibration energy $\hbar\omega_0 = 0.01\,eV$, cutoff $\hbar\omega_c = 0.03\,eV$, linewidth $\Gamma = 0.1\,eV$ and room temperature $k_BT = 0.025\,eV$. The density of states is fragmented into 'bunches' of strongly localized states with very low elastic transmission.

4.3.2. Inhomogeneous DNA

Inhomogeneous DNA sequences show a transport behavior which differs significantly from that of the homogeneous Poly-(GC) sequence. As a specific example, we analyze the sequence 5'-CAT TAA TGC TAT GCA GAA AAT CTT AG-3' (plus complementary strand), which has been investigated experimentally by Porath et al. [65]. The density of states is displayed in Fig. 4.6. Rather than traces of bands it now shows discrete 'bunches' of states due to the disorder in the sequence. All states are strongly localized, extending over at most a few base pairs [108]. The right-most (largest energy) bunch of states is due to the GC base pairs. Two of these GC pairs are the only base pairs that are directly coupled to the metallic electrodes. Note that the equilibrium Fermi level is set at $E_F = 0\,eV$, roughly $0.35\,eV$ above these states. The first states with mostly AT character are located around $-0.7\,eV$.

As to be expected the elastic transmission through these localized states is extremely low. The largest contribution to the elastic transmission stems from the AT-like states around an energy $\epsilon_A = -0.86\,eV$ (note that the considered sequence is AT rich). But even these states have an elastic transmission of less than 10^{-14} for the parameters we use. Consequently, the 'elastic' quasi-ballistic transmission of electrons is completely negligible for the considered sequence.

In spite of the localization of the electron states, a rather significant current can be transmitted, as displayed in Fig. 4.7. It is due to the inelastic contributions to transport, where electrons dissipate (or absorb) energy during their motion through the DNA. Roughly speaking, the transported electrons excite the vibrations which in turn either

dissipate their energy to the environment or 'promote' other electrons, thus increasing their probability to hop to neighboring but energetically distant base pairs. This inelastic transmission strongly depends on the specific states (in contrast to the band-like transmission for the homogeneous sequence). As a consequence, the inelastic transmission of different states can differ by several orders of magnitude. Together with the bunched density of states this leads to the step-like behavior for the current displayed in Fig. 4.7. The first step centered around $V_b \sim 0.7\,\mathrm{V}$ roughly corresponds to states with GC character, whereas the second step at 1.4 V corresponds to hybridized states with mixed AT-GC character. Here, the GC states display a larger inelastic transmission as can be seen from the large non-linear conductance peak around $V_b \sim 0.6 - 0.7\,\mathrm{V}$ (see inset of Fig. 4.7).

The non-local electron-vibration coupling λ_1 for this sequence leads to qualitative change of the I-V-characteristics, depending on the details of the nature of the states and therefore explicitly on the DNA sequence. The current on the lowest bias plateau is increased relative to the case with only local electron-vibration coupling, although the GC states do barely shift towards the Fermi energy. However, the inelastic transmission of the states is slightly increased (see inset), leading to an increased current on the first plateau (dashed line).

In contrast, the conductance due to states with mixed AT-GC nature is much reduced (almost by a factor of two, see middle peak in the inset of Fig. 4.7) which leads to a smaller increase of the current for the middle step. Obviously, the transmission of these mixed states is reduced by the 'vibration assisted electron hopping'. On the other hand, the last step at $\sim 2V$ is almost unaffected.

While the changes of the I-V-characteristics due to non-local electron-vibration coupling are relatively small for the present sequence and model parameters, the observed sensitivity of the inelastic transmission suggests that other sequences could display much larger effects. Furthermore, quantum chemistry calculations [50] suggest that the local and non-local electron-vibration couplings can be of the order of $\sim 10\,\mathrm{meV}$, i.e. larger than what we considered here. Inhomogeneities in the electron-vibration coupling, not covered in the present calculation, might have a further impact.

The DNA sequence we considered was investigated in transport experiments, and we should compare the experimental and theoretical results. As some important factors are still not well determined, a quantitative comparison is not feasible. However, we observe both in experiment and theory roughly a 'semiconducting' I-V-characteristics with (sometimes) steplike features. The size of the currents is roughly comparable, of the order of $\sim 80\,\mathrm{nA}$ at a bias of $V_b = 1\,\mathrm{V}$. As the choice of the position of the Fermi energy defines the size of the 'semiconducting' gap, this gap could be adjusted to fit the experiment. On the other hand, the value of the current for this sequence (with parameters derived from quantum chemistry calculations) can not be simply scaled by changing a single 'free' parameter like the electrode-DNA coupling Γ.

For the case of the homogeneous sequence, the current at a given bias (say, at $V_b = 1\,\mathrm{V}$) grows monotonically with increasing Γ (as long Γ is smaller than the hopping amplitude t_{ij}), as is expected from quasi-ballistic Landauer-type transport. In contrast, for the inhomogeneous sequence, the current is a *non-monotonic* function of Γ, see Fig. 4.8. In particular, the current at the first plateau (at $V_b = 1\mathrm{V}$) initially grows as we decrease Γ from the value used in the above figures ($\Gamma = 0.1\,e\mathrm{V}$), up to a point at which the

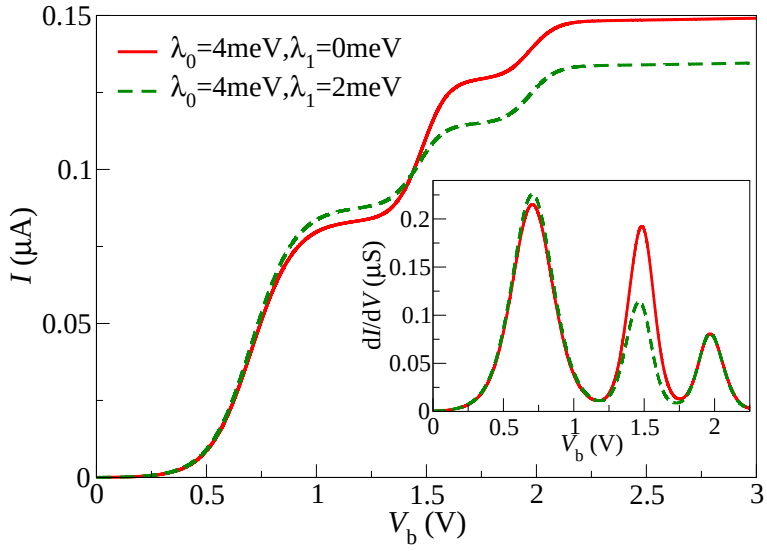

Figure 4.7: I-V-characteristics and differential conductance for an inhomogeneous DNA with sequence (5'-CAT TAA TGC TAT GCA GAA AAT CTT AG-3'). Parameters are the same as in Fig. 4.6. The inclusion of a non-local electron-vibration coupling λ_1 leads to changes in the conductance, depending on the nature of the relevant state.

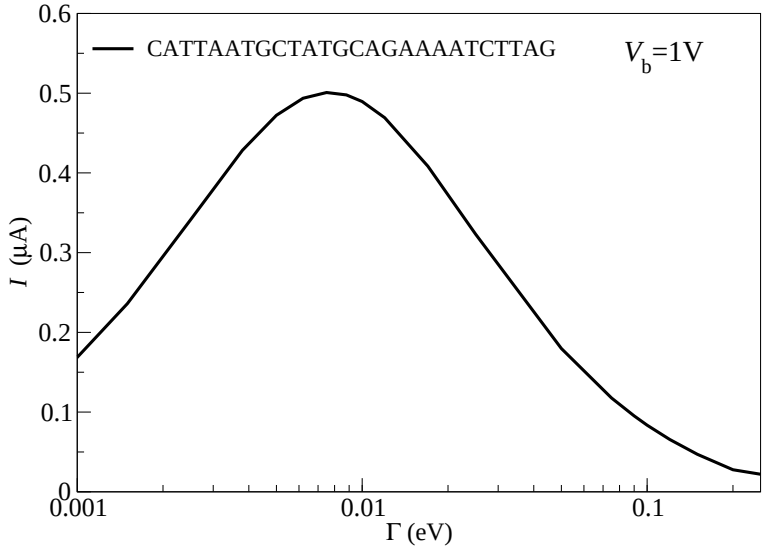

Figure 4.8: Current at a bias of $V_b = 1$V as a function of electrode-DNA coupling Γ for the inhomogeneous DNA with sequence (5'-CAT TAA TGC TAT GCA GAA AAT CTT AG-3'). Other parameters are the same as in Fig. 4.6. The current is a non-monotonous function of Γ and peaks around a value Γ_{max} where the imaginary part of the vibration self energy $\Sigma_{\rm vib}$ is of the same size as Γ.

imaginary part of the vibration self energy $\Sigma_{\rm vib}$ is of the same size as Γ. This happens around $\Gamma_{max} \sim 0.01\,e$V. The current at Γ_{max} is of order of $\sim 500\,$nA. If Γ is decreased further, the current drops rapidly from the maximal value.[1] On the other hand, if Γ is increased above the value $\Gamma = 0.1\,e$V, the current also drops initially, before at very large Γ quasi-ballistic transport becomes dominant and the current increases again (not shown in the figure).

Summarizing these results, we conclude that for the given model parameters, i.e. for values of Γ in the large range $1-200\,$meV, likely to be realistic for present-days transport experiments in DNA, the current at the first plateau lies in the range of $50-500\,$nA.

4.4. Summary

To summarize, in this chapter we have presented a technique that allows the computation of electron transport through short sequences of DNA, including local and non-local coupling to vibrations and a dissipative environment. Using an equation-of-motion approach we identify elastic and inelastic contributions to the current. For homogeneous DNA sequences, the transport is dominated by elastic quasi-ballistic contributions through a band-like density of states (Fig. 4.3,4.4), which display an asymmetry due to the non-local electron-vibration coupling. The coupling to vibrations strongly enhances the zero-bias conductance at low temperatures. The current at finite bias above the 'semiconducting' gap, however, is only quantitatively modified by the non-local electron-vibration coupling (Fig. 4.5). For inhomogeneous DNA sequences, the transport is almost entirely due to inelastic processes, the effectiveness of which is strongly sequence dependent (Fig. 4.6). For the considered example sequence the non-local electron-vibration coupling qualitatively modifies the I-V-characteristics (Fig. 4.7). We also point out that the current through inhomogeneous DNA sequences depends non-monotonically on the electrode-DNA coupling Γ (Fig. 4.8).

[1] Note that our assumption $\Gamma >> \lambda_0$ breaks down at some point. Nevertheless, the decrease of the current at very small Γ makes physical sense.

5. Incoherent polaron hopping: Fermi's Golden Rule

5.1. Definition of the Problem

In the previous chapter we have studied the influence of vibrations on the electronic transport in DNA when some coherence of transport is retained and we do not have a self-trapping of the electrons due to interaction with the vibrations. With this transport mechanism extremely high current as measured in the groups of Porath or Tao [64,65] are explainable. On the other hand, many experiments and *ab initio* calculations indicate that small polarons are formed in DNA, as argued in Chapter 2. The actual size of the polaron is still controversially discussed, but it is at most a few bases, maybe even restricted to a single base. In this limit, the electrons become localized and transport is a sequence of incoherent hopping processes. The interaction with vibrations is on one hand the source of localization, but on the other hand it provides the necessary energy to overcome the barriers posed by the localization.

We model the electronic properties of the DNA just as explained in the previous Sections 4.1 and 2.1. In contrast to the previous chapter, where we considered vibrations extended over the whole molecule, we now consider local vibrations to allow the formation of small polarons. We therefore consider that every base pair i can vibrate independently from the other base pairs, i. e. every site is connected to independent oscillators. The vibrational frequency $\omega_{\alpha i}$ and the strength of the local coupling to the charge density (here we only consider diagonal electron-vibration coupling terms) $\lambda_{\alpha i}$ can in general depend on the vibrational mode α and on the base pair i that is vibrating. Throughout this chapter we will restrict ourselves to one vibrational mode per base pair.

We will evaluate the rates for polaron hopping in the spirit of what is known as the $P(E)$-theory for electron tunneling in a dissipative environment modeled by a bath of oscillators [117–119]. Here, instead of a bath of oscillators we have for each DNA base pair one localized vibrational mode which, however, is broadened due to the coupling to a dissipative environment.

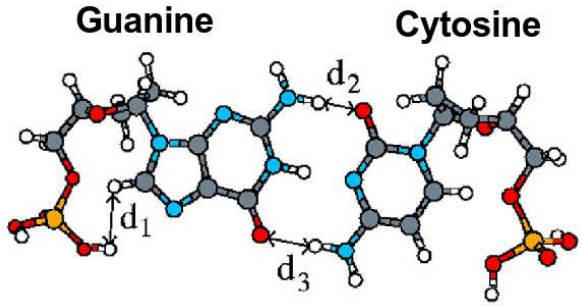

Figure 5.1: Ball-stick representation of a guanine-cytosine base pair. The labeled bonds d_1, d_2 and d_3 are distorted the most, when the base pair is charged. The charge is mainly localized on the guanine base (not shown). The picture is taken from [47].

5.2. Model and technique

5.2.1. Hamiltonian

To describe the situation discussed above, we consider the Hamiltonian $H = H_{\mathrm{el}} + H_{\mathrm{L}} + H_{\mathrm{R}} + H_{\mathrm{T,L}} + H_{\mathrm{T,R}} + H_{\mathrm{vib}} + H_{\mathrm{el-vib}} + H_{\mathrm{bath}}$, with

$$\begin{aligned} H_{\mathrm{el}} &= \sum_i \epsilon_i a_i^\dagger a_i - \sum_{<ij>} t_{ij} a_i^\dagger a_j \\ H_{\mathrm{T,L}} + H_{\mathrm{T,R}} &= \sum_{\nu,r,i} \left[t^r c_{\nu r}^\dagger a_i + t^{r*} a_i^\dagger c_{\nu r} \right] \\ H_{\mathrm{vib}} &= \sum_i \hbar\omega_i \left(B_i^\dagger B_i + \frac{1}{2} \right) \\ H_{\mathrm{el-vib}} &= \sum_i \lambda_i \, a_i^\dagger a_i \left(B_i + B_i^\dagger \right) \ . \end{aligned} \tag{5.1}$$

The first term H_{el} describes the electrons in the DNA chain just as introduced in the previous chapter, with onsite energies and hopping integrals for next-neighbor hopping taken from *ab initio* calculations. Also, the terms $H_{\mathrm{L,R}}$(not written explicitly, see Chap. 4) with $r = \mathrm{L}, \mathrm{R}$ refer to the left and right electrodes, with a flat density of states ρ_e (wide band limit). The details of the coupling between the DNA and the electrodes are not the focus of this work. For our purposes it is sufficiently described by $H_{\mathrm{T,L}} + H_{\mathrm{T,R}}$ with tunneling amplitudes assumed to be independent of the base pair i and the quantum numbers of the electrode states ν. The coupling strength is then characterized by the parameter $\Gamma^{\mathrm{L,R}} \propto \rho_e |t^{\mathrm{L,R}}|^2$.

The vibrational degrees of freedom of base i are described by H_{vib}, with bosonic operators $B_i^\dagger$ and B_i for the mode with frequency ω_i. The coupling of the electrons on the DNA to the vibrational modes is described by $H_{\mathrm{el-vib}}$, where λ_i is the local electron-vibration coupling strength. Here we only consider the so-called stretch mode with frequency $\hbar\omega_i = 16\,\mathrm{meV}$ for a GC base pair and $\hbar\omega_i = 11\,\mathrm{meV}$ for an AT base pair, which couple strongly to the electrons, as shown by Starikov [50]. Furthermore, Alexandre *et al.*

showed that in the formation of a polaron by placing an additional charge on a guanine-cytosine base pair, the bonds with the strongest distortion, where the hydrogen bonds (labeled d_2 and d_3 in Fig. 5.1) between G and C [47]. The stretch mode is exactly the vibrational mode which changes this bond distance (see also Fig. 4.2).

The coupling strengths are chosen in such a way that the reorganization energy or polaron shifts fit the values extracted from experiments and listed by Olofsson *et al*, $\Delta_{\mathrm{A}} = 0.18\,\mathrm{eV}$ and $\Delta_{\mathrm{G}} = 0.47\,\mathrm{eV}$ [46]. These values probably underestimate the effect of the solvent on the reorganization energy, but give an idea of the magnitude of energies involved in the polaron formation.

The vibration of each base pair i is coupled to the local environment, $H_{i,\mathrm{bath}}$, the microscopic details of which do not matter. Just as explained in the previous section, this changes the vibrations' spectra from discrete modes ω_i to continuous spectra, different for both types of base pairs,

$$\begin{aligned} D_i(\omega) =& -i \int dt e^{i\omega t}\theta(t) \left\langle \left\{ B_i^\dagger(t) + B_i(t), B_i^\dagger + B_i \right\} \right\rangle \\ =& \frac{1}{\pi} \left(\frac{\eta_i(\omega)}{(\omega-\omega_i)^2 + \eta_i(\omega)^2} - \frac{\eta_i(\omega)}{(\omega+\omega_i)^2 + \eta_i(\omega)^2} \right) . \end{aligned} \tag{5.2}$$

with frequency dependent broadening $\eta_i(\omega)$. [115] The actual form of $\eta_i(\omega)$ depends on the properties of the bath. A reasonable choice which assures also convergence at low and high frequencies is $\eta_i(\omega) = \eta_0 \frac{\omega^3}{\omega_i^3}\,\theta(\omega_c - \omega)$ with $\eta_0 = 0.5\,\mathrm{meV}$ and a cutoff of the order of $\hbar\omega_c = 0.045\,\mathrm{meV}$. The coupling to the bath introduces the dissipation, which is crucial for the stability of the DNA molecule in current carrying situations where substantial amount of heat can be produced in the DNA.

5.2.2. Lang-Firsov Transformation

In order to describe the system with strong electron-vibration coupling we first apply the so-called polaron or Lang-Firsov unitary transformation just as explained previously, but now considering the local nature of the vibrations,

$$\tilde{H} = e^S H e^{-S} .$$

The generator of the Transformation is given by

$$S = -\sum_i \frac{\lambda_i}{\hbar\omega_i}\, a_i^\dagger a_i \left[B_i - B_i^\dagger \right] .$$

We introduce transformed electron and vibrational operators,

$$\begin{aligned} \tilde{a}_i &= a_i \chi_i \\ \tilde{B}_i &= B_i - \frac{\lambda_i}{\hbar\omega_i}\, a_i^\dagger a_i \end{aligned}$$

and polaron operators

$$\chi_i = \exp\left[\frac{\lambda_i}{\hbar\omega_i} \left(B_i - B_i^\dagger \right) \right] .$$

Operators χ_i with different indices i act on different vibrational states, therefore they commute at all times. In terms of these quantities the Hamiltonian reads

$$\tilde{H} = \tilde{H}_0 + \tilde{H}' \tag{5.3}$$

$$\tilde{H}_0 = \sum_i (\epsilon_i - \Delta_i) a_i^\dagger a_i + \sum_i \hbar\omega_i \left(B_i^\dagger B_i + \frac{1}{2} \right) + H_\mathrm{L} + H_\mathrm{R} \tag{5.4}$$

$$\tilde{H}' = -\sum_{<ij>} t_{ij}\, a_i^\dagger \chi_i^\dagger a_j \chi_j \tag{5.5}$$

$$+ \sum_{\nu,r,i} \left[t^r c_{\nu r}^\dagger a_i \chi_i + t^{r*} a_i^\dagger \chi_i^\dagger c_{\nu r} \right] \tag{5.6}$$

$$\Delta_i = \int d\omega D_i(\omega) \frac{\lambda_i^2}{\hbar\omega} \,. \tag{5.7}$$

In contrast to the Hamiltonian $\tilde{H}$ (Eq. 4.3) of the previous chapter, here no effective electron–electron interactions $\tilde{H}_\mathrm{ee}$ arise. The reason for their occurrence was, that we considered a vibration extended over the whole molecule, so electrons could 'interact' with each other via the vibration. The local nature of the vibrations considered here does not lead to such an interaction. From the definition of the polaron shift (Eq. 5.7) we can calculate the electron-vibration coupling strengths assuming polaron shifts and vibrational frequencies listed above

$$\lambda_\mathrm{G} = 0.086\,\mathrm{eV} \tag{5.8}$$

$$\lambda_\mathrm{A} = 0.045\,\mathrm{eV} \,. \tag{5.9}$$

A perturbative treatment of the Hamiltonian H would not make sense, due to the strong electron-vibration coupling strengths, but after the Lang-Firsov transformation we can proceed studying the effect of strong electron-vibration coupling in perturbation theory in $\tilde{H}'$. The small parameters are t_{ij}/Δ_i and t^r/Δ_i, which allows truncating the perturbation expansion at lowest non-vanishing order in these parameters. From here on we will use the shifted onsite energy $\tilde{\epsilon}_i = \epsilon_i - \Delta_i$ in all expressions.

Rate equation and current

As remarked in Sec. 3.1, the small-polaron theory covers two limits of transport. At sufficiently low temperatures polarons form bands with bandwidth

$$W \simeq W_0 \exp\left[-\left(\frac{\lambda}{\hbar\omega} \right)^2 \coth\left(\frac{\hbar\omega}{2k_B T} \right) \right] \,,$$

where W_0 denotes the electronic bandwidth without vibrations. [83] At high temperatures the bandwidth W decreases exponentially as the increasing number of multi-phonon processes destroy the coherence, and the band picture ceases to be valid. Transport is then accomplished by a sequence of incoherent polaron hops. A rough estimate for

the cross-over temperature is $k_B T \simeq \hbar\omega \left[4 \ln \left(\lambda/\hbar\omega\right)\right]^{-1}$. [80] For the electron-vibration coupling strengths of interest in the present problem, room temperature is already well above this limit.

To describe room-temperature transport it is therefore sufficient to consider a rate equation for the diagonal elements of the single-particle density matrix, i.e. the occupation numbers of the sites $\rho_l(t) = \left\langle a_l^\dagger(t) a_l(t) \right\rangle$. These occupation numbers evolve according to a master equation with transition rates which we obtain in an expansion in $\tilde{H}'$ from Fermi's Golden Rule. If we consider the rate for a hopping process from base pair (site) l to m, we have to take into account that also the vibrational states may change. If the initial and final states of the coupled system are denoted by I and F, the rates are

$$\mathcal{W}_{lm} \quad = \tfrac{2\pi}{\hbar} |t_{lm}|^2 \left| \left\langle F \left| a_m^\dagger \chi_m^\dagger a_l \chi_l \right| I \right\rangle \right|^2 \delta(E_I - E_F).$$

In the following the vibrational states are not explicitly considered. Therefore, we trace out the vibrational degrees of freedom X_l by summing over all initial vibrational states weighted by the appropriate thermal probability and over all final states. Thus the transition rate from a state with site l initially occupied and site m initially empty becomes

$$\begin{aligned} \mathcal{W}_{lm} =& \frac{2\pi}{\hbar} |t_{lm}|^2 \sum_{X_l, X_l'} \varrho_l(X_l) \left| \left\langle X_l' \left| \chi_l \right| X_l \right\rangle \right|^2 \\ & \times \sum_{X_m, X_m'} \varrho_m(X_m) \left| \left\langle X_m' \left| \chi_m^\dagger \right| X_m \right\rangle \right|^2 \\ & \times \delta(\tilde{\epsilon}_l - \tilde{\epsilon}_m + E_{X_l} - E_{X_l'} + E_{X_m} - E_{X_m'}) \,, \end{aligned}$$

where $\varrho_l(X_l)$ is the probability of finding vibration l in state X_l. Rewriting the energy conserving delta-function by its Fourier transform we obtain

$$\mathcal{W}_{lm} = \frac{1}{\hbar^2} |t_{lm}|^2 \int dt \, e^{\frac{i}{\hbar}(\tilde{\epsilon}_l - \tilde{\epsilon}_m)t} P_l(t) P_m(t) \,, \tag{5.10}$$

where

$$\begin{aligned} P_l(t) =& \sum_{X_l} \varrho_l(X_l) \left\langle X_l \left| \chi_l^\dagger(t) \chi_l(0) \right| X_l \right\rangle \qquad (5.11) \\ =& \mathcal{L}_l \exp \left[\int d\omega D_l(\omega) \left(\frac{\lambda_l}{\hbar\omega} \right)^2 \frac{\cos\left(\omega \left[t + i\hbar\beta/2\right]\right)}{\sinh\left(\hbar\omega\beta/2\right)} \right] \,, \end{aligned}$$

with

$$\mathcal{L}_l = \exp \left\{ - \int d\omega D_l(\omega) \left(\frac{\lambda_l}{\hbar\omega} \right)^2 \coth\left(\hbar\omega\beta/2\right) \right\} \,. \tag{5.12}$$

The function $P_l(t)$ is known from the '$P(E)$ theory', which describes tunneling in a dissipative electromagnetic environment, modeled by an infinite set of oscillators. Here,

instead of such a bath we have broadened local vibrational modes of two DNA base pairs involved in the hopping process. Figure 5.2 shows the $P(E)$ function and the combinations of it appearing in the rates introduced above and below. The parameters used in the calculation were introduced in the previous section (Sec. 5.2). The functions in Fig. 5.2 give the probability for a hopping or tunneling process for an energy difference E between initial and final state. The general shape is a Gaussian with maximum at $-\Delta$ and height about $\propto \Delta$.

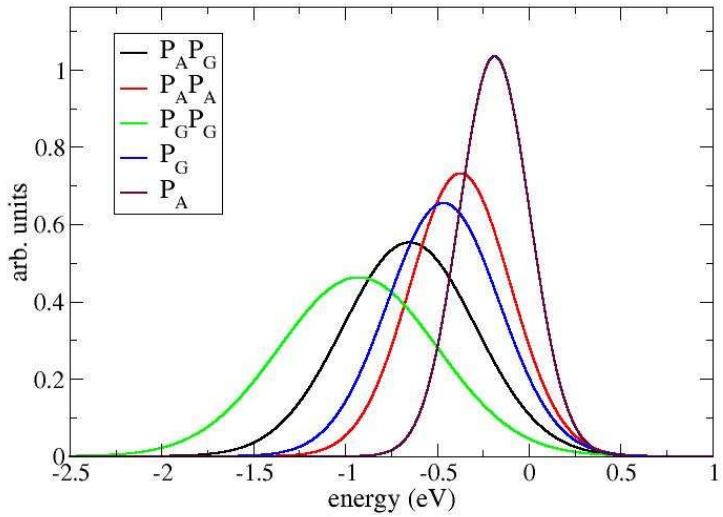

Figure 5.2: Various combinations of P(E) functions, where the index indicates the two types of bases, G (guanine) and A (adenine). The combination $P_{\mathrm{A}}P_{\mathrm{G}}$ stands for the convolution $\int dE' P_{\mathrm{A}}(E-E')P_{\mathrm{G}}(E')$ and similar for the other combinations, which are relevant in the hopping transitions from e. g. an A base to a G base. The used parameters were introduced in Sec. 5.2, in particular, the polaron shifts are $\Delta_{\mathrm{A}} = 0.18\,\mathrm{eV}$ and $\Delta_{\mathrm{G}} = 0.47\,\mathrm{eV}$.

The calculation for the tunneling transition between the left (L) and right (R) electrodes and the first or last site of the DNA chain $l = 1$ or $l = N$ proceeds similarly, except that one has to trace also over the electrodes' electronic states, while we have to consider only the local vibration of the one site involved. Hence we have for the rates on the left and right junction between electrodes and DNA chain

$$W_{-}^{\mathrm{L}} = \Gamma^{\mathrm{L}} \int \frac{dE}{2\pi\hbar} (1 - f_{\mathrm{L}}(E)) P_1(\tilde{\epsilon}_1 - E) \tag{5.13}$$

$$W_{+}^{\mathrm{L}} = \Gamma^{\mathrm{L}} \int \frac{dE}{2\pi\hbar} f_{\mathrm{L}}(E) P_1(E - \tilde{\epsilon}_1) \ , \tag{5.14}$$

where $\Gamma^{\mathrm{L/R}} = 2\pi |t^{\mathrm{L/R}}|^2 \rho_e$, $f_{\mathrm{L/R}}(E)$ is the Fermi function in left/right lead, and $P_{1/N}(E)$ is the Fourier transform of $P_{1/N}(t)$.

The master equation for sites in the DNA chain thus reads

$$\frac{d}{dt}\rho_l = \sum_m \Big[-\rho_l\,(1-\rho_m)\,\mathcal{W}_{lm} + (1-\rho_l)\,\rho_m \mathcal{W}_{ml}\Big], \tag{5.15}$$

where the sum over m is restricted to nearest neighbors of l [1]. For the base pair at the left end of the chain we get

$$\begin{aligned}\frac{d}{dt}\rho_1 = &-\rho_1 W_-^{\mathrm{L}} + (1-\rho_1)\,W_+^{\mathrm{L}} \\ &+ \Big[-\rho_1\,(1-\rho_2)\,\mathcal{W}_{12} + (1-\rho_1)\,\rho_2 \mathcal{W}_{21}\Big]\,,\end{aligned} \tag{5.16}$$

and similar for the right interface.

As is obvious from Eqs. 5.15 and 5.16 the single-particle charge densities are considered to be uncorrelated. This, of course, is only true approximatively, since the occupations of different sites are effectively linked by the hopping rates. As we only consider next neighbor hopping, the most important charge–charge correlation is the one between neighboring sites. As we will explain in the next chapter, the correlations can introduce another energy scale depending on the considered sequence. For now we will neglect these correlations as the most important features arise already without them.

We are interested in the steady state, $d\rho_l/dt = 0$, which develops for a constant applied bias. After solving the resulting self-consistent equations iteratively we can calculate the non-equilibrium current through the left lead,

$$I_{\mathrm{L}} = e\Big[-\rho_1 W_-^{\mathrm{L}} + (1-\rho_1)\,W_+^{\mathrm{L}}\Big] \tag{5.17}$$

or for the right lead, which is the same since the current is conserved, $I_{\mathrm{L}} = -I_{\mathrm{R}}$.

Discussion of the hopping rates

For the hopping rates Eq. (5.10) the situation differs from the usual $P(E)$ theory: instead of one infinite vibrational bath each base pair (m and l) has its own vibration degree of freedom and we get products $P_m(t)P_l(t)$, which become convolutions in energy space. The rates still satisfy detailed balance

$$\mathcal{W}_{lm} = \mathcal{W}_{ml} \exp\left[\frac{\tilde{\epsilon}_l - \tilde{\epsilon}_m}{k_{\mathrm{B}}T}\right]\,, \tag{5.18}$$

where $\tilde{\epsilon}_m$ and $\tilde{\epsilon}_l$ are the onsite energies of base pairs m and l, respectively.

For large times, $P_l(t)$ approaches a constant, $\lim\limits_{t\to\infty} P_l(t) = \mathcal{L}_l$. Therefore it can be separated into two terms, one decaying in time and one constant:

$$P_l(t) = \tilde{P}_l(t) + \mathcal{L}_l\,. \tag{5.19}$$

[1] Including also hopping to more distant bases, one could account for the superexchange mechanism, dominant for guanine bases closer than three base pairs. This is, however, not important for the sequences considered in this work, so it was not included in the numerical evaluation.

Accordingly we can write

$$P_l(t)P_m(t) = \tilde{P}_l(t)\tilde{P}_m(t) + \mathcal{L}_m\tilde{P}_l(t) + \mathcal{L}_l\tilde{P}_m(t) + \mathcal{L}_m\mathcal{L}_l\,.$$

The product $\tilde{P}_l(t)\tilde{P}_m(t)$ describe transitions, where the number of vibrations changes on both sites, the next two terms describe changes in one of the two sites only, while the last term describes transitions without changes in the vibration state. When performing the time integration in Eq. (5.10), this last term leads to a divergence when the two site energies are degenerate

$$\frac{1}{2\pi\hbar}\int dt\, e^{\frac{i}{\hbar}(\tilde{\epsilon}_l-\tilde{\epsilon}_m)t}\mathcal{L}_m\mathcal{L}_l = \mathcal{L}_l\mathcal{L}_m\delta\left(\tilde{\epsilon}_l-\tilde{\epsilon}_m\right)\,, \tag{5.20}$$

since in this situation the phenomenon of resonant tunneling occurs. In this situation the perturbation theory limited to second order is not sufficient. Rather, one should sum up in a 'ladder'-approximation an infinite series of such terms, leading to a result with finite rates. [76, 120, 121] In the next chapter we will study the same system in more detail using a diagrammatic approach and, as we will show, this 'ladder'-approximation will give rise to the correlation effects mentioned in the previous section.

Alternatively, we can phenomenologically regularize the divergence of Eq. (5.20) by formally introducing an imaginary part to the level energies $\tilde{\epsilon}_l$. This is motivated by the fact that they acquire a finite width due to the interaction with the vibrations or leads. In this way the hopping rates become finite. We further note that the contribution of the vibration-free transitions (the constant term of Eq. 5.20) is multiplied by the factor $\mathcal{L}_l\mathcal{L}_m$. In our case, this factor is exponentially small. This corresponds to the fact that we consider the limit where polaron hopping by far dominates polaron band transport. We therefore can ignore the terms $\propto \mathcal{L}_m\mathcal{L}_l$ in our analysis all together, i.e. we subtract them in Eq. (5.10). The regularized hopping rates are therefore

$$\mathcal{W}_{lm} = \frac{|t_{l,m}|^2}{\hbar^2}\int dt\, e^{\frac{i}{\hbar}(\tilde{\epsilon}_l-\tilde{\epsilon}_m)t}\left[P_l(t)P_m(t) - \mathcal{L}_l\mathcal{L}_m\right]\,. \tag{5.21}$$

To give a feeling for the relationship between current in a system and the occupation numbers, let us consider two neighboring sites (1 and 2) of a system with a current I and a given occupation of of site 1. The rate for a hopping process from site 1 to 2 is $\mathcal{W}_{12}$ and the backward hopping rate is $\mathcal{W}_{21} = \mathcal{W}_{12}\exp\left[-\beta\Delta E\right]$, where ΔE is the difference between the onsite energies of site 1 and 2. The occupation of site 2 is then given by

$$\rho_2 = \frac{\rho_1 + \frac{I}{e\mathcal{W}_{12}}}{\rho_1(1-e^{-\beta\Delta E}) + e^{-\beta\Delta E}}\,.$$

In Figure 5.3 the occupation of site 2 is shown as a function of the onsite energy difference for four different values of $I/e\mathcal{W}_{12}$, where the occupation of site 1 is assumed to be $\rho_1 = 0.9$. Clearly, the occupation of site 2 is always lower if site 2 has higher energy (negative ΔE). If site 2 has lower energy, the occupation strongly depends on the current. For low current the occupation can be higher than on site 1. The current, of course, will be determined by the applied bias and the structure of the whole system.

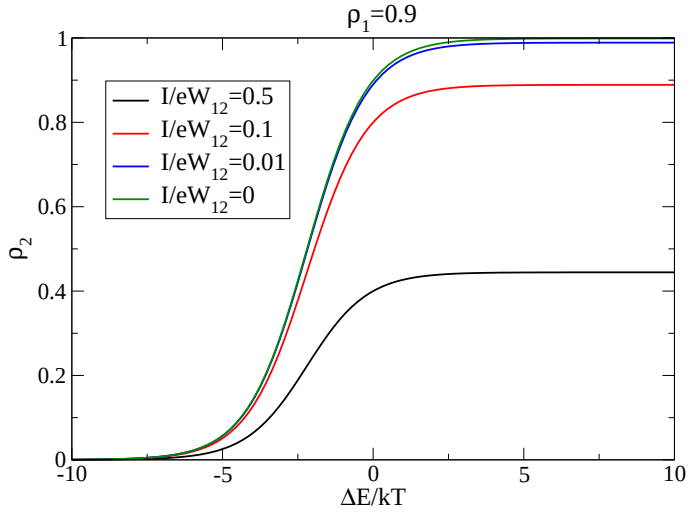

Figure 5.3: Occupation of site 2 for given occupation of site 1 as a function of the onsite energy difference for four different values of the current.

5.3. Results

5.3.1. Sequence effects

Using the rate equation we will study now the charge transport and the non-equilibrium occupation of the sites for various DNA sequences. Both quantities depend strongly on the specific sequence. All DNA sequences are 'semi-conducting' since the Fermi energy lies in the HOMO-LUMO gap, i.e. well above the HOMO states which carry the transport.

Figure 5.4 shows the I-V characteristics for two such sequences, 5'-GGGGGGGG-3' (green, dash-dotted line) and 5'-GAAAAAAG-3' (black, solid line). The first sequence displays the 'semi-conducting' behavior with a gap characterized by the distance of the Fermi energy to the onsite energy of the G base (shifted by Δ_{G}). Due to its electronic symmetry the I-V characteristic is symmetric with respect to the applied bias. On the other hand, the second DNA sequence shows strong rectifying behavior, despite of its seemingly symmetric sequence. The reason for this asymmetry lies in the electronic asymmetry of the hopping amplitudes, together with the incoherence of the hopping processes between DNA base pairs. This can easily be understood: For positive bias the hopping 'bottleneck' of the system is at the crossover from A to G at the 3' end of the strand. There, the polaron needs to overcome an energy barrier mediated by vibrational excitations. For negative bias the 'bottleneck' is at the crossover from A to G at the 5' end of the strand. Due to the opposite direction of the dominating hopping process, with $|t_{\mathrm{GA}}| > |t_{\mathrm{AG}}|$ (compare Table 2.1), the current for negative bias is higher than for positive bias. Thus, inhomogeneous sequences will in general display a rectifying, semi-conducting I-V characteristic. The rectification effect will be weaker for longer and more disordered sequences, as more 'bottlenecks' in either direction appear. Note that no rectifying behavior would be observed if we model the transport as a coherent transition through the total length of the chain ('Landauer approach'). [96, 122, 123]

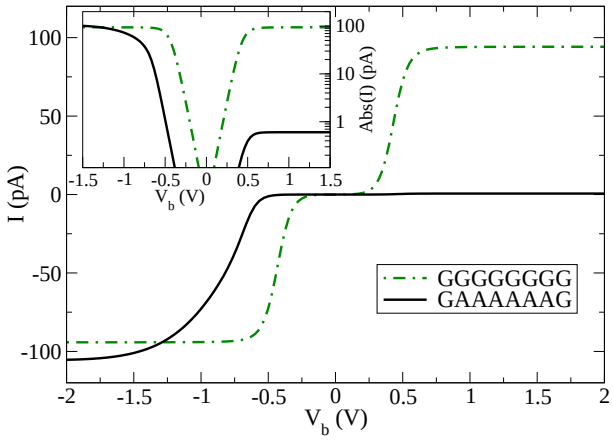

Figure 5.4: I-V characteristics for two DNA strands with sequences 5'-GGGGGGGG-3' (dash-dotted line) and 5'-GAAAAAAG-3' (solid line) with the following parameters: Base pair onsite energies $\epsilon_A = -0.26\,\text{eV}$, $\epsilon_G = +0.25\,\text{eV}$, polaron shifts $\Delta_A = 0.18\,\text{eV}$ and $\Delta_G = 0.47\,\text{eV}$, Fermi energy $E_F = 0\,\text{eV}$, symmetric coupling to leads with linewidths $\Gamma_L = \Gamma_R = 0.01\,\text{eV}$, vibrational energies $\hbar\omega_A = 11\,\text{meV}$, $\hbar\omega_G = 16\,\text{meV}$, and room temperature $k_BT = 25\,\text{meV}$. The inset shows the absolute value of the current on logarithmic scale. The current for the second sequence shows rectification by a factor of ~ 200.

We now study the sequence dependence of the current threshold, or equivalently the position of the peak in the differential conductance dI/dV_b (both differ only by a term proportional to temperature). Figure 5.5 shows the differential conductance as a function of the applied bias for 5 different DNA sequences 5'-AAAAAAAA-3', 5'-GAAAAAAG-3', 5'-GGAAAAGG-3', 5'-GGGAAGGG-3', and 5'-GGGGGGGG-3'. For the homogeneous sequences the threshold is equal to the onsite energy of the considered base pairs ($eV_b = 2\tilde{\epsilon}_A$ for 5'-AAAAAAAA-3' and $eV_b = 2\tilde{\epsilon}_G$ for 5'-GGGGGGGG-3'). For the inhomogeneous sequences the threshold lies in between the limits set by the homogeneous sequences, i.e. it is not determined by the internal energy scales alone. The varying threshold is a consequence of the way the charges are rearranged along the DNA molecule, which of course is very sensitive to the considered sequence.

As discussed above, Eqs. (5.14) describe the tunneling rate from the electrode to the adjacent DNA base pair. The tunneling is modified by the vibrational modes which can be excited, depending on the applied bias. This 'renormalized' tunneling can lead to a very broad differential conductance peak which is very different from the usual (derivative of) Fermi function form, as observed most prominently for the sequence 5'-GAAAAAAG-3'. Note that there is nearly no modification on the low bias side of the peak.

5.3.2. Local chemical potential

As discussed above, the I-V characteristic of a DNA molecule is affected by bias and sequence dependent charge rearrangements on the DNA base pairs. For the ease of

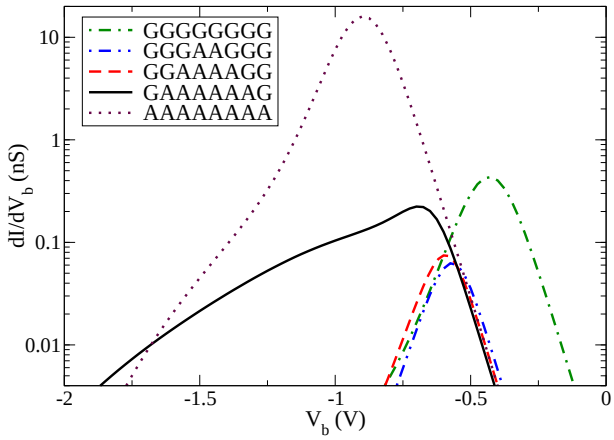

Figure 5.5: Differential conductance (logarithmic scale) as a function of applied bias for five different DNA sequences with parameters as in Fig. 5.4. For the homogeneous sequences the threshold, i.e. the position of the maximum of the differential conductance, is set by onsite energy of the considered base pairs. For the inhomogeneous sequences, however, the threshold is not determined by the internal energy scales alone. The sequence-dependent thresholds lie in between the limits set by the homogeneous sequences. For some sequences (e.g. 5'-GAAAAAAG-3'), the peaks are broadened due to 'renormalized' tunneling.

displaying these effects, i.e, both small deviations from an occupation 1, as well as occupations near 0, we introduce a local chemical potential Φ_i, defined by

$$\Phi_i(V_\mathrm{b}) = \tilde{\epsilon}_i - k_\mathrm{B}T \ln\left(\frac{1}{\rho_i(V_\mathrm{b})} - 1\right). \tag{5.22}$$

This quantity is superior to the occupation in visualizing the non-equilibrium charge rearrangement, because it reacts sensitively to even small changes in the occupation.

Figure 5.6 shows the I-V curves for the two DNA molecules 5'-GAAAAAAG-3' (black, solid line) and 5'-GGAAAAGG-3' (red, dashed line), and the inset shows the local chemical potential Φ for the last guanine base (at the 3' end) for both sequences. Although the sequences are very similar, the I-V characteristics differ strongly in the maximum current and in the way the current increases for increasing bias voltage. The current of the second sequence has reached a plateau already at about $V_\mathrm{b} = -0.8\,\mathrm{V}$, whereas the black curve has not leveled off even for $V_\mathrm{b} = -1.5V$. This strong deviation from a Fermi function behavior is in part a consequence of the renormalization of the tunneling rates by the vibrations.

This difference in the I-V characteristics is reflected in the local chemical potential Φ, most prominently at the last guanine base of both sequences, as shown in the inset. At low bias both sequences behave in the same way: the potential increases equally with the applied bias. The DNA is not conducting and therefore, the situation is similar to the charging of a capacitor. At the drop-off around $V_\mathrm{b} = -0.3\,\mathrm{V}$, the current sets in and a potential drop between base pair and lead is established. In correspondence to the current, the local chemical potential for the second sequence 5'-GGAAAAGG-3' levels

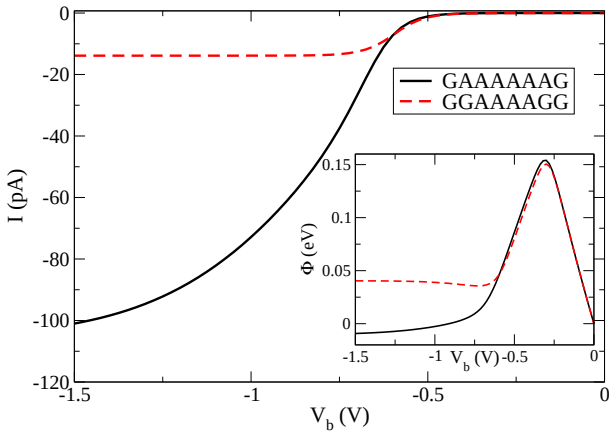

Figure 5.6: I-V curves for the two sequences 5'-GAAAAAAG-3' (solid line) and 5'-GGAAAAGG-3' (dashed line) (parameters see Fig. 5.4). Despite the very similar sequences, the I-V show clear differences. The inset shows the local chemical potential Φ for the last guanine base (at the 3' end) for both sequences at various bias voltages. Equivalent behavior between local potential and I-V is visible

off, whereas the potential of the first sequence 5'-GAAAAAAG-3' never reaches a plateau in the range up to $V_\mathrm{b} = -1.5\,\mathrm{V}$.

To give a feeling for the total charge rearrangement Figure 5.7 shows the local chemical potential Φ_i of the two DNA sequences for all base pairs i and all voltages. The chemical potential landscape also suggests how the bias voltage V_b applied to the leads drops over the entire DNA molecule. Regions of good conductivity show almost no voltage drop, as seen for the stretches of adenine bases in the middle of both sequences. On the other hand most of the voltages drops at the base pairs close to the interfaces. The potential/voltage drop over for the entire sequence 5'-GAAAAAAG-3' is less than for 5'-GGAAAAGG-3'. This suggests that the the first sequence is better conducting than the latter, which is in accordance with their I-V curves (Fig. 5.6).

5.3.3. Temperature dependence and activation energy

In the experiments of Ref. [62] the current through bundles of long homogeneous DNA molecules showed a strong temperature dependence. The data could be fitted by an activation law $I(V) = \alpha(V) \exp\left[\frac{-E_a}{k_\mathrm{B}T}\right]$, with a voltage dependent prefactor $\alpha(V)$ that also shows a temperature dependence for the case poly(dG)-poly(dC) bundles. Asai [53] has used the Kubo formula for a polaron hopping model to obtain a similar relation for the linear response conductivity.

Our results are obtained in a non-equilibrium situation and also show a strong temperature dependence. An Arrhenius plot of the current vs. temperature shows linear behavior, indicating that the current is indeed an activated quantity (though we also observe deviations from a perfect Arrhenius law). Fitting the temperature dependence of our data by an Arrhenius law allows us to estimate the activation energy for a given bias voltage and polaron shift Δ. Figure 5.8 shows the activation energy E_a obtained by this

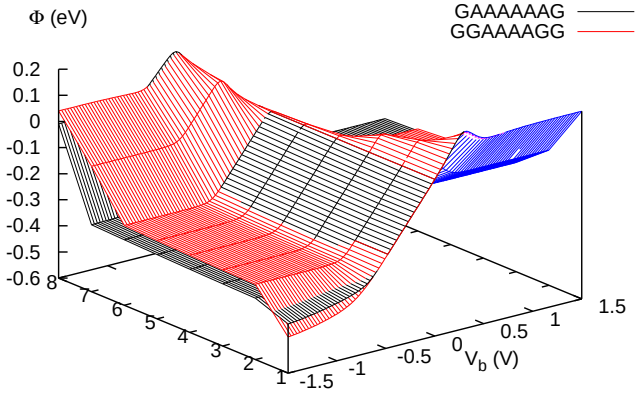

Figure 5.7: Local chemical potential Φ for all base pairs of the DNA strand with sequence 5'-GAAAAAAG-3' (black lines) and 5'-GGAAAAGG-3' (red lines) at various bias voltages and with parameters as in Fig. 5.4. The local potential drops differently for the two sequences, implying different conduction properties.

fitting as a function of the polaron shift at three different bias voltages for a homogeneous DNA strand with 15 GC base pairs. [2] The activation energy is proportional to Δ_G, but the proportionality factor differs depending on the applied bias voltages. For voltages smaller than the gap, the activation energy also includes the energy needed to overcome the gap. For voltages above the threshold the proportionality factor between activation energy and polaron shift is about 1/2, consistent with the high-temperature value for the bulk polaron hopping conduction $E_a = 0.5\Delta$ (see green/dotted line in Fig. 5.8) [76].

5.4. Summary

In this chapter we have investigated the non-equilibrium polaron hopping transport in short DNA chains with various sequences, coupled to voltage-biased leads in the frame of rate equations which take into account inelastic transitions in the local vibration degrees of freedom. Our theory is formally an extension of the so-called $P(E)$ theory of tunneling in a dissipative electromagnetic environment. We find semi-conducting I-V characteristics with thresholds that are very sensitive to the considered DNA sequence. For all non-symmetric sequences (which is the typical case) we observe rectifying behavior (Fig. 5.4). The sequence dependent thresholds are not directly connected to intrinsic energy scales (Fig. 5.5), rather they are intimately related to the non-trivial charge

[2] We chose to set the polaron shift in the electronic part of the Hamiltonian to zero, so that the gap between onsite energy $\tilde{\epsilon}_G$ and the Fermi level is constant for all electron-vibration coupling strengths ($|\tilde{\epsilon}_G - E_F| = 0.25eV$). This allows us to keep the bias voltages fixed for the range of polaron shifts considered.

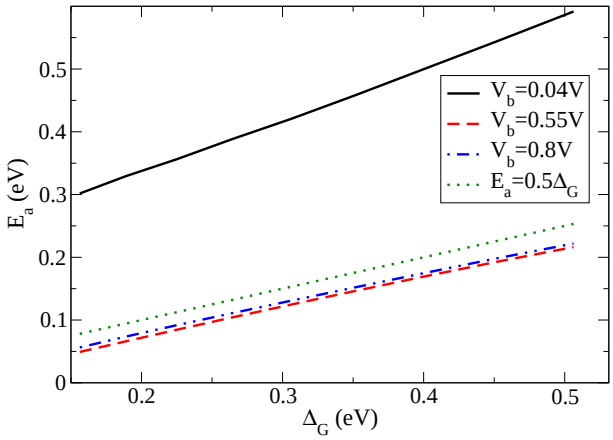

Figure 5.8: Activation energy E_a for polaron hopping of a homogeneous DNA with 15 G-C base pairs as a function of the polaron shift Δ for voltages $V_\mathrm{b} = 0.04\,\mathrm{V}$ (solid line), $V_\mathrm{b} = 0.55\,\mathrm{V}$ (dashed line), and $V_\mathrm{b} = 0.8\,\mathrm{V}$ (dash-dotted line). All other parameters as in Fig. 5.4. For comparison, the dotted line shows the activation energy of polaron hopping conduction in bulk at high temperatures ($E_a = 0.5\Delta$) [76].

rearrangement along the DNA molecule at finite bias. We have visualized this effect by displaying the local chemical potential Φ_i (Fig. 5.7). As expected for polaron hopping, the current is thermally activated with a temperature dependence following an Arrhenius-law. The activation energy E_a is voltage dependent and approaches the bulk polaron value $E_a = 1/2\Delta$ (Δ: polaron shift) for voltages above the threshold (Fig. 5.8).

6. Incoherent polaron hopping: Diagrammatic approach

In the previous chapter, we developed a description of polaron hopping in terms of a rate equation with rates obtained by golden rule arguments. This description is restricted to diagonal components of the density matrix and it neglects correlations between charge densities of different base pairs mediated by the hopping processes. In this chapter we will introduce a diagrammatic approach for polaron hopping in one dimensional system coupled to two biased leads. This approach is a real-time expansion on the Keldysh contour and is an extension of a technique developed by Böttger and Bryskin in the late 1970s for bulk systems. [76]

6.1. Theory

6.1.1. Real-time density matrix expansion

The Hamiltonian we consider has been introduced in detail in the previous chapter. We start with the form $\tilde{H}$, which was obtained after the Lang-Firsov transformation

$$\tilde{H} = \tilde{H}_0 + \tilde{H}' \tag{6.1}$$

$$\tilde{H}_0 = \sum_i (\epsilon_i - \Delta_i) a_i^\dagger a_i + \sum_i \hbar\omega_i \left(B_i^\dagger B_i + \frac{1}{2} \right) + H_\mathrm{L} + H_\mathrm{R} \tag{6.2}$$

$$\tilde{H}' = -\sum_{<ij>} t_{ij}\, a_i^\dagger \chi_i^\dagger a_j \chi_j \tag{6.3}$$

$$+ \sum_{\nu,r,i} \left[t^r c_{\nu r}^\dagger a_i \chi_i + t^{r*} a_i^\dagger \chi_i^\dagger c_{\nu r} \right] \tag{6.4}$$

$$\Delta_i = \int d\omega D_i(\omega) \frac{\lambda_i^2}{\hbar\omega} \,. \tag{6.5}$$

To calculate quantities of interest, e. g. the occupation number $\left\langle a_i^\dagger(t) a_i(t) \right\rangle$ and the current in a non-equilibrium situation with applied bias, we make a real time expansion of the density matrix along the Keldysh contour. The evolution in the interaction picture introduces the time dependence

$$\begin{aligned} a_i(t) &= a_i e^{-i(\epsilon_i - \Delta_i)t} = a_i e^{-i\tilde{\epsilon}_i t} \\ B_i(t) &= B_i e^{-i\omega_i t}. \end{aligned}$$

From here on we will use the shifted onsite energy $\tilde{\epsilon}_i = \epsilon_i - \Delta_i$ in all expressions.

The single-particle density matrix of the DNA chain can be written as $\rho_k^l(t) = \left\langle a_k^\dagger(t) a_l(t) \right\rangle_{\tilde{H}}$. We express it in the interaction picture, assuming that the perturbation $\tilde{H}'$ is adiabatically turned on from the time $t_0 = -\infty$,

$$\rho_k^l(t) = \left\langle U_{\tilde{H}_0}^\dagger(t,-\infty) a_k^\dagger a_l U_{\tilde{H}_0}(t,-\infty) \right\rangle_{\tilde{H}_0} e^{-i(\tilde{\epsilon}_l - \tilde{\epsilon}_k)t},$$

with time evolution operator

$$U_{\tilde{H}_0}(t,-\infty) = \mathrm{T}\left\{ \exp\left[-i \int_{-\infty}^{t} dt \tilde{H}'_{\tilde{H}_0}(t) \right] \right\}. \tag{6.6}$$

A Taylor expansion of the time evolution operators in $\tilde{H}'$ defines a diagrammatic expansion. The forward time-evolution operator $U_{\tilde{H}_0}(t,-\infty)$ is expanded on the upper branch of the Keldysh contour, whereas the backward time-evolution operator $U_{\tilde{H}_0}^\dagger(t,-\infty)$ is expanded on the lower branch (see Fig. 6.1). The index $\tilde{H}_0$ indicates that these operators are written in the interaction picture. The time ordering operator 'T' in Eq. 6.6

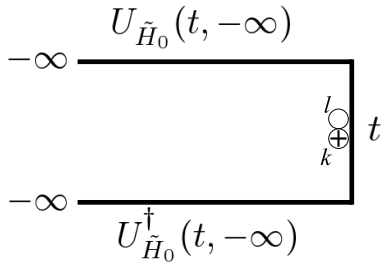

Figure 6.1: Schematic drawing of the Keldysh contour and the forward and backward time-evolution operators. The open and crossed circle (the clamp) represent the two operators a_l and $a_k^\dagger$, respectively, which are evaluated at time t.

(anti-time ordering operator '$\tilde{\mathrm{T}}$') ensures that the different times t_i, arising from the Taylor expansion of the forward (backward) time evolution operator, are ordered in the correct way along the contour. Note, oftentimes forward and backward time evolution operators are combined and a contour ordering operator '$\mathrm{T_k}$' is introduced to ensure the correct ordering of times along the Keldysh contour. [94, 124]

In performing the expansion in the time evolution operators, we obtain certain operator products, which we have to average thermally. Since $\tilde{H}_0$ is quadratic in the fermion operators, these can be treated using Wick's theorem. On the other hand, the vibrational operator products, involving various operators $\chi_i(t_j)$, cannot be factored. The rules for the evaluation of these operator products are given in Appendix E. A specific term in the Taylor expansion, is represented by diagram with a certain number of vertices on the upper and lower branch of the Keldysh contour, where each vertex is proportional either to t_{ij} (a hopping vertex) or $t_{i\nu}^r$ (a tunneling vertex). The different vertices are connected by fermion and vibrational lines and belong to different times t_i, which have to be (anti-) time ordered along the (lower) upper branch of the contour.

A feature of this expansion is that certain diagrams are diverging even in first order. These diagrams can be identified by so called free sections (we will introduce the concept of free sections below in more detail), that cut at least one pair of fermion lines, where both lines are associated with sites (the same or different), that have the same onsite energy. This is equivalent to the situation of resonant tunneling. In such a case an infinite number of diagrams has to be summed up in a way similar to a 'ladder'-approximation [76, 120, 121].[1] Note, when considering only diagonal elements of the single-particle matrix, every diagram is diverging. In the derivation of the diagrammatic rules listed below such a ladder summation is performed. This leads to a relation for the time derivative of the density matrix

$$\begin{aligned}\frac{d}{dt}\rho_k^l(t) = &- i\left(\epsilon_l - \epsilon_k\right)\rho_k^l(t) \\ &+ \int_{-\infty}^{t} dt_1 \sum_{\{m_i, m_i'\}} \Bigg[\rho_{m_1'}^{m_1}(t_1)\mathcal{W}_{m_1' k}^{m_1 l}(t_1, t) + \left(\delta_{m_1' m_1} - \rho_{m_1'}^{m_1}(t_1)\right)\mathcal{V}_{m_1' k}^{m_1 l}(t_1, t) \\ &+ \rho_{m_1' m_2'}^{m_1 m_2}(t_1)\mathcal{W}_{m_1' m_2' k}^{m_1 m_2 l}(t_1, t) + \rho_{m_1' m_2' m_3'}^{m_1 m_2 m_3}(t_1)\mathcal{W}_{m_1' m_2' m_3' k}^{m_1 m_2 m_3 l}(t_1, t) + \dots \Bigg] . \end{aligned} \tag{6.7}$$

The important property of the irreducible blocks $\mathcal{W}$ and $\mathcal{V}$ is, that they do not diverge. Clearly, this is not a self-consistent equation for the single-particle density matrix, as it depends also on higher order density matrices, e. g.

$$\rho_{m_1' m_2'}^{m_1 m_2}(t_1) = \left\langle U_{\tilde{H}_0}^{\dagger}(t_1) a_{m_2'}^{\dagger} a_{m_2} a_{m_1'}^{\dagger} a_{m_1} U_{\tilde{H}_0}(t_1) \right\rangle . \tag{6.8}$$

Then, also a similar equations for the higher order density matrices has to be computed, i. e. one has to deal with an infinite hierarchy of equations. For practicability an appropriate decoupling scheme has to be applied.

Why does a many-particle density matrix affect the behavior of a single-particle density matrix? This becomes obvious, when considering a hopping process between two sites m and n, where the two-particle density occurs. Such a hopping process is determined by the hopping probability, which is represented by a second order irreducible diagram, and the occupation of the final site n. The two-particle density matrix combines the probability to find the initial site m occupied and the final site n empty. In general, the occupation of different sites is correlated, except for situations, where the charge density is very low. To describe the situation of uncorrelated occupation numbers, the density matrix can be factorized in a Hartree-Fock type way

$$\rho_{m_1' m_2'}^{m_1 m_2} \approx \rho_{m_1'}^{m_1}\rho_{m_2'}^{m_2} + \rho_{m_2'}^{m_1}\left(\delta_{m_2 m_1'} - \rho_{m_1'}^{m_2}\right) . \tag{6.9}$$

This approximation was taken in the previous chapter.

[1] For example, a second order diagram with a diverging free section contributes to a similar first order diagram. This can be incorporated, by the convolution of the first order block diagram with the single density matrix, as in Eq. 6.7. If the second order block has a non-diverging free section, than the first order block is just multiplied by Fermi function. For such situations, the density matrices in Eq. 6.7 have to replaced by Fermi functions. For example $\rho_{m_1'}^{m_1} \to \delta_{m_1' m_1} f_{m_1}$.

6.1.2. Construction of irreducible block diagrams

Below we will state the rules for the construction and evaluation of irreducible block diagrams. The rules for pure hopping diagrams, i. e. those containing only vertices $\propto t_{ij}$, were developed by Böttger and Bryksin [76]. We extended their theory adding new rules to treat diagrams with tunneling vertices $\propto t^r_{i\nu}$.

The perturbative expansion can be visualized by the construction of diagrams which are equivalent to expressions in the analytic expansion. The main contribution to the diagrams comes from so called irreducible blocks, which, as the name implies, cannot be decomposed into more simple diagrams. The main feature of an irreducible block diagram is, that it does not diverge, when integrating over the internal times t_i. Irreducible blocks can be identified by their property of not allowing free sections. A free section is a vertical line drawn between the leftmost vertex and the rightmost vertex (except for the clamp) that does not cross either a phonon line or an external fermion (tunneling) line.

The rules come in two sets: the first for the construction and labeling of possible diagram, the second set for the evaluation of a particular diagram. The rules are general for all orders of perturbation theory. We give a concrete example of a third order contribution to the block $\mathcal{W}^{m_1 m_2 l}_{m'_1 m'_2 k}(t)$ in Fig. 6.2.

1. Draw the Keldysh time contour as a rectangle which is open to the left, corresponding to $t \to -\infty$.

2. For a diagram of order n we draw on the contour $n+1$ pair vertices consisting of one open circle $\bigcirc$ (symbolizing a destruction operator) and one crossed circle $\bigoplus$ (symbolizing a creation operator). All circles belonging to operators acting on the molecule (DNA) are drawn on the inside of the contour, whereas circles belonging to electrode operators are drawn on the outside of the contour. Therefore, if the pair vertex is due to a tunneling process $t^r_{i,\nu}$ one circle is on the inside and the other one is on the outside of the contour. The circles of a hopping process are both drawn on the inside of the contour where the open circle is always 'earlier' along the Keldysh contour than the crossed circle. As we calculate diagrams to evaluate the density matrix, we draw one pair vertex (also called 'clamp' [76]) at the inside of the right vertical line of the Keldysh contour, corresponding to time t. The other n vertices are drawn at n times t_i on either the upper or lower branch of the Keldysh contour (where t_2 is the leftmost, earliest time and t_1 is the rightmost, latest time).

3. Each open circles $\bigcirc$ on the inside of the contour has one ingoing fermion line (arrow pointing to the vertex) and each crossed circle $\bigoplus$ has one outgoing fermion line (arrow pointing away from the vertex) which is locally directed along the Keldysh contour.

4. Complementary circles outside the contour are pairwise connected by a fermion line drawn *outside* of the contour. Since this line corresponds to an electron propagating in electrode r the connected circles have to belong to the same electrode r, otherwise the diagram contribution is zero.

5. The clamp is always connected by a fermion line to the rightmost vertex (other than the clamp) drawn *inside* of the contour. If the rightmost vertex is a hopping vertex, the fermion line is directed along the contour. If the rightmost vertex is a tunneling vertex, the inside circle (open or crossed) is connected to the complementary circle of the clamp, no matter what the direction of the fermion line.

6. The remaining unconnected inside circles have fermion lines going into (coming from) the region left of the diagram ($t \to -\infty$) without intersecting each other.

7. Each circle belongs to one specific state for the molecule or the electrode. We label the molecule states (sites) by latin characters (e.g. $m, m', \ldots$) and the electrode states by Greek characters (e.g. ν). Note that the two circles of a hopping vertex can not correspond to the same state (site). Since we want to calculate the density matrix ρ^l_k then the crossed circle of the clamp is associated with the state (site) k and the open circle corresponds to state (site) l.

8. Except for the clamp, the circles on the inside of the contour must be connected by phonon lines so that the diagram has no free section, as defined above. One circle can be connected to more than one phonon line. All diagrams with different number of phonon lines (but still without free sections) have to be considered. Only circles belonging to the same state (site) can be connected by a phonon line. Therefore, the two circles of a hopping vertex can not be connected.

The rules for evaluating a diagram are as follows.

1. A hopping vertex at time t_i is associated with a factor $\pm i t_{m'm} \mathcal{K}_{m'} \mathcal{K}_m e^{-i(\epsilon_{m'} - \epsilon_m)(t_i - t_2)}$ where the creation operator (crossed circle) corresponds to site label m' and the destruction operator to the site label m (recall that t_2 is the leftmost time of the diagram). A tunneling vertex is associated with a factor $\pm i t^{r*}_{\nu m} \mathcal{K}_m e^{-i(\epsilon_\nu - \epsilon_m)(t_i - t_2)}$ or $\pm i t^{r}_{m'\nu} \mathcal{K}_{m'} e^{-i(\epsilon_{m'} - \epsilon_\nu)(t_i - t_2)}$ if the creation operator acts on the electrode or on the molecule, respectively. Vertices on the upper half of the contour have the minus sign, vertices on the lower half of the contour have the plus sign. The factor

$$\mathcal{K}_m = \exp\left\{ -\frac{1}{2} \int d\omega D_m(\omega) \left(\frac{\lambda_m}{\omega} \right)^2 (2N(\omega) + 1) \right\}.$$

   The clamp circles contribute a factor $e^{-i(\epsilon_l - \epsilon_k)(t_1 - t_2)}$, where the open circle of the clamp corresponding to the state l and crossed one corresponding to state k.

2. The outside fermion lines of the electrodes r contribute a factor $1 - f^r_\nu$ or f^r_ν depending whether they run in the direction of the contour or against it. Here f^r_ν is the Fermi function at energy $\epsilon_\nu - \mu_r$, with the chemical potential μ_r.

3. The fermion lines entering (leaving) the irreducible block from (to) the left are labeled from top to bottom. The labels determine the indices of the irreducible block, e.g. $\mathcal{W}^{m_1 m_2 l}_{m'_1 m'_2 k}(t)$. The lines leaving the diagram correspond to the lower labels

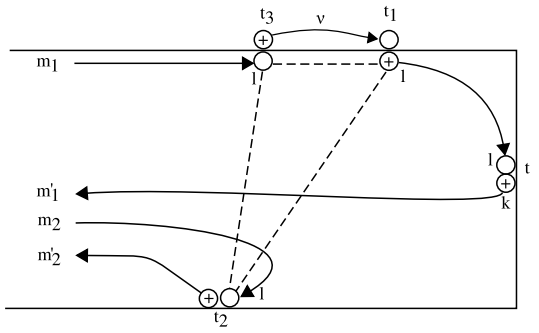

Figure 6.2: A third order diagram to the rate $\mathcal{W}^{m_1 m_2 l}_{m_1' m_2' k}(t_2, t_1)$

(primed labels in the example Fig. 6.2) whereas the lines entering the diagram from the left correspond to the upper labels (unprimed labels). Since the fermion lines are connected to circles on the inside of the diagram (which belonged to some state (site) j) a Kronecker factor has to be added, e.g. $\delta_{m_1 l}$ and $\delta_{m_1' k}$ for the example of Fig. 6.2.

4. A phonon line connecting two circles both associated to a state (site) m has a value

$$F_m^\zeta(t_i - t_j) = \exp\left\{\zeta A_m(t_i - t_j)\right\} - 1 \text{ , with}$$
$$A_m(t) = \int d\omega D_m(\omega) \left(\frac{\lambda_m}{\omega}\right)^2 \frac{\cos\left(\omega\left[t + i\hbar\beta/2\right]\right)}{\sinh\left(\hbar\omega\beta/2\right)} \text{ ,}$$

where the circle at time t_i is later on the contour than the circle at time t_j. The factor ζ is determined by the type of circles the line connects. If the circles are different $\zeta = +1$, otherwise $\zeta = -1$.

5. Multiply with a factor $(-1)^{M+N}$, where M is the number of intersections of fermion lines on the *outside* of the contour (tunneling lines) and N is the number of intersections of fermion lines on the *inside* of the contour.

6. We integrate over all internal times t_i (except t_1 and t_2) and sum over all electrode states ν and all internal molecule states i, j, *except* the states associated with the clamp.

Let us have a look at the third order example in Fig. 6.2. This diagram is part of the rate $\mathcal{W}^{m_1 m_2 l}_{m_1' m_2' k}(t_2 - t_1)$. Full lines are fermion lines and dashed lines are phonon lines. For easier readability we introduce renormalized hopping and tunneling strengths $\tilde{t}_{m_1' m_1} = t_{m_1' m_1}\mathcal{K}_{m_1'}\mathcal{K}_{m_1}$, $\tilde{t}^{r*}_{l\nu} = t^{r*}_{l\nu}\mathcal{K}_l$ and $\tilde{t}^{r}_{\nu l} = t^{r}_{\nu l}\mathcal{K}_l$. The diagram has the value:

$$\begin{aligned}\mathcal{W}^{m_1 m_2 l}_{m_1' m_2' k}(t_2 - t_1) =& (-i)^2 i \sum_{r\nu} \tilde{t}_{m_2' m_2}\, \tilde{t}^{r*}_{l\nu}\, \tilde{t}^{r}_{\nu l}\, \delta_{m_1 l}\, \delta_{m_1' k}\, \delta_{m_2 l}\, (1 - f^r_\nu) \\ &\times e^{-i(\epsilon_\nu - \epsilon_l)(t_1 - t_2)} e^{-i(\epsilon_l - \epsilon_k)(t_1 - t_2)} F_l^+(t_2 - t_1) \\ &\times \int_{t_2}^{t_1} dt_3 e^{-i(\epsilon_l - \epsilon_\nu)(t_3 - t_2)} F_l^-(t_2 - t_3) F_l^+(t_1 - t_3)\,.\end{aligned}$$

As can be seen from Eqs. 6.7 and 6.10, the irreducible blocks are convoluted with single- and many-particle density matrices or correlation functions. The order of the labels of the irreducible block rate determine the correlation function it will be convoluted with. Lines leaving the block (primed labels) correspond to creation operators in Eq.6.8, lines entering the block (unprimed labels) correspond to destruction operators. The order of operators from left to right corresponds to the order of the lines leaving/entering the diagram from bottom to top.

For example, let us consider some rate $\mathcal{W}^{m_1 m_2 m_3 l}_{m_1' m_2' m_3' k}(t_2 - t_1)$ which has the following order of the terminals at the left of the diagram from bottom to top: m_3', m_2', m_3, m_1', m_2, and m_1 (the primed labels correspond to fermion lines leaving the diagram, the unprimed to lines entering the diagram as in Fig. 6.2). This rate will be convoluted with the higher order correlation function

$$\left\langle a_{m_3'}(t_2) a_{m_2'}(t_2) a^\dagger_{m_3}(t_2) a_{m_1'}(t_2) a^\dagger_{m_2}(t_2) a^\dagger_{m_1}(t_2) \right\rangle_{\tilde{H}}$$

The above rules apply to the most general situation of polaron transport, where coherence effects are considered by including non-diagonal elements of the single and many-particle density matrices. As explained in the previous chapter, for the situation of strong electron-vibration coupling and high temperature it is sufficient to consider only diagonal components of the density matrices. In the rest of the work, we will resort to this limit and discuss a situation of finite bias applied to a DNA molecule, which has reached steady-state. Thus, equation 6.7 for the time derivative of the single-particle density matrix reduces to

$$\begin{aligned} 0 = \int_{-\infty}^{0} dt_1 \sum_{\{m_i\}} \Big[& \rho_{m_1} \mathcal{W}_{m_1 l}(t_1) + (1 - \rho_{m_1}) \mathcal{V}_{m_1 l}(t_1) \\ & + \rho_{m_1 m_2} \mathcal{W}_{m_1 m_2 l}(t_1) + \rho_{m_1 m_2 m_3} \mathcal{W}_{m_1 m_2 m_3 l}(t_1) + \dots \Big] . \end{aligned} \tag{6.10}$$

6.1.3. First and second order diagrams

In the previous chapter we obtained the rates for hopping transport in DNA molecules from golden rule arguments. Equivalently, the rate equation and the associated rates can be obtained from diagram using the above rules. The advantage of this procedure is, that no divergences occur and that correlation effects are incorporated naturally, that were not considered in the previous chapter. As explained before, we will restrict ourselves to diagonal components of the density matrices. The rates are given by the eight diagram depicted in Figure 6.3 and 6.4, where Table 6.1 list the values of the diagrams. Inserting these rates into Eq. 6.10, the rate equations 5.15 and 5.16 are obtained.

Each of the tunneling diagrams depicted in Fig. 6.3 is the sum of two almost identical diagrams arising from the rules given above, one with a vibrational line and one without it. This is reflected in the fact that the generalized vibrational line (dashed line in the diagrams) has a value of $F_l^+(t_1 - t_2) + 1$. Similarly, each hopping diagram is the sum of three diagrams, one with two vibrational lines and two with a single vibrational line.

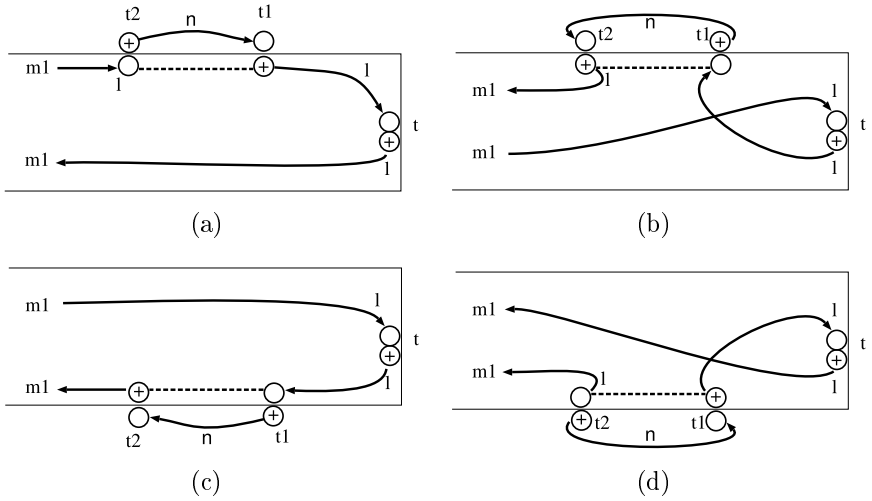

Figure 6.3: The four tunnel diagrams. The two diagrams on top of each other are their respective complex conjugates. The full lines represent fermion lines. The dashed line represents the sum of all possible vibrational lines arising from the diagrammatic rules, e. g. for diagram (a) it has a value $F_l^+(t_1 - t_2) + 1$.

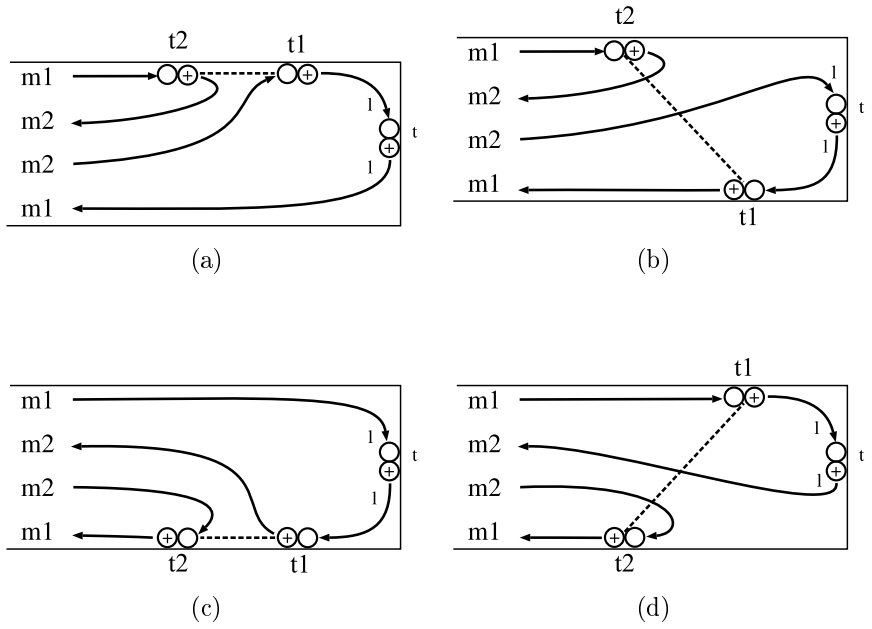

Figure 6.4: The four hopping diagrams. The two diagrams on top of each other are their respective complex conjugates. The full lines represent fermion lines. The dashed line represents the sum of all possible vibrational lines arising from the diagrammatic rules, e. g. for diagram (a) it has a value $F_l^+(t_1 - t_2)F_{m_2}^+(t_1 - t_2) + F_l^+(t_1 - t_2) + F_{m_2}^+(t_1 - t_2)$.

diagrams	value	Eq.
6.3(a)+6.3(c)	$W^{\mathrm{r}}_{m_1 l} = -\Gamma^{\mathrm{r}} \int \frac{dE}{2\pi\hbar}(1 - f_{\mathrm{r}}(E))P_l(\tilde{\epsilon}_l - E)\delta_{lm_1}$	5.13
6.3(b)+6.3(d)	$V^{\mathrm{r}}_{m_1 l} = \Gamma^{\mathrm{r}} \int \frac{dE}{2\pi\hbar} f_{\mathrm{r}}(E)P_l(E - \tilde{\epsilon}_l)\delta_{lm_1}$	5.14
6.4(a)+6.4(c)	$\mathcal{W}_{m_1 m_2 l} = -\frac{\lvert t_{l,m_2}\rvert^2}{\hbar^2} \int dt\, e^{\frac{i}{\hbar}(\tilde{\epsilon}_l - \tilde{\epsilon}_{m_2})t} \left[P_l(t)P_{m_2}(t) - \mathcal{K}^2_l \mathcal{K}^2_{m_2}\right] \delta_{lm_1}$	5.21
6.4(b)+6.4(d)	$\mathcal{W}_{m_1 m_2 l} = \frac{\lvert t_{m_1,l}\rvert^2}{\hbar^2} \int dt\, e^{\frac{i}{\hbar}(\tilde{\epsilon}_{m_1} - \tilde{\epsilon}_l)t} \left[P_{m_1}(t)P_l(t) - \mathcal{K}^2_{m_1} \mathcal{K}^2_l\right] \delta_{lm_2}$	5.21

Table 6.1: Values for the diagrams of Fig. 6.3 and 6.4. For the evaluation of the tunneling diagrams the wide band limit was assumed. The index $r = L/R$ stands for the left/right electrode.

The value of the generalized vibrational line is therefore $F^+_l(t_1 - t_2)F^+_{m_2}(t_1 - t_2) + F^+_l(t_1 - t_2) + F^+_{m_2}(t_1 - t_2)$. In the previous chapter, the influence of the vibrations was described by the functions $P_l(t)$, which were known from the 'P(E)' theory. In the diagrammatic rules the vibrations are described by functions $F^{+/-}_l(t)$. The relation between these two functions is given by $P_l(t) = \mathcal{K}^2_l \left(F^+_l(t) + 1\right) = \mathcal{L}_l \left(F^+_l(t) + 1\right)$. In the previous chapter, the function $\mathcal{L}_l = \mathcal{K}^2_l$ was introduced for simplicity.

The rates from the various diagrams are convoluted with different correlation functions, depending on the fermion lines leaving to the left as explained above. The diagrams presented in Fig. 6.3 and 6.4 are convoluted with correlation functions as listed in Table 6.2.

diagrams	correlation function
6.3(a)+6.3(c)	$\left\langle a^\dagger_l a_l \right\rangle = \rho_l$
6.3(b)+6.3(d)	$\left\langle a_l a^\dagger_l \right\rangle = 1 - \rho_l$
6.4(a)+6.4(c)	$\left\langle a^\dagger_l a_{m_2} a^\dagger_{m_2} a_l \right\rangle = \rho_l - \rho_{l m_2}$
6.4(b)+6.4(d)	$\left\langle a^\dagger_{m_1} a_l a^\dagger_l a_{m_1} \right\rangle = \rho_{m_1} - \rho_{m_1 l}$

Table 6.2: Diagrams and the correlation functions they are convoluted with. The two-particle density matrix is given by $\rho_{lm} = \left\langle a^\dagger_l a_l a^\dagger_m a_m \right\rangle$.

Inserting the rates and the associated correlation function into Eq. 6.10 one obtains the rate equation for the single-particle density matrix ρ_l.

6.1.4. Two-particle density matrix

In the previous chapter the two-particle correlation functions were factorized $\rho_{lm_2} \approx \rho_l \rho_{m_2}$. In the following we will investigate which influence the correlations have on the transport through DNA. For this we have to state equations for the two-particle density matrices, as well. The rules for the diagrams arising from the expansion of the

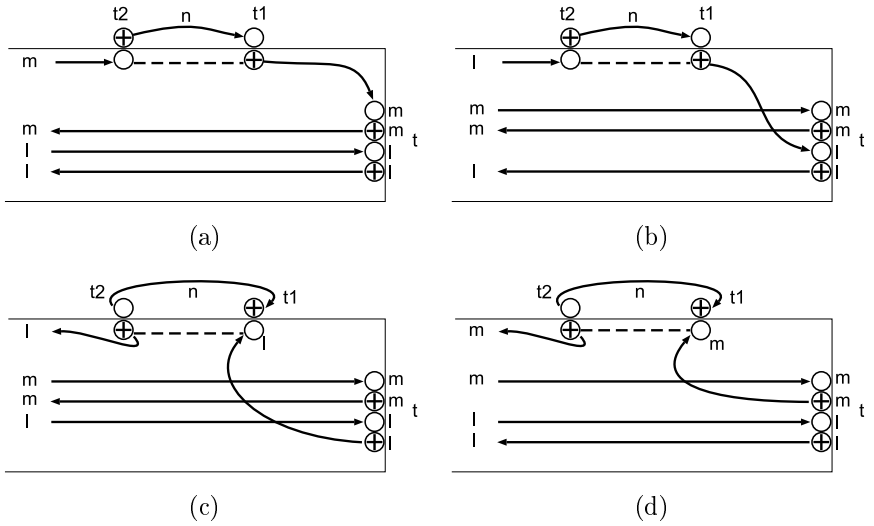

Figure 6.5: Four tunnel diagrams. To each of these diagrams there exists another that is their respective complex conjugate. The full lines represent fermion lines. The dashed line represents the sum of all possible vibrational lines arising from the diagrammatic rules, e. g. for diagram (a) it has a value $F_m^+(t_1 - t_2) + 1$. Note the various orderings of the indices on the left of the irreducible block.

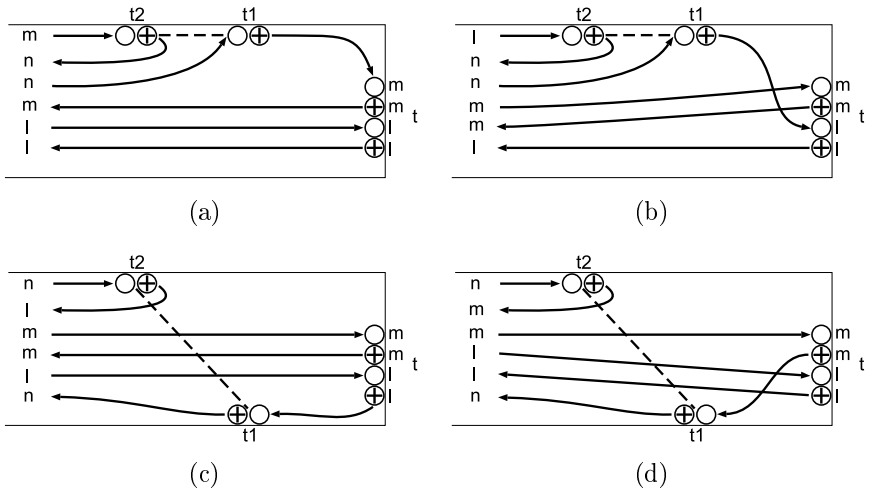

Figure 6.6: Four hopping diagrams. To each of these diagrams there exists another that is their respective complex conjugate. The full lines represent fermion lines. The dashed line represents the sum of all possible vibrational lines arising from the diagrammatic rules, e. g. for diagram (a) it has a value $F_m^+(t_1 - t_2)F_n^+(t_1 - t_2) + F_m^+(t_1 - t_2) + F_n^+(t_1 - t_2)$.

two-particle density matrix are almost identical to the ones stated above for the single-particle density matrix. The only difference arises from the clamp, which now consists of four circles (two empty, two crossed) representing the four fermion operators of the two-particle density matrix. There are now two possibilities to connect the rightmost vertex with the clamp, which both have to be considered. Furthermore, not only one but three fermion lines from the remaining terminals of the clamp leave to (enter from) the region left of the irreducible block without intersecting each other. The equation for the time derivative of the two-particle density matrix has the same structure as Eq. 6.7 and 6.10.

The diagrams up to second order are given in Figure 6.5 and 6.6. As for the single-particle density matrix, there are always two diagrams which are their respective complex conjugates. So, only one of them is shown. The irreducible blocks, i. e. the rates, have the same value as the ones derived previously, except for some δ-functions due to the additional terminals of the clamp and the correlators, they are convoluted with.

The rate, that every diagram (plus its complex conjugate) represents, is listed in the second column of Table 6.3. The values of these rates correspond to the ones given in Table 6.1. In the third column the correlators are shown with which the rates are convoluted. In the second section of the table, i. e. for $n = l$ or $n = m$, the relation $\hat{n}_l^2 = \hat{n}_l$ was used, where $\hat{n}_l = a_l^\dagger a_l$ is the number operator of site l. In the third section, the three-particle correlation functions have been factorized into two- and single-particle correlation functions to obtain closed equations. The rule for the factorization is given by

$$\begin{aligned}\langle ABC\rangle \approx \langle A\rangle\langle B\rangle\langle C\rangle &+ [\langle AB\rangle\langle C\rangle - \langle A\rangle\langle B\rangle\langle C\rangle] \\ &+ [\langle AC\rangle\langle B\rangle - \langle A\rangle\langle B\rangle\langle C\rangle] \\ &+ [\langle BC\rangle\langle A\rangle - \langle A\rangle\langle B\rangle\langle C\rangle] \ ,\end{aligned}$$

where the capital letters represent pairs of fermion operators, i. e. $a_l^\dagger a_l$. With the above rates one obtains the following rate equation for the two-particle density matrix in the inside of the DNA molecule

$$\begin{aligned}\frac{d}{dt}\rho_{lm} = \sum_n \Big\{ \quad & [\rho_{lm}(1-\rho_n) - \rho_{ln}\rho_m - \rho_{mn}\rho_l + 2\rho_l\rho_m\rho_n]\,\mathcal{W}_{lnl} \\ & + [\rho_{lm}(1-\rho_n) - \rho_{mn}\rho_l - \rho_{ln}\rho_m + 2\rho_l\rho_m\rho_n]\,\mathcal{W}_{mnm} \\ & + [\rho_{nl}(1-\rho_m) - \rho_{lm}\rho_n - \rho_{nm}\rho_l + 2\rho_n\rho_m\rho_l]\,\mathcal{W}_{nll} \\ & + [\rho_{nm}(1-\rho_l) - \rho_{lm}\rho_n - \rho_{ln}\rho_m - 2\rho_l\rho_n\rho_m]\,\mathcal{W}_{nmm} \Big\} \ . \end{aligned} \tag{6.11}$$

For a two-particle density matrix at the left junction the rate equation has the following form

$$\begin{aligned}\frac{d}{dt}\rho_{12} = & \rho_{12}W_{11}^{\mathrm{L}} + (\rho_2 - \rho_{12})\,V_{11}^{\mathrm{L}} \\ & + [\rho_{12}(1-\rho_3) - \rho_{23}\rho_1 - \rho_{13}\rho_2 + 2\rho_1\rho_2\rho_3]\,\mathcal{W}_{232} \\ & + [\rho_{13}(1-\rho_2) - \rho_{32}\rho_1 - \rho_{12}\rho_3 + 2\rho_1\rho_3\rho_2]\,\mathcal{W}_{322} \ . \end{aligned} \tag{6.12}$$

diagrams	value	correlation function
6.5(a)+c.c.	W^{r}_{ll}	ρ_{lm}
6.5(b)+c.c.	W^{r}_{mm}	ρ_{lm}
6.5(c)+c.c.	V^{r}_{ll}	$\rho_m - \rho_{lm}$
6.5(d)+c.c.	V^{r}_{mm}	$\rho_l - \rho_{lm}$
6.6(a)+c.c. $n = l$	$\mathcal{W}_{lml}$	$\left\langle a_l^\dagger a_l a_l a_l^\dagger a_m^\dagger a_m \right\rangle = 0$
6.6(b)+c.c. $n = m$	$\mathcal{W}_{mlm}$	$\left\langle a_l^\dagger a_m^\dagger a_m a_m a_m^\dagger a_l \right\rangle = 0$
6.6(c)+c.c. $n = m$	$\mathcal{W}_{mll}$	$\left\langle a_l a_l^\dagger a_m^\dagger a_m^\dagger a_m a_m \right\rangle = 0$
6.6(d)+c.c. $n = l$	$\mathcal{W}_{lmm}$	$\left\langle a_l^\dagger a_l^\dagger a_l a_m a_m^\dagger a_l \right\rangle = 0$
6.6(a)+c.c. $n \neq l$	$\mathcal{W}_{lnl}$	$\left\langle a_l^\dagger a_l a_m^\dagger a_n a_n^\dagger a_m \right\rangle \approx \rho_{lm}(1-\rho_n) - \rho_{ln}\rho_m - \rho_{mn}\rho_l + 2\rho_l\rho_m\rho_n$
6.6(b)+c.c. $n \neq m$	$\mathcal{W}_{mnm}$	$\left\langle a_l^\dagger a_m^\dagger a_m a_n a_n^\dagger a_l \right\rangle \approx \rho_{lm}(1-\rho_n) - \rho_{mn}\rho_l - \rho_{ln}\rho_m + 2\rho_l\rho_m\rho_n$
6.6(c)+c.c. $n \neq m$	$\mathcal{W}_{nll}$	$\left\langle a_n^\dagger a_l a_m^\dagger a_m a_l^\dagger a_n \right\rangle \approx \rho_{nl}(1-\rho_m) - \rho_{lm}\rho_n - \rho_{nm}\rho_l + 2\rho_n\rho_m\rho_l$
6.6(d)+c.c. $n \neq l$	$\mathcal{W}_{nmm}$	$\left\langle a_n^\dagger a_l^\dagger a_l a_m a_m^\dagger a_n \right\rangle \approx \rho_{nm}(1-\rho_l) - \rho_{lm}\rho_n - \rho_{ln}\rho_m - 2\rho_l\rho_n\rho_m$

Table 6.3: Values for the diagrams of Fig. 6.5 and 6.6 plus their complex conjugates. For the evaluation of the tunneling diagrams the wide band limit was assumed. The index $r = L/R$ stands for the left/right electrode. In the second section, for the situations $n = l$ or $n = m$ the relation $\hat{n}_l^2 = \hat{n}_l$ was used, where $\hat{n}_l = a_l^\dagger a_l$ is the number operator of site l. In the third section, the three-particle correlation functions have been factorized into two- and single-particle correlation functions to obtain closed equations.

Note, for the two-particle density matrix the relation $\rho_{lm} = \rho_{ml}$ holds. The rate equations for single-particle density matrices have the following form, similar to Eq. 5.15 and 5.16,

$$\frac{d}{dt}\rho_l = \sum_m \Big[(\rho_l - \rho_{lm})\, \mathcal{W}_{lml} + (\rho_m - \rho_{ml})\, \mathcal{W}_{mll} \Big] \tag{6.13}$$

$$\frac{d}{dt}\rho_1 = \rho_1 W_{11}^{\mathrm{L}} + (1-\rho_1)\, V_{11}^{\mathrm{L}} + (\rho_1 - \rho_{12})\, \mathcal{W}_{121} + (\rho_2 - \rho_{21})\, \mathcal{W}_{211}\ . \tag{6.14}$$

The rate equations for all other single and two-particle density matrices have a similar structure following Table 6.3. The rate equations for the single and two-particle density matrices have to be solved simultaneously. The current can then be calculated using Equation 5.17.

Correlations

To see which terms in the rate equation for the two-particle density matrix give rise to correlation effects, we exemplary compare Eq. 6.12 with

$$\begin{aligned}
\frac{d}{dt}\left[\rho_1\rho_2\right] =& \frac{d}{dt}\left[\rho_1\right]\rho_2 + \rho_1 \frac{d}{dt}\left[\rho_2\right] \\
=& \rho_1\rho_2 W_{11}^{\mathrm{L}} + (\rho_2 - \rho_1\rho_2)\, V_{11}^{\mathrm{L}} \\
&+ (\rho_1 - \rho_{12})\, \rho_2 \mathcal{W}_{121} + (\rho_2 - \rho_{21})\, \rho_2 \mathcal{W}_{211} \\
&+ \rho_1 (\rho_2 - \rho_{21})\, \mathcal{W}_{212} + \rho_1 (\rho_1 - \rho_{12})\, \mathcal{W}_{122} \\
&+ \rho_1 (\rho_2 - \rho_{23})\, \mathcal{W}_{232} + \rho_1 (\rho_3 - \rho_{32})\, \mathcal{W}_{322}\ .
\end{aligned}$$

For the second and last line the corresponding terms in Eq. 6.12 are easily found when identifying $\rho_{12} \equiv \rho_1\rho_2$. On the other hand, the corresponding terms for the third and fourth line are not obvious. The reason lies in the use of the identity $\hat{n}_l^2 = \hat{n}_l$ in deriving Eq. 6.12, where $\hat{n}_l = a_l^\dagger a_l$ is the number operator of site l (see Table. 6.1). When factorizing the three-particle correlators in the middle section of Table. 6.1 directly, without using the above identity, one obtains exactly the expressions in the third and fourth line of the above equation. Consequently, all hopping terms contribute to the correlation effects.

6.2. Results

In this section we study the I-V characteristics of short DNA molecules including correlation effects and compare with the results obtained in the previous chapter. Firstly, it should be noted that correlation effects do not influence the transport properties of homogeneous DNA sequences, as can be seen from Eqs. 6.13 and 6.14. In homogeneous DNA the onsite energies of all base pairs are identical therefore the hopping rates for a forward and backward hopping process are equal in magnitude but with opposite sign. Since $\rho_{ij} = \rho_{ji}$ holds, the two-particle density matrices drop out of the equations and the

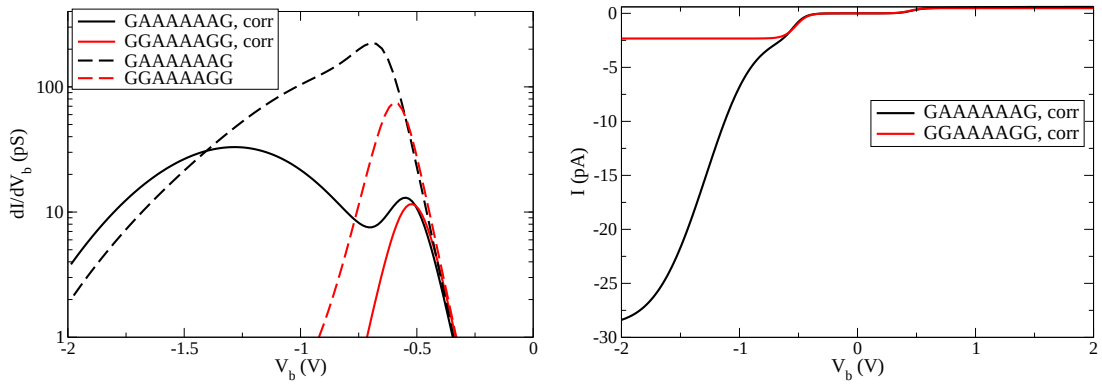

Figure 6.7: (a) Differential conductance (logarithmic scale) as a function of applied bias for two DNA sequences including (solid lines) and neglecting (dashed lines) correlation effects. (b) Corresponding I-V characteristics of the two solid curves in (a). All results are obtained with the following parameters: base pair onsite energies $\epsilon_{\mathrm{A}} = -0.26\,\mathrm{eV}$, $\epsilon_{\mathrm{G}} = +0.25\,\mathrm{eV}$, polaron shifts $\Delta_{\mathrm{A}} = 0.18\,\mathrm{eV}$ and $\Delta_{\mathrm{G}} = 0.47\,\mathrm{eV}$, Fermi energy $E_{\mathrm{F}} = 0\,\mathrm{eV}$, symmetric coupling to leads with linewidth $\Gamma_{\mathrm{L}} = \Gamma_{\mathrm{R}} = 0.01\,\mathrm{eV}$, vibrational energies $\hbar\omega_{\mathrm{A}} = 11\,\mathrm{meV}$, $\hbar\omega_{\mathrm{G}} = 16\,\mathrm{meV}$, and room temperature $k_{\mathrm{B}}T = 25\,\mathrm{meV}$.

occupation and consequently the current, only depends on the single-particle densities. The I-V curves are therefore identical with or without correlation effects.

Throughout this chapter we will present various results which include correlations effects, i. e. when the single- and two-particle density matrix are calculated by simultaneous numerical iteration of the corresponding rate equations. The number of rate equation for the two-particle density matrices increases quadratically with the number of DNA bases, leading to numerical difficulties in the calculations for large systems. We therefore consider only nearest-neighbor correlation functions $\rho_{i,i+1}$ (unless indicated differently), as they have the most important influence on the transport properties of the DNA. This is obvious as only these two-particle density matrix elements directly enter in the rate equations for the single-particle density matrix (Eqs. 6.13 and 6.14). The other two-particle correlation functions only indirectly enter through the rate equation for the two-particle density matrix. In a later part of this chapter we will explicitly show the validity of this assumptions, as the correlation functions of more distant base pairs only slightly change the results. The main physical effects remain unchanged.

6.2.1. Correlation effects

Figure 6.7(a) shows a comparison of the differential conductance with (full lines) and without (dashed lines) correlation effects for the sequences GAAAAAAG (black lines) and GGAAAAGG (red lines). The dashed curves are identical to the ones presented in Fig. 5.5 of the previous chapter. Figure 6.7(b) displays the corresponding I-V characteristics for the situation with correlation effects. For both sequences the current at negative bias is reduced by about an order of magnitude when correlation effects are

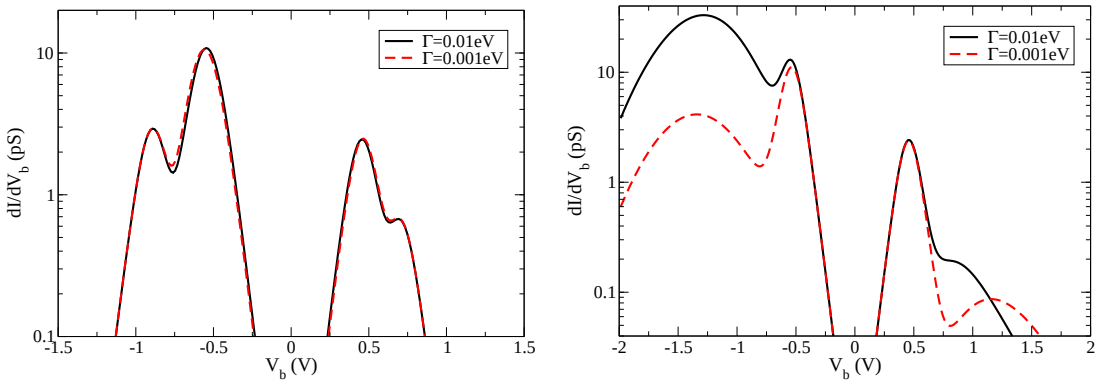

Figure 6.8: Differential conductance as a function of applied bias for DNA molecules with sequence AAAAGAAA (a) and GAAAAAAG (b) for two different electrode coupling strengths $\Gamma_{\mathrm{L/R}} = 0.01\,\mathrm{eV}$ (black lines) and $\Gamma_{\mathrm{L/R}} = 0.001\,\mathrm{eV}$ (red lines). For AAAAGAAA there is only a very weak dependence on $\Gamma_{\mathrm{L/R}}$, in particular the secondary peak at high positive and negative bias is not effected. For GAAAAAAG the secondary maxima are strongly lowered and broadened for smaller $\Gamma_{\mathrm{L/R}}$. The primary maxima are only weakly affected. All parameters as in Fig. 6.7.

considered as can be estimated from the area under the differential conductance curves. For positive bias (not shown) the reduction is only about a factor of 2. As discussed in the previous chapter the position of the current threshold, i. e. the primary maximum in the differential conductance, is not determined by an internal energy scale alone, but also by the specific charge rearrangements in the DNA. This is also seen for the case of correlations, where the position of the conductance peak has slightly shifted to lower bias voltages, as compared to the uncorrelated results. The most prominent change, though, is the additional secondary maximum in the dI/dV_{b} of the sequence GAAAAAAG, when correlation effects are considered. Without correlation effects the differential conductance only shows a very broad single peak. This indicates that a new energy scale is introduced into the system by the correlation.

Additional energy scale

In the following we will show some situations in which secondary peaks in the differential conductance or likewise steps in the I-V characteristics arise. Figure 6.8 shows the differential conductance dI/dV_{b} as a function of applied bias V_{b} for two DNA molecules with sequences AAAAGAAA (6.8(a)) and GAAAAAAG (6.8(b)) for two different electrode coupling strengths $\Gamma_{\mathrm{L/R}} = 0.01\,\mathrm{eV}$ and $\Gamma_{\mathrm{L/R}} = 0.001\,\mathrm{eV}$. For the sequence AAAAGAAA we can identify two maxima in the differential conductance for positive and negative bias, respectively — at $V_{\mathrm{b}} = -0.9\,\mathrm{V}$, -0.55 V, 0.46 V, and 0.7 V. The primary peak or threshold indicates the voltage at which the current sets in. As discussed in the previous chapter, the position of the the primary peak is not given by an internal energy scale alone. Rather the position is determined by internal energies and the way the charges rearrange for an applied bias voltage, which depends very sensitively on the DNA sequence.

The secondary peaks for both positive and negative bias can be identified with new energy scales arising from the correlations. The position of these peaks is also strongly dependent on the sequence, as will become clear from the results for other sequences. Changing the coupling to the electrodes by one order of magnitude does not change the transport characteristics for the sequence AAAAGAAA, as the bottleneck of the system is the hopping to guanine on the inside of the DNA[2]. Astonishingly, by adding a second guanine in the center (AAAGGAAA, not shown), the secondary maxima vanish completely, whereas the primary maxima remain unchanged. This indicates that the correlations only introduce a new energy scale when a single isolated guanine is present in the sequence. Nevertheless, the correlations change the transport characteristics, even when no secondary maximum arises. A similar effect is always seen when a single base is surrounded by other bases with a different onsite energy (not shown).

For the sequence GAAAAAAG there are also two maxima at positive and negative bias, but for positive bias, the second always seen, peak is strongly suppressed as compared to AAAAGAAA. The positions of the primary peaks for GAAAAAAG agree well with the values for AAAAGAAA, but the positions of the secondary maxima clearly differ. The main difference of GAAAAAAG to the other sequence is the dependence on the electrode coupling Γ. For smaller Γ the secondary maxima are strongly reduced, broadened, and the positions are shifted. This behavior is a clear indication that these maxima arise from correlations associated with the injection onto the guanine base from the interface (or the reverse process). In contrast, the secondary peaks for the sequence AAAAGAAA arise from correlations associated with a hopping process onto the guanine base in the center of the sequence.

If a controlled way to vary the coupling between DNA molecule and electrode were at hand, this effect could be easily studied experimentally. If indeed it was found, that secondary maxima existed and were, depending on the sequence, either sensitive or insensitive to the electrode coupling, then this could be an indication that the physics involved in charge migration along DNA was similar to the one we described. It should also be noted, that by adding further guanine bases at the front and at the end of GAAAAAAG (GGAAAAGG) the secondary maxima vanish as can be seen in Fig. 6.7. As mentioned above the same phenomena was found for AAAAGAAA.

Correlation function

To further explain what happens when a new energy scale is introduced, we take a look at the correlation functions ρ_{ij}, to identify the voltage at which the correlations become important. In particular, we discuss the relative correlation $\Delta\rho_{ij}$, i.e. the quantity

$$\Delta\rho_{ij} = \frac{\rho_{ij} - \rho_i\rho_j}{\rho_i\rho_j} \,. \tag{6.15}$$

When correlations are irrelevant $\Delta\rho_{ij} = 0$, but when correlations exist $\Delta\rho_{ij}$ is either positive or negative. The influence of the correlation function $\rho_{i,i+1}$ on the current is most

[2]In real DNA there would be a competing process, i. e. tunneling through the G between the surrounding A bases, which is so far not considered in our model.

important when the bases i and $i+1$ have different onsite energies. For equal energies the terms involving the correlation functions $\rho_{i,i+1}$ drop out of the rate equations for the single-particle density matrix (Eq. 6.13 and 6.14) as discussed above for homogeneous sequences. In Figure 6.9 and 6.10 the characteristics of the correlation functions $\Delta\rho_{ij}$ are displayed for the two sequences AAAAGAAA and GAAAAAAG, respectively.

In Fig. 6.9(a) the relative correlations $\Delta\rho_{45}$ (AG) and $\Delta\rho_{56}$ (GA) are compared with the differential conductance for the sequence AAAAGAAA. These correlations are the most interesting as the single guanine base is at position 5 in the sequence. As indicated by the dashed vertical lines, the correlations set in at the same voltage V_b as the secondary maxima in the differential conductance arise. It is therefore, reasonable to assume that the secondary peak in the dI/dV_b and the correlations at this link are connected. Figure 6.9(b) shows a comparison of $\Delta\rho_{i,i+1}$ for all bases i of the sequence AAAAGAAA for the two different electrode coupling strengths $\Gamma = 0.01\,\mathrm{eV}$ and $\Gamma = 0.001\,\mathrm{eV}$ at the two bias voltages $V_\mathrm{b} = -0.88\,\mathrm{V}$ (top panel) and $V_\mathrm{b} = -0.68\,\mathrm{V}$ (bottom panel). These voltages agree with the secondary maxima (for both negative and positive bias voltage) in the differential conductance shown in Fig. 6.8(a). As in Figure 6.8(a) for the dI/dV_b there is no difference between the correlation functions for the two electrode coupling strengths.

The transport bottlenecks of the sequence AAAAGAAA are the transitions $4 \to 5$ for positive and $6 \to 5$ for negative bias. The relative correlations associated with these transitions $\Delta\rho_{45}$ ($\Delta\rho_{56}$) are negative for positive (negative) bias. For the sequence AAAGGAAA, which does not have a secondary maximum, the relative correlations associated with the respective bottleneck transitions are zero. One could therefore argue that $\Delta\rho_{i,i+1} < 0$ at bottlenecks leads to secondary maxima in the differential conductance. Unfortunately, for more complicated sequences this argument is too simple. For the sequence AAAAGAAA, the 'non-bottleneck' transition from guanine to adenine ($5 \to 6$ for positive and $5 \to 4$ for negative bias) lead to $\Delta\rho_{i,i+1} > 0$.

For the sequence GAAAAAAG the dependence of the correlation functions on Γ is different. Figure 6.10(b) shows a comparison of $\Delta\rho_{i,i+1}$ for all bases i of the sequence GAAAAAAG for $\Gamma = 0.01\,\mathrm{eV}$ and $\Gamma = 0.001\,\mathrm{eV}$. The two bias voltages $V_\mathrm{b} = -1.28\,\mathrm{V}$ (top panel) and $V_\mathrm{b} = -1.00\,\mathrm{V}$ (bottom panel) are chosen to agree with the secondary maxima (for both negative and positive bias voltage) in the differential conductance shown in Fig. 6.8(b)[3]. The value of $\Delta\rho_{12}$ ($\Delta\rho_{78}$) for negative (positive) bias voltage changes strongly with Γ just as the secondary maxima of the differential conductance (Fig. 6.8(b)). Again a strong relationship between correlations and secondary maxima in the differential conductance is obvious.

For positive bias the transport bottleneck of the DNA molecule is the hopping transition from the adenine (base 7) to the guanine (base 8). For negative bias the bottleneck is the transition from base 2 to base 1. As with the sequence AAAAGAAA, these bottlenecks produce negative relative correlation ($\Delta\rho_{i,i+1} < 0$). For all other sites i $\Delta\rho_{i,i+1} = 0$. In Fig. 6.10(a) the relative correlation $\Delta\rho_{12}$ and $\Delta\rho_{78}$ are compared with the differential

[3]Since the position of the secondary maxima shift with Γ a value between the maxima for both couplings is chosen.

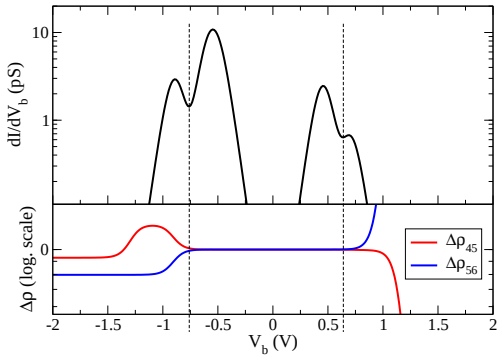

(a) top panel: Differential conductance (logarithmic scale) vs. bias voltage. bottom panel: correlation functions $\Delta\rho_{45}$ (red line) and $\Delta\rho_{56}$ (blue line) (logarithmic scale) vs. bias voltage (with $\Gamma = 0.01\,\mathrm{eV}$).

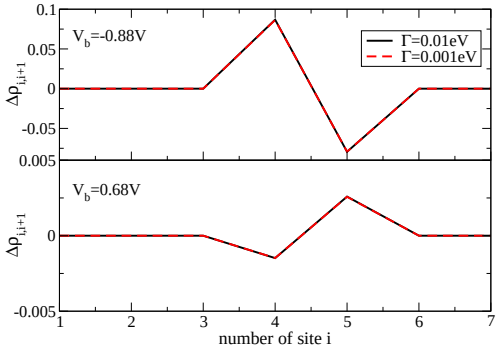

(b) correlation function $\Delta\rho_{i,i+1}$ with electrode coupling $\Gamma = 0.01\,\mathrm{eV}$ (black line) and $\Gamma = 0.001\,\mathrm{eV}$ (red line) for $V_\mathrm{b} = -0.88\,\mathrm{V}$ (top panel) and $V_\mathrm{b} = 0.68\,\mathrm{V}$ (bottom panel).

Figure 6.9: Characteristics of DNA molecule with sequence AAAAGAAA. All parameters as in Fig. 6.7.

conductance for the sequence GAAAAAAG. The dashed vertical lines again indicate that the correlations set in at the same voltage V_b as the secondary maxima in the differential conductance arise (compare to Fig. 6.9(a)).

More complicated sequences

So far we have only discussed the influence of the correlations on relatively simple DNA sequences. For those systems, the connection between correlations and current or differential conductance is quite easily established. Nevertheless, the physical reason why correlations arise at a specific bias voltage is not clear.

For more complicated sequences the above discussed behavior holds also, i. e. when single guanine or adenine bases are present in the sequence an additional energy scale arise, which is reflected as a secondary maximum in the differential conductance. Figure 6.11 shows the characteristics of a DNA molecule with sequence GAATGAC, with single guanine (cytosine) at the ends and in the center and a single adenine between a guanine and a cytosine. The shape of the differential conductance curve (Fig. 6.11(a)) is similar to the one of AAAAGAAA. On the other hand, the fact that the secondary maxima decrease strongly with the electrode coupling Γ indicates that they arise from the correlations at the electrode interfaces. This is partly supported by the relative correlation $\Delta\rho_{i,i+1}$ shown in Fig. 6.11(b). The relative correlations are shown for the voltages that agree with the secondary maxima at negative and positive bias. For negative bias only $\Delta\rho_{12} \neq 0$, which decreases with Γ. For positive bias $\Delta\rho_{67} < 0$ but $\Delta\rho_{56} > 0$, i. e. correlations between the guanine and adenine at positions 5 and 6 also seem to be relevant for positive bias voltages at the secondary maximum. Nevertheless, both correlations decrease with the coupling to the electrodes. The influence of the correlations $\Delta\rho_{56}$ is not quite clear. At higher bias more correlations arise (not shown), but a connection of these with the I-V could so far not be established.

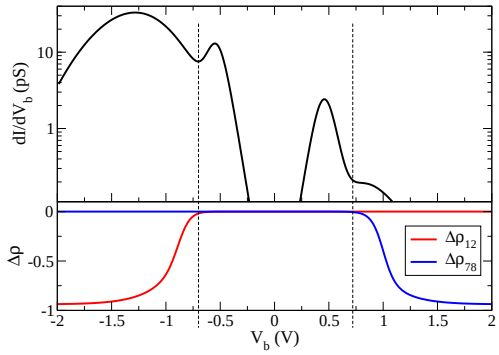

(a) top panel: Differential conductance (logarithmic scale) vs. bias voltage. bottom panel: correlation functions $\Delta\rho_{12}$ (red line) and $\Delta\rho_{78}$ (blue line) vs. bias voltage (with $\Gamma = 0.01\,\mathrm{eV}$).

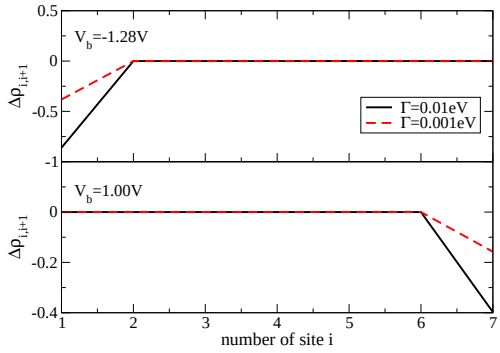

(b) correlation function $\Delta\rho_{i,i+1}$ with electrode coupling $\Gamma = 0.01\,\mathrm{eV}$ (black line) and $\Gamma = 0.001\,\mathrm{eV}$ (red line) for $V_\mathrm{b} = -1.28\,\mathrm{V}$ (top panel) and $V_\mathrm{b} = 1.00\,\mathrm{V}$ (bottom panel).

Figure 6.10: Characteristics of DNA molecule with sequence GAAAAAAG. All parameters as in Fig. 6.7.

It can be summarized that the correlations due to single guanine bases at the electrode junctions dominate the behavior of the secondary maxima with respect to Γ. Additional single guanine (or adenine) bases in the center of the sequence do not lead to Γ independent secondary maxima, as was observed for AAAAGAAA (Fig. 6.8(a)).

6.2.2. Long-range vs. short-range correlation

In the entire chapter we restricted our calculations to nearest-neighbor correlations and ignored correlations between more distant base pairs. The inclusion of long-range correlations to some degree changes the I-V characteristics, but the essential physical effects are not affected. Figure 6.12(a) shows the current and differential conductance of the DNA sequence GAAAAAAG including and neglecting long-range correlations. The first step at negative bias in the I-V characteristics is flattened out when long-range correlations are considered. This reduces the primary maximum in the differential conductance to a shoulder. The same happens to the secondary maximum at positive bias. For high bias voltages the currents including or neglecting long-range correlations are equal, showing that at these voltages long-range correlations are irrelevant.

This interpretations is validated by Fig. 6.12(b), which shows the (absolute value of the) relative correlation $|\Delta\rho_{1j}|$ between the first and jth base as a function of j. The black line shows the distance dependence for a bias voltage $V_\mathrm{b} = -1.24\,\mathrm{V}$, i. e. at the position of the secondary maximum at negative bias. The relative correlation decrease exponentially with the distance — already for $j = 3$ the correlations are one order of magnitude smaller than for $j = 2$. At a bias $V_\mathrm{b} = -0.56\,\mathrm{V}$, where the differential conductances in Fig. 6.12(a) differ the most, the relative correlations decrease far slower but still exponentially. Therefore, long-range correlations at this bias voltage are more important. Note that the data point for the eighth base differs from the exponential

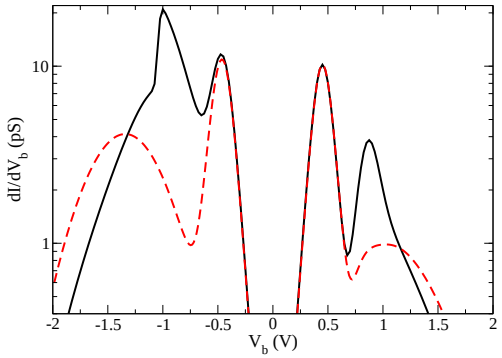

(a) Differential conductance vs. bias voltage for $\Gamma_{\mathrm{L/R}} = 0.01\,\mathrm{eV}$ (black line) and $\Gamma_{\mathrm{L/R}} = 0.001\,\mathrm{eV}$ (red line).

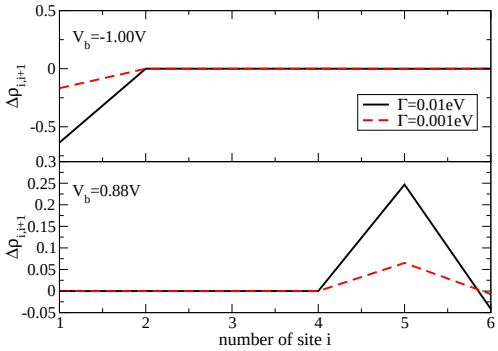

(b) correlation function $\Delta\rho_{i,i+1}$ with electrode coupling $\Gamma = 0.01\,\mathrm{eV}$ (black line) and $\Gamma = 0.001\,\mathrm{eV}$ (red line) for $V_\mathrm{b} = -1.00\,\mathrm{V}$ (top panel) and $V_\mathrm{b} = 0.88\,\mathrm{V}$ (bottom panel).

Figure 6.11: Characteristics of DNA molecule with sequence GAATGAC. All parameters as in Fig. 6.7.

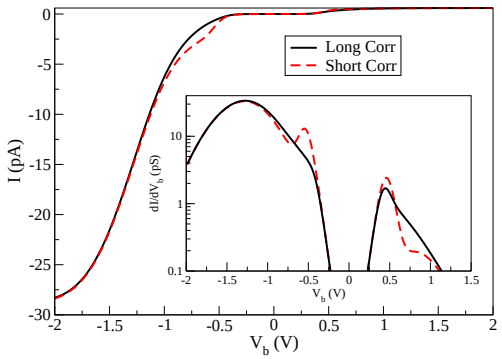

(a) Current and differential conductance as a function of applied bias. The black lines show the results when correlation between all base pairs were included. The red lines show the approximative result, where only correlations between nearest neighbors were considered.

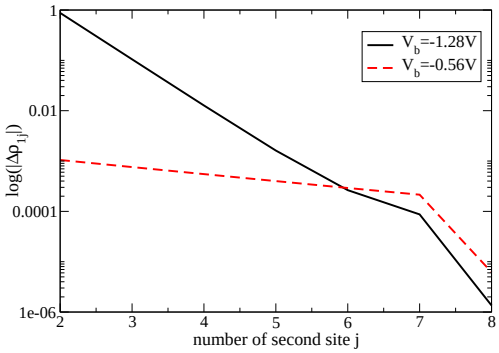

(b) Relative correlation between first and jth base $|\Delta\rho_{1j}|$ (logarithmic scale) vs. j. The bias voltage $V_\mathrm{b} = -1.24\,\mathrm{V}$ and $V_\mathrm{b} = -0.56\,\mathrm{V}$ are chosen to agree with the position of the first and second maximum at negative bias.

Figure 6.12: Characteristics of DNA sequence GAAAAAAG including long-range correlations. All parameters as in Fig. 6.7.

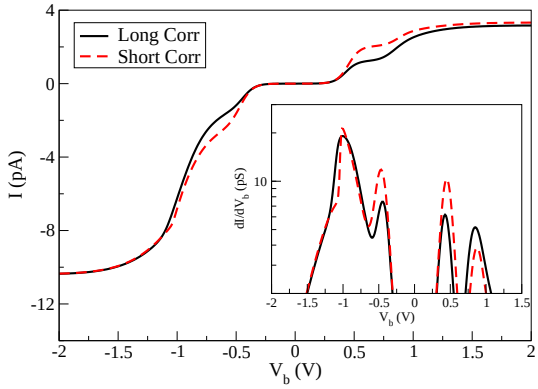

Figure 6.13: Current and differential conductance as a function of applied bias for GAATGAC. The black lines show the results when correlation between all base pairs were included. The red lines show the approximative result, where only correlations between nearest neighbors were considered. All parameters as in Fig. 6.7.

behavior for both voltages as it is a guanine base, whereas the other six bases are adenine bases.

To show that these arguments hold also for more complicated DNA sequences, Fig. 6.13 depicts the current and differential conductance as a function of applied bias for the sequence GAATGAC, which we studied above. Here all primary and secondary maxima in the differential conductance are clearly visible. The inclusion of long-range correlations slightly changes the shape and height of these peaks in the differential conductance, but for high positive and negative voltages the current is again identical with the approximation of nearest-neighbor correlations.

Non-local electron-vibration coupling

As we have explained in the fourth chapter, non-local or non-diagonal electron vibration coupling is also strong in DNA. Disregarding such coupling may neglect some important physical effects. Consequently, it might be interesting to generalize our approach to include non-local electron vibration coupling. In the following we shortly sketch how this could be done by extending the diagrammatic approach described above.

One would have to consider the following non-local electron vibration coupling term as an addition to the perturbative Hamiltonian $\tilde{H}'$

$$\sum_{ij} \lambda_{ij}\, a_i^\dagger \chi_i^\dagger a_j \chi_j \left(B_i + B_i^\dagger + B_j + B_j^\dagger \right) . \tag{6.16}$$

The inclusion of this term into the diagrammatic expansion is not straight forward. Firstly, a new kind of vertex with value $\pm i\lambda_{ij}\mathcal{K}_i\mathcal{K}_j e^{-i(\epsilon_i-\epsilon_j)(t_i-t_2)}$ is obtained. The fermion lines of the diagrams are not affected, but there are all kinds of new vibrational lines. These lines arise from operator products of the kind

$$\begin{aligned} &\left\langle \chi_k(t_1)\chi_j \left(B_k(t_1) + B_k^\dagger(t_1) \right) \chi_k^\dagger(t_2)\chi_k(t_3)\chi_k^\dagger(t_4) \right. \\ &\left. \cdots \chi_k(t_{n-1}) \left(B_k(t_{n-1}) + B_k^\dagger(t_{n-1}) \right) \chi_k^\dagger(t_n) \right\rangle_{H_0} \end{aligned} \tag{6.17}$$

with $(B_k(t_i) + B_k^\dagger(t_i))$ at various positions in the product. A closed formula which describes the value of the vibrational lines is therefore not easily found (compare to Appendix E).

6.3. Summary and outlook

In this chapter we have developed a diagrammatic approach to polaron transport in small molecules coupled to biased metallic electrodes. This approach is based on a real-time expansion of the single-particle density matrix along the Keldysh contour. It extends a technique for polaron transport in bulk systems which was developed by Böttger and Bryskin. We have applied this technique to short DNA molecules with various sequences. This diagrammatic approach includes effects arising from correlations between the occupations of different base pairs, which were not considered in the previous chapter. Correlations are only relevant for inhomogeneous DNA sequences and, in general, they lead to a reduction of the current. For sequences which include single isolated bases surrounded by bases with other onsite energies, a new energy scale arises. This new energy scale stems from correlations associated with the isolated base and leads to a secondary maximum in the differential conductance. Correlations associated with isolated bases in the center of a sequence are insensitive to the coupling to the electrodes, whereas correlations associated with bases at the electrode interface are strongly reduced for decreased coupling to the electrodes. A decrease in the correlations is accompanied by a reduction of the secondary maxima in the differential conductance. We have also shown that correlations between different bases decrease exponentially with the distance, i. e. correlations between nearest-neighbors are the most important.

There are some interesting effects associated with correlations between different bases in DNA molecules, but there remains an open question: What determines the specific voltage, i. e. the energy scale, at which the correlations develop. Some simpler model has to be found that allows more insight into the physical effects that govern such correlations. Furthermore, in real DNA there are other processes, which compete with the nearest-neighbor hopping. These processes are tunneling transitions between bases with equal onsite energies that are no further apart than two or three base pairs. The inclusion of such processes into our theoretical model would lead to a better understanding which effect tunneling has on hopping transport through DNA.

7. Conclusions

In this thesis we have studied electronic transport through short DNA molecules, stressing the influence of base pair vibrations. Experiments and earlier theoretical investigations have shown that vibrations are important in the electronic transport through DNA, although there is still some controversy over the exact influence of vibrations. In particular, the question whether polarons are formed in DNA is not conclusively answered, as only some experimental results favor the idea of polarons. Other experiments show relatively high maximum currents, which agrees better with a (quasi)-coherent transport picture. Therefore, we have discussed transport through DNA in these two limits, by developing independent theoretical methods to study these situations. In both these situations the DNA is described by a minimum tight-binding model, identifying each base pair with one tight-binding site, with parameters taken from experiments and/or *ab initio* calculations.

Firstly, we have investigated the quasi-coherent situation, where the coupling to vibrations introduces inelastic contributions to the current, but a partial coherence of transport is conserved. We have developed an equation-of-motion (EOM) approach for the single-particle Green function of the electrons in the DNA, which describes vibrational effects arising from local *and* non-local electron-vibration coupling. To describe the limit of relatively strong electron-vibration coupling we apply a unitary transformation to the Hamiltonian, canceling the local interaction term. This procedure allows for a truncation of the series of higher-order Green functions arising from the EOM. The truncation is physically justified for small non-local coupling. As we assume that the chemical potential of the DNA coupled to the electrodes lies in the gap between highest occupied and lowest unoccupied molecular orbital (HOMO and LUMO), DNA molecules will in general experience 'semiconducting' I-V characteristics.

We showed that homogeneous DNA sequences have a band-like density of states with distinct electronic resonances due to finite size. Additionally, vibrational satellites arise energetically above and below the corresponding electronic resonance due to the local electron-vibration coupling. The distance of these vibrational satellites to the corresponding electronic resonance agrees with integer multiples of the vibration energy, where more distant satellites have strongly reduced spectral weights. Furthermore, the density of states displays a strong asymmetry due to the non-local electron-vibration coupling, but, nevertheless, its effect on the current is rather small. The transport through a homogeneous DNA molecule is dominated by elastic quasi-ballistic contributions. For finite bias and room temperature, scattering of the electrons with the vibrations decreases the current by about 30% as compared to the vibrationless case. On the other hand, the coupling to vibrations enhances the zero-bias conductance at low temperatures by several orders of magnitude. The reason for this lies in the emergence of vibrational satellites in the gap, which have non-zero transmission.

As inhomogeneous DNA sequences experience Anderson localization, the density of states is highly fragmented. As for the homogeneous sequence, there are electronic resonances and vibrational satellites. For such DNA molecules electronic transport is almost entirely governed by inelastic processes. That means that the energy to overcome the potential barriers in the DNA, associated with the inhomogeneous sequence, is provided by the base pair vibrations. We exemplary studied the sequence 5'-CAT TAA TGC TAT GCA GAA AAT CTT AG-3', which I-V characteristics show distinct steps associated with the energies of either pure or hybridized states of guanine and adenine. This states can be identified in the density of states at $E - E_\mathrm{F} = -0.3\,\mathrm{eV}$, -0.7 eV, and -0.95 eV. We could show, that in contrast to homogeneous DNA, the non-local electron-vibration coupling qualitatively modifies the I-V characteristics for inhomogeneous DNA molecules. In particular, for our model sequence the transmission of the states around $E - E_\mathrm{F} = -0.7\,\mathrm{eV}$ was halved.

Astonishingly, we found that the current through such inhomogeneous DNA sequences depends non-monotonically on the electrode-DNA coupling Γ. The current reaches a maximum value when Γ is about equal to the imaginary part of the vibrational self-energy $\Sigma_\mathrm{vib} \approx 0.01\,\mathrm{eV}$. This shows that it is not always better to maximize the coupling of the DNA to the electrodes and that a systematic (experimental) study of the coupling is needed.

Secondly, we studied the limit of incoherent polaron hopping transport through short DNA molecules coupled to biased leads. The polarons are formed due to strong interaction between electrons and base pair vibrations, which are assumed to be independent of the vibrations of other base pairs. To describe strong local electron-vibration coupling a unitary transformation is performed on the Hamiltonian, giving rise to new parameters for a perturbative expansion. These are the hopping (t_{ij}/Δ) and tunneling $(t_i^{\mathrm{L/R}}/\Delta)$ strengths normalized by the polaron binding energy Δ, which is $\Delta_\mathrm{G} = 0.47\,\mathrm{eV}$ and $\Delta_\mathrm{A} = 0.18\,\mathrm{eV}$ for guanine and adenine, respectively. To derive the current through such a system, we stated a set of rate equations for the occupation number of the various DNA base pairs, with rates obtained from Golden Rule arguments. These rates take into account inelastic hopping transitions involving excitation or absorption of local base pair vibrations.

For all DNA molecules we observe semi-conducting I-V characteristics, which are symmetric for homogeneous and symmetric sequences, but show rectifying behavior for all non-symmetric sequences. The reason for this, lies in the fact that the 'bottlenecks' for transport are hopping transitions, where a potential step has to be overcome. Since these steps are, in general, different for positive or negative bias voltage they lead to different currents. We showed that the current thresholds are very sensitive to the considered sequence. For homogeneous sequences they agree with the polaron shifted onsite energy of the corresponding base pairs, but for inhomogeneous sequences the thresholds are not directly related to intrinsic energy scales. For such DNA molecules the non-trivial charge rearrangement at finite bias determine the exact position of the threshold, which is somewhere in between the limits set by the onsite energies of guanine and adenine. The shape of the thresholds differs from the Fermi function form. This change in shape is the most prominent for the sequence 'GAAAAAAG' with only single guanine base pairs at both ends, which shows a very broad peak, whereas for other sequences, comprising

more than a single guanine at the ends, the thresholds are only slightly broadened. The effect of charge rearrangements is visualized by displaying the local chemical potential Φ_i, which illustrates how the applied bias voltage 'drops' over the entire DNA molecule. As expected most of the voltage drops at the junctions to the electrodes and at the 'bottlenecks' of the sequence.

We show that the current for a homogeneous DNA molecule is thermally activated with a temperature dependence following an Arrhenius-law, which is expected for polaron hopping transport. This result agrees well with some recent experiments. The obtained activation energy E_a depends on the applied bias voltage and approaches the bulk polaron value $E_a = \Delta/2$ for voltages above the threshold.

In the third part of this thesis we have developed a general approach to polaron transport through mesoscopic systems coupled to biased electrodes, which is not restricted to DNA. The approach is based on a diagrammatic real-time expansion of the single particle density matrix along the Keldysh contour. The consideration of non-diagonal elements of the single-particle density matrix allows the inclusion of coherence effects in the description of polaron hopping. Furthermore, by nature of the diagrammatic expansion, divergences associated with resonant tunneling, which where neglected in the previous part by phenomenological arguments, do not occur. Instead, the possibility of resonant tunneling gives rise to correlation effects between occupations of different sites.

We apply this approach to polaron hopping transport through DNA. In the limit of strong electron-vibration coupling and high temperature coherence effects can be neglected and we consider only the diagonal elements of the single particle density matrix. In contrast to the previous part, we now consider correlations between the occupation of different sites and study when such correlations occur and which changes they promote in the transport characteristics. We showed that these correlations only affect inhomogeneous DNA sequences and, in general, lead to a reduction of the current of up to one order of magnitude for high voltages. Most importantly, for some DNA sequences they can introduce a new energy scale, which manifests itself as an additional peak in the differential conductance. This new energy scale arises from correlations associated with DNA bases in a sequence that are surrounded by bases with other onsite energies, e. g. the guanine in AAAAGAAA. At bias voltages where these relative correlations (Eq. 6.15) start to differ strongly from zero, the secondary maxima arise in the differential conductance. These secondary peaks arise at voltage above the primary current threshold, but their exact position strongly depends on the considered DNA sequence.

We find that correlations which are associated with isolated bases at the electrode interface (e. g. GAAAAAAG) strongly depend on the electrode coupling strength Γ. For decreased coupling the correlations and also the associated secondary peaks in the differential conductance are strongly reduced. On the other hand, correlations associated with isolated bases in the center of a sequence (e. g. AAAAGAAA) are insensitive to the electrode coupling and consequently also the secondary maxima do not vary. This behavior changes, if additional to the isolated base in the center there are isolated bases at the electrode junctions (e. g. GAATGAC). In such a case the correlations associated with the base in the center are also reduced when the electrode coupling is decreased. We have also shown that correlations between nearest-neighbors are the most important, as the correlations decrease exponentially with the distance.

Inelastic effects are important to transport in DNA and can lead to different behavior, depending on the strength and nature of the coupling between electronic and vibrational degrees of freedom. Hopefully this work will help to interpret the results of electronic transport experiments with short DNA molecules and lead to a deeper understanding of the physics involved.

Appendix A. Useful relations

A.1. Green functions

The various Green functions are defined by

$$G^{>}_{kl}(t,t') = -i\left\langle a_k(t)a_l^{\dagger}(t')\right\rangle \tag{A.1}$$

$$G^{<}_{kl}(t,t') = i\left\langle a_l^{\dagger}(t')a_k(t)\right\rangle \tag{A.2}$$

$$G^{\mathrm{ret}}_{kl}(t,t') = -i\theta(t-t')\left\langle\left\{a_k(t),a_l^{\dagger}(t')\right\}\right\rangle \tag{A.3}$$

$$= \theta(t-t')\left(G^{>}_{kl}(t,t') - G^{<}_{kl}(t,t')\right) \tag{A.4}$$

$$G^{\mathrm{adv}}_{kl}(t,t') = i\theta(t'-t)\left\langle\left\{a_k(t),a_l^{\dagger}(t')\right\}\right\rangle \tag{A.5}$$

$$= \theta(t'-t)\left(G^{<}_{kl}(t,t') - G^{>}_{kl}(t,t')\right)\ , \tag{A.6}$$

where only three of the four Green functions defined above are independent. The fourth Green function is given by the relations

$$G^{>}_{kl}(t,t') - G^{<}_{kl}(t,t') = G^{\mathrm{ret}}_{kl}(t,t') - G^{\mathrm{adv}}_{kl}(t,t') \tag{A.7}$$

$$G^{>}_{kl}(E) - G^{<}_{kl}(E) = G^{\mathrm{ret}}_{kl}(E) - G^{\mathrm{adv}}_{kl}(E)\ . \tag{A.8}$$

The retarded Green functions follows the Dyson equation given by

$$G^{\mathrm{ret}}(E) = \left[\left(G_0^{\mathrm{ret}}(E)\right)^{-1} - \Sigma^{\mathrm{ret}}(E)\right]^{-1}\ ,\ \text{with} \tag{A.9}$$

$$G_0^{\mathrm{ret}}(E) = \left[E - H + i0^{+}\right]^{-1}\ , \tag{A.10}$$

where H is the Hamiltonian of the system.

The lesser Green can be calculated from the retarded and advanced Green functions and the respective self-energies by the kinetic equation

$$G^{<}(E) = G^{\mathrm{ret}}(E)\left[\Sigma^{<}(E)\right]G^{\mathrm{adv}}(E)\ , \tag{A.11}$$

where for the last three equations the Green functions where assumed to be matrices in the site indices k, l.

The complex conjugate of the Green functions read

$$\left[G^{>/<}_{kl}(t,t')\right]^{*} = -G^{>/<}_{lk}(t',t) \quad \text{and} \quad \left[G^{>/<}_{kl}(E)\right]^{*} = -G^{>/<}_{lk}(E) \tag{A.12}$$

$$\left[G^{\mathrm{ret}}_{kl}(t,t')\right]^{*} = G^{\mathrm{adv}}_{lk}(t',t) \quad \text{and} \quad \left[G^{\mathrm{ret}}_{kl}(E)\right]^{*} = G^{\mathrm{adv}}_{lk}(E)\ . \tag{A.13}$$

In equilibrium the fluctuation-dissipation relation is valid

$$G^{>}_{kl}(E) = \left(1 - f(E)\right)\left(G^{\mathrm{ret}}_{kl}(E) - G^{\mathrm{adv}}_{kl}(E)\right) \tag{A.14}$$

$$G^{<}_{kl}(E) = -f(E)\left(G^{\mathrm{ret}}_{kl}(E) - G^{\mathrm{adv}}_{kl}(E)\right)\ . \tag{A.15}$$

A.2. Langreth rules

Let us consider some contour ordered Green functions (A, B, C, and D) which are evaluated at specific times τ_i on the Keldysh contour [94, 124]. The associated real-time Green functions (lesser, retarded ...) of products and convolutions of these contour ordered Green functions are found from the Langreth rules.

For easier readability we do not explicitly write out the time arguments for convolutions with respect to time. That implies for a convolution on the contour $C = \int_C AB \rightarrow C(\tau,\tau') = \int_C d\tau_1 A(\tau,\tau_1)B(\tau_1,\tau')$ and similar for a convolution on the real-time axis.

Contour	Real-time axis
$C = \int_C AB$	$C^< = \int_t \left[A^{\rm ret}B^< + A^<B^{\rm adv}\right]$
	$C^{\rm ret} = \int_t A^{\rm ret}B^{\rm ret}$
$D = \int_C ABC$	$D^< = \int_t \left[A^{\rm ret}B^{\rm ret}C^< + A^{\rm ret}B^<C^{\rm adv} + A^<B^{\rm adv}C^{\rm adv}\right]$
	$D^{\rm ret} = \int_t A^{\rm ret}B^{\rm ret}C^{\rm ret}$
$C(\tau,\tau') = A(\tau,\tau')B(\tau,\tau')$	$C^<(t,t') = A^<(t,t')B^<(t,t')$
	$C^{\rm ret}(t,t') = A^<(t,t')B^{\rm ret}(t,t') + A^{\rm ret}(t,t')B^<(t,t') + A^{\rm ret}(t,t')B^{\rm ret}(t,t')$
$C(\tau,\tau') = A(\tau,\tau')B(\tau',\tau)$	$C^<(t,t') = A^<(t,t')B^>(t',t)$
	$C^{\rm ret}(t,t') = A^<(t,t')B^{\rm adv}(t',t) + A^{\rm ret}(t,t')B^<(t',t)$

The above expressions are taken from [124].

Appendix B. Boson correlator

B.1. Commutation relation with the Hamiltonian

We want to calculate the commutator $[\tilde{H}, \chi]$, where the only relevant parts of the Hamiltonian (Eq. 4.3) are the ones including vibrational operators B_α, since χ commutes with all fermion operators and with itself ($[\chi, \chi] = [\chi^\dagger, \chi] = 0$). Using the Feynman rule for disentangling of operators

$$e^{A+B} = e^A e^B e^{-\frac{1}{2}[A,B]} \quad \text{if } [A,[A,B]] = [B,[A,B]] = 0$$

we can write

$$\begin{aligned}
\chi &= \exp\left[\sum_\alpha \left(\frac{\lambda_0}{\omega_\alpha} B_\alpha - \frac{\lambda_0}{\omega_\alpha} B_\alpha^\dagger\right)\right] \\
&= \prod_\alpha \exp\left[\frac{\lambda_0}{\omega_\alpha} B_\alpha - \frac{\lambda_0}{\omega_\alpha} B_\alpha^\dagger\right] \\
&= \prod_\alpha \underbrace{\exp\left[\frac{\lambda_0}{\omega_\alpha} B_\alpha\right]}_{I_\alpha} \underbrace{\exp\left[-\frac{\lambda_0}{\omega_\alpha} B_\alpha^\dagger\right]}_{J_\alpha} \underbrace{\exp\left[-\frac{\lambda_0^2}{2\omega_\alpha^2}\right]}_{K_\alpha} .
\end{aligned}$$

We now perform the commutation

$$\begin{aligned}
\left[\tilde{H}, \chi\right] &= \sum_\alpha \prod_{\alpha' \neq \alpha} I_{\alpha'} J_{\alpha'} K_{\alpha'} \cdot \left[\tilde{H}, I_\alpha J_\alpha K_\alpha\right] \\
&= \sum_\alpha \prod_{\alpha' \neq \alpha} I_{\alpha'} J_{\alpha'} K_{\alpha'} \cdot \left\{\left[\tilde{H}, I_\alpha\right] J_\alpha K_\alpha + I_\alpha \left[\tilde{H}, J_\alpha\right] K_\alpha\right\} ,
\end{aligned}$$

since $\left[I_{\alpha'} J_{\alpha'} K_{\alpha'}, \left[\tilde{H}, I_\alpha J_\alpha K_\alpha\right]\right] = 0$ for $\alpha' \neq \alpha$.
Let us look at the two remaining commutators separately.

(1)

$$\begin{aligned}
\left[\tilde{H}, I_\alpha\right] &= \sum_n \frac{1}{n!} \left(\frac{\lambda_0}{\omega_\alpha}\right)^n [\tilde{H}, B_\alpha^n] \\
&= \sum_n \frac{n}{n!} \left(\frac{\lambda_0}{\omega_\alpha}\right)^n [\tilde{H}, B_\alpha] \, B_\alpha^{n-1} \quad \text{since } [B_\alpha, [\tilde{H}, B_\alpha]] = 0 .
\end{aligned}$$

Using

$$\begin{aligned}\left[\tilde{H}, B_\alpha\right] &= -\omega_\alpha B_\alpha - \sum_{<ij>} \lambda_1 \, a_i^\dagger a_j \quad \text{and} \\ \left[\tilde{H}, B_\alpha^n\right] &= 0 \quad \text{for n=0 ,}\end{aligned}$$

we obtain

$$\begin{aligned}\left[\tilde{H}, I_\alpha\right] &= \sum_{n=1}^{\infty} \frac{1}{(n-1)!} B_\alpha^{n-1} \left(\frac{\lambda_0}{\omega_\alpha}\right)^{n-1} \left[\frac{\lambda_0}{\omega_\alpha}\left\{-\omega_\alpha B_\alpha - \sum_{<ij>} \lambda_1 \, a_i^\dagger a_j\right\}\right] \\ &= I_\alpha \left[-\lambda_0 B_\alpha - \sum_{<ij>} \frac{\lambda_0 \lambda_1}{\omega_\alpha} \, a_i^\dagger a_j\right] .\end{aligned}$$

(2)

$$\begin{aligned}\left[\tilde{H}, J_\alpha\right] &= \sum_n \frac{1}{n!} \left(\frac{-\lambda_0}{\omega_\alpha}\right)^n [\tilde{H}, B_\alpha^{\dagger n}] \\ &= \sum_n \frac{n}{n!} \frac{-\lambda_0}{\omega_\alpha}^n [\tilde{H}, B_\alpha^\dagger] \, B_\alpha^{\dagger(n-1)} \quad \text{since } [B_\alpha^\dagger, [\tilde{H}, B_\alpha^\dagger]] = 0 .\end{aligned}$$

Using

$$\begin{aligned}\left[\tilde{H}, B_\alpha^\dagger\right] &= \omega_\alpha B_\alpha^\dagger + \sum_{<ij>} \lambda_1 \, a_i^\dagger a_j \quad \text{and} \\ \left[\tilde{H}, B_\alpha^{\dagger n}\right] &= 0 \quad \text{for n=0 ,}\end{aligned}$$

we obtain

$$\begin{aligned}\left[\tilde{H}, J_\alpha\right] &= \sum_{n=1}^{\infty} \frac{1}{(n-1)!} B_\alpha^{\dagger(n-1)} \left(\frac{-\lambda_0}{\omega_\alpha}\right)^{n-1} \left[\frac{-\lambda_0}{\omega_\alpha}\left\{\omega_\alpha B_\alpha^\dagger + \sum_{<ij>} \lambda_1 \, a_i^\dagger a_j\right\}\right] \\ &= J_\alpha \left[-\lambda_0 B_\alpha^\dagger - \sum_{<ij>} \frac{\lambda_0 \lambda_1}{\omega_\alpha} \, a_i^\dagger a_j\right] .\end{aligned}$$

Combining everything, we get

$$\begin{aligned}\left[\tilde{H}, \chi\right] &= \sum_\alpha \prod_{\alpha' \neq \alpha} I_{\alpha'} J_{\alpha'} K_{\alpha'} \cdot \left\{ \left[-\lambda_0 B_\alpha - \sum_{<ij>} \frac{\lambda_0 \lambda_1}{\omega_\alpha} \, a_i^\dagger a_j\right] I_\alpha J_\alpha K_\alpha \right. \\ &\quad \left. + I_\alpha J_\alpha K_\alpha \left[-\lambda_0 B_\alpha^\dagger - \sum_{<ij>} \frac{\lambda_0 \lambda_1}{\omega_\alpha} \, a_i^\dagger a_j\right] \right\} \\ &= \sum_\alpha \left\{ \left[-\lambda_0 B_\alpha - \sum_{<ij>} \frac{\lambda_0 \lambda_1}{\omega_\alpha} \, a_i^\dagger a_j\right] \chi + \chi \left[-\lambda_0 B_\alpha^\dagger - \sum_{<ij>} \frac{\lambda_0 \lambda_1}{\omega_\alpha} \, a_i^\dagger a_j\right] \right\} .\end{aligned}$$

B.2. Explicit expressions for higher order correlators

Explicitely, for the different correlators in the equation for $G^{(1)}_{kl}(t)$ we have

$$\begin{aligned}
\left\langle a_j(t)B_\alpha(t)\chi(t)a_l^\dagger\chi^\dagger\right\rangle &\approx -\frac{\lambda_\alpha}{\omega_\alpha}(N(\omega_\alpha)+1)(1-e^{-i\omega_\alpha t})\left\langle a_j(t)\chi(t)a_l^\dagger\chi^\dagger\right\rangle \\
\left\langle a_j(t)B_\alpha^\dagger(t)\chi(t)a_l^\dagger\chi^\dagger\right\rangle &\approx \frac{\lambda_\alpha}{\omega_\alpha}N(\omega_\alpha)(1-e^{i\omega_\alpha t})\left\langle a_j(t)\chi(t)a_l^\dagger\chi^\dagger\right\rangle \\
\left\langle a_j(t)\chi(t)B_\alpha^\dagger(t)a_l^\dagger\chi^\dagger\right\rangle &\approx \frac{\lambda_\alpha}{\omega_\alpha}\left(1+N(\omega_\alpha)(1-e^{i\omega_\alpha t})\right)\left\langle a_j(t)\chi(t)a_l^\dagger\chi^\dagger\right\rangle
\end{aligned}$$

and for $G^{(2)}_{kl}(t)$

$$\begin{aligned}
\left\langle a_l^\dagger\chi^\dagger a_j(t)B(t)\chi(t)\right\rangle &\approx -\frac{\lambda_\alpha}{\omega_\alpha}\left(1+N(\omega_\alpha)(1-e^{-i\omega_\alpha t})\right)\left\langle a_l^\dagger\chi^\dagger a_j(t)\chi(t)\right\rangle \\
\left\langle a_l^\dagger\chi^\dagger a_j(t)B^\dagger(t)\chi(t)\right\rangle &\approx \frac{\lambda_\alpha}{\omega_\alpha}(N(\omega_\alpha)+1)(1-e^{i\omega_\alpha t})\left\langle a_l^\dagger\chi^\dagger a_j(t)\chi(t)\right\rangle \\
\left\langle a_l^\dagger\chi^\dagger a_j(t)\chi(t)B^\dagger(t)\right\rangle &\approx \frac{\lambda_\alpha}{\omega_\alpha}\left[(N(\omega_\alpha)+1)(1-e^{i\omega_\alpha t})-1\right]\left\langle a_l^\dagger\chi^\dagger a_j(t)\chi(t)\right\rangle \ .
\end{aligned}$$

In the next section the derivation of the first line in the above formulas, is shortly sketched.

Calculation of the higher order boson correlators

Here we sketch the approximation taken to truncate the hierarchy at the first level and how the expressions listed above are calculated. The approximation we take is the following

$$\left\langle a_j(t)B_\alpha(t)\chi(t)a_l^\dagger\chi^\dagger\right\rangle_{\tilde H} \approx F_\alpha(t)\left\langle a_j(t)\chi(t)a_l^\dagger\chi^\dagger\right\rangle_{\tilde H}. \tag{B.1}$$

The function $F_\alpha(t)$ is obtained by considering a Hamiltonian $\tilde H_0$ equivalent to $\tilde H$, but without electron-vibration coupling terms and calculating the same higher order correlation function $\left\langle a_j(t)B_\alpha(t)\chi(t)a_l^\dagger\chi^\dagger\right\rangle_{\tilde H_0}$, where now the average is taken with respect to $\tilde H_0$. Then the electronic and vibrational correlators factorize,

$$\left\langle a_j(t)B_\alpha(t)\chi(t)a_l^\dagger\chi^\dagger\right\rangle_{\tilde H_0} = \left\langle a_j(t)a_l^\dagger\right\rangle_{\tilde H_0^{\rm el}}\left\langle B_\alpha(t)\chi(t)\chi^\dagger\right\rangle_{\tilde H_0^{\rm vib}}, \tag{B.2}$$

where $\tilde H_0^{\rm el}$ and $\tilde H_0^{\rm vib}$ are the electronic and vibrational parts of $\tilde H_0$.

After some straight-forward algebra (see below) we obtain

$$\left\langle B_\alpha(t)\chi(t)\chi^\dagger\right\rangle_{\tilde H_0^{\rm vib}} = F_\alpha(t)\left\langle\chi(t)\chi^\dagger\right\rangle_{\tilde H_0^{\rm vib}}$$

and consequently

$$\left\langle a_j(t)B_\alpha(t)\chi(t)a_l^\dagger\chi^\dagger\right\rangle_{\tilde H_0} = F_\alpha(t)\left\langle a_j(t)\chi(t)a_l^\dagger\chi^\dagger\right\rangle_{\tilde H_0}.$$

So, we want to find an expression for the correlator $\left\langle B_\alpha(t)\chi(t)\chi^\dagger\right\rangle_{\tilde{H}_0^{\rm vib}}$, where $\tilde{H}_0^{\rm vib} = \sum_\alpha \omega_\alpha B_\alpha^\dagger B_\alpha$. For this case the time-evolution for the boson operators become trivial $B_\alpha(t) = B_\alpha e^{-i\omega_\alpha t}$. This derivation proceeds, using ideas from [76]. First we rewrite the correlator and divide it into two parts.

$$\begin{aligned}
&\left\langle B_\alpha(t)\chi(t)\chi^\dagger\right\rangle \\
&= < B_\alpha(t)\exp\Big[\sum_{\alpha'}\frac{\lambda_{\alpha'}}{\omega_{\alpha'}}(B_{\alpha'}(t)-B_{\alpha'}^\dagger(t))\Big]\exp\Big[-\sum_{\alpha'}\frac{\lambda_{\alpha'}}{\omega_{\alpha'}}(B_{\alpha'}-B_{\alpha'}^\dagger)\Big] > \\
&= \prod_{\alpha'\neq\alpha}\underbrace{< \exp\Big[\frac{\lambda_{\alpha'}}{\omega_{\alpha'}}(B_{\alpha'}(t)-B_{\alpha'}^\dagger(t))\Big]\exp\Big[-\frac{\lambda_{\alpha'}}{\omega_{\alpha'}}(B_{\alpha'}-B_{\alpha'}^\dagger)\Big] >}_{F_{\alpha'}(t)} \\
&\quad \times \underbrace{< B_\alpha(t)\exp\Big[\frac{\lambda_\alpha}{\omega_\alpha}(B_\alpha(t)-B_\alpha^\dagger(t))\Big]\exp\Big[-\frac{\lambda_\alpha}{\omega_\alpha}(B_\alpha-B_\alpha^\dagger)\Big] >}_{<Ia>} .
\end{aligned}$$

Now we look at Ia, where we explicitly write the density matrix $\varrho_{\rm vib} = \exp\Big[-\beta\hbar\omega_\alpha n_\alpha\Big]$ and the sum over all quantum mechanical states $|n_\alpha>$, i. e. the occupation numbers of vibrational mode α,

$$\begin{aligned}
< Ia > &= \frac{1}{Z}\sum_{n_\alpha=0}^{\infty}\exp\Big[-\beta\hbar\omega_\alpha n_\alpha\Big] \\
&\times < n_\alpha|B_\alpha(t)\exp\Big[\frac{\lambda_\alpha}{\omega_\alpha}(B_\alpha(t)-B_\alpha^\dagger(t))\Big]\exp\Big[-\frac{\lambda_\alpha}{\omega_\alpha}(B_\alpha-B_\alpha^\dagger)\Big]|n_\alpha> ,
\end{aligned}$$

with $Z = \sum_{n_\alpha=0}^{\infty}\exp\Big[-\beta\hbar\omega_\alpha n_\alpha\Big]$.
Applying the Feynman rule for disentangling of operators (see previous section), we can rewrite

$$\begin{aligned}
&\exp\Big[\frac{\lambda_\alpha}{\omega_\alpha}(B_\alpha e^{-i\omega_\alpha t}-B_\alpha^\dagger e^{i\omega_\alpha t})\Big]\exp\Big[-\frac{\lambda_\alpha}{\omega_\alpha}(B_\alpha-B_\alpha^\dagger)\Big] = \\
&\quad \exp\Big[-\frac{\lambda_\alpha^2}{\omega_\alpha^2}\Big]\exp\Big[-\frac{\lambda_\alpha}{\omega_\alpha}B_\alpha^\dagger e^{i\omega_\alpha t}\Big]\exp\Big[\frac{\lambda_\alpha}{\omega_\alpha}B_\alpha e^{-i\omega_\alpha t}\Big]\exp\Big[\frac{\lambda_\alpha}{\omega_\alpha}B_\alpha^\dagger\Big]\exp\Big[-\frac{\lambda_\alpha}{\omega_\alpha}B_\alpha\Big] .
\end{aligned}$$

using the commutator relationship

$$\begin{aligned}
&\exp\Big[\frac{\lambda_\alpha}{\omega_\alpha}B_\alpha e^{-i\omega_\alpha t}\Big]\exp\Big[\frac{\lambda_\alpha}{\omega_\alpha}B_\alpha^\dagger\Big] = \\
&\quad \exp\Big[\Big(\frac{\lambda_\alpha}{\omega_\alpha}\Big)^2 e^{-i\omega_\alpha t}\Big]\exp\Big[\frac{\lambda_\alpha}{\omega_\alpha}B_\alpha^\dagger\Big]\exp\Big[\frac{\lambda_\alpha}{\omega_\alpha}B_\alpha e^{-i\omega_\alpha t}\Big] ,
\end{aligned}$$

the above expression becomes

$$\begin{aligned}
&\exp\Big[\frac{\lambda_\alpha}{\omega_\alpha}(B_\alpha e^{-i\omega_\alpha t}-B_\alpha^\dagger e^{i\omega_\alpha t})\Big]\exp\Big[-\frac{\lambda_\alpha}{\omega_\alpha}(B_\alpha-B_\alpha^\dagger)\Big] \\
&= \underbrace{\exp\Big[-\Big(\frac{\lambda_\alpha}{\omega_\alpha}\Big)^2(1-e^{-i\omega_\alpha t})\Big]}_{K(t)}\exp\Big[\frac{\lambda_\alpha}{\omega_\alpha}B_\alpha^\dagger(1-e^{i\omega_\alpha t})\Big]\exp\Big[-\frac{\lambda_\alpha}{\omega_\alpha}B_\alpha(1-e^{-i\omega_\alpha t})\Big] .
\end{aligned}$$

Ia now reads

$$\begin{aligned} Ia &= B_\alpha(t)\,\exp\Big[\frac{\lambda_\alpha}{\omega_\alpha}(B_\alpha(t)-B_\alpha^\dagger(t))\Big]\exp\Big[-\frac{\lambda_\alpha}{\omega_\alpha}(B_\alpha-B_\alpha^\dagger)\Big] \\ &= K(t)\,B_\alpha(t)\,\exp\Big[\frac{\lambda_\alpha}{\omega_\alpha}B_\alpha^\dagger(1-e^{i\omega_\alpha t})\Big]\exp\Big[-\frac{\lambda_\alpha}{\omega_\alpha}B_\alpha(1-e^{-i\omega_\alpha t})\Big]\,. \end{aligned}$$

We want to move all term containing $B^\dagger$ to the left. For that we need the relation

$$B_\alpha(t)\,\exp\Big[\frac{\lambda_\alpha}{\omega_\alpha}B_\alpha^\dagger(1-e^{i\omega_\alpha t})\Big] = \exp\Big[\frac{\lambda_\alpha}{\omega_\alpha}B_\alpha^\dagger(1-e^{i\omega_\alpha t})\Big]\underbrace{\exp\Big[-\frac{\lambda_\alpha}{\omega_\alpha}B_\alpha^\dagger(1-e^{i\omega_\alpha t})\Big]B_\alpha e^{-i\omega_\alpha t}\exp\Big[\frac{\lambda_\alpha}{\omega_\alpha}B_\alpha^\dagger(1-e^{i\omega_\alpha t})\Big]}_{B_\alpha e^{-i\omega_\alpha t}-\frac{\lambda_\alpha}{\omega_\alpha}(1-e^{-i\omega_\alpha t})}\,,$$

which was derived using

$$e^{\hat S}\hat B e^{-\hat S} = \hat B + \Big[\hat S,\hat B\Big] + \frac{1}{2}\Big[\hat S,\Big[\hat S,\hat B\Big]\Big] + \dots\,.$$

Defining $u=\frac{\lambda_\alpha}{\omega_\alpha}(1-e^{i\omega_\alpha t})$, we can write

$$\begin{aligned} Ia &= -u^*\,K(t)\,\exp\Big[u\,B_\alpha^\dagger\Big]\exp\Big[-u^*\,B_\alpha\Big] \\ &\quad + K(t)\,\exp\Big[u\,B_\alpha^\dagger\Big]B_\alpha e^{-i\omega_\alpha t}\exp\Big[-u^*\,B_\alpha\Big]\,. \end{aligned}$$

We can now write an expression for $< Ia >$, that we can use to calculate the explicit result,

$$\begin{aligned} &< Ia > \\ &= -\frac{\lambda_\alpha}{\omega_\alpha}(1-e^{-i\omega_\alpha t})F(t) \\ &+ \underbrace{\frac{K(t)}{Z}\sum_{n_\alpha=0}^{\infty}\exp\Big[-\beta\hbar\omega_\alpha n_\alpha\Big] < n_\alpha|\exp\Big[u\,B_\alpha^\dagger\Big]B_\alpha e^{-i\omega_\alpha t}\exp\Big[-u^*\,B_\alpha\Big]|n_\alpha >}_{Ib}\,. \end{aligned}$$

To calculate Ib, we state the following rules, when acting with the boson operators on the states,

$$\begin{aligned} < n_\alpha|e^{u\,B_\alpha^\dagger} &= \sum_{m=0}^{n_\alpha}\frac{u^m}{m!}\Big[\frac{n_\alpha!}{(n_\alpha-m)!}\Big]^{\frac{1}{2}} < n_\alpha-m| \\ B_\alpha e^{-i\omega_\alpha t}e^{-u^*\,B_\alpha}|n_\alpha > &= \sum_{l=0}^{n_\alpha-1}\frac{(-u^*)^l}{l!}\Big[\frac{n_\alpha!}{(n_\alpha-l-1)!}\Big]^{\frac{1}{2}}e^{-i\omega_\alpha t}|n_\alpha-l-1> \\ < n_\alpha-m|n_\alpha-l-1 > &= \delta_{m,l+1}\,. \end{aligned}$$

Using these, the expression in brackets of I_b reads

$$< n_\alpha | e^{u\, B_\alpha^\dagger} B_\alpha e^{-i\omega_\alpha t} e^{-u^*\, B_\alpha} | n_\alpha >= \sum_{m=0}^{n_\alpha} \frac{u^m}{m!} \Big[\frac{n_\alpha!}{(n_\alpha - m)!} \Big]^{\frac{1}{2}} \sum_{l=0}^{n_\alpha - 1} \frac{(-u^*)^l}{l!} \Big[\frac{n_\alpha!}{(n_\alpha - l - 1)!} \Big]^{\frac{1}{2}} e^{-i\omega_\alpha t} \delta_{m,l+1} \; .$$

Performing the sum over l we end up with

$$\begin{aligned} < n_\alpha | e^{u\, B_\alpha^\dagger} B_\alpha e^{-i\omega_\alpha t} e^{-u^*\, B_\alpha} | n_\alpha > &= \sum_{m=1}^{n_\alpha} \frac{u^m}{m!} \frac{n_\alpha!}{(n-m)!} \frac{(-u^*)^{m-1}}{(m-1)!} e^{-i\omega_\alpha t} \\ &= \sum_{m=1}^{n_\alpha} \frac{(-|u|^2)^{(m-1)}}{[(m-1)!]^2} \frac{n_\alpha!}{(n_\alpha - m)!} \cdot \frac{u}{m} e^{-i\omega_\alpha t} \; . \end{aligned}$$

Together with $Z = \sum_{n_\alpha=0}^{\infty} \exp\Big[-\beta\hbar\omega_\alpha n_\alpha \Big] = \big[1 - e^{-\beta\hbar\omega_\alpha} \big]^{-1}$, this makes

$$Ib = (1 - e^{-\beta\hbar\omega_\alpha}) \sum_{n_\alpha=1}^{\infty} e^{-\beta\hbar\omega_\alpha n_\alpha} \sum_{m=1}^{n_\alpha} \frac{(-|u|^2)^{(m-1)}}{[(m-1)!]^2} \frac{n_\alpha!}{(n-m)!} \cdot \frac{u}{m} e^{-i\omega_\alpha t} \; .$$

Using the variable transform $l = n_\alpha - 1$ and $k = m - 1$, Ib becomes

$$\begin{aligned} Ib &= K(t)\,(1 - e^{-\beta\hbar\omega_\alpha}) \sum_{l=0}^{\infty} e^{-\beta\hbar\omega_\alpha (l+1)} \sum_{k=0}^{l} \frac{(-|u|^2)^k}{(k!)^2} \frac{(l+1)!}{(l-k)!} \cdot \frac{u}{k+1} e^{-i\omega_\alpha t} \\ &= K(t)\,(1 - e^{-\beta\hbar\omega_\alpha}) e^{-\beta\hbar\omega_\alpha}\, u\, e^{-i\omega_\alpha t} \sum_{l=0}^{\infty} \sum_{k=0}^{l} e^{-\beta\hbar\omega_\alpha l} \frac{(-|u|^2)^k}{(k!)^2} \frac{(l+1)!}{(l-k)!} \cdot \frac{1}{k+1} \\ &= K(t)\,(1 - e^{-\beta\hbar\omega_\alpha}) e^{-\beta\hbar\omega_\alpha}\, u\, e^{-i\omega_\alpha t} \sum_{l=0}^{\infty} \sum_{k=0}^{\infty} e^{-\beta\hbar\omega_\alpha (l+k)} \frac{(l+k+1)!}{(l!)^2 (k)!} (-|u|^2)^l \cdot \frac{1}{l+1} \; , \end{aligned}$$

where in the last step we set the upper limit of k to infinity, together with changing the accordant values in the formula, which is not straight forward, but can be checked by explicit comparison between the terms from the second and third line. Using the identity for the faculty $(l+k+1)! = \int_0^\infty dx x^{l+k+1}\, e^{-x}$, we obtain

$$\begin{aligned} Ib &= K(t)\,(1 - e^{-\beta\hbar\omega_\alpha}) e^{-\beta\hbar\omega_\alpha}\, u\, e^{-i\omega_\alpha t} \\ &\times \sum_{l=0}^{\infty} e^{-\beta\hbar\omega_\alpha l} \frac{(-|u|^2)^l}{(l!)^2 (l+1)} \underbrace{\int_0^\infty dx \sum_{k=0}^{\infty} x^{l+k+1}\, e^{-x} e^{-\beta\hbar\omega_\alpha k} \frac{1}{k!}}_{Ic} \; . \end{aligned}$$

The expression Ic can be computed to

$$\begin{aligned} Ic &= \int_0^\infty dx\, x^{l+1} e^{-x} \sum_{k=0}^{\infty} x^k\, e^{-\beta\hbar\omega_\alpha k} \frac{1}{k!} \\ &= \int_0^\infty dx\, x^{l+1} e^{-x(1-\exp[-\beta\hbar\omega_\alpha])} \\ &= (1-e^{-\beta\hbar\omega_\alpha})^{-(l+1)} \int_0^\infty dx\, [x(1-e^{-\beta\hbar\omega_\alpha})]^{l+1} e^{-x(1-\exp[-\beta\hbar\omega_\alpha])} \ . \end{aligned}$$

Using $y = x(1-e^{-\beta\hbar\omega_\alpha})$ and $dy = dx(1-e^{-\beta\hbar\omega_\alpha}) \rightarrow$

$$\begin{aligned} Ic &= (1-e^{-\beta\hbar\omega_\alpha})^{-(l+2)} \int_0^\infty dy\, y^{l+1} e^{-y} \\ &= (1-e^{-\beta\hbar\omega_\alpha})^{-(l+2)} (l+1)! \ . \end{aligned}$$

Consequently, we get

$$\begin{aligned} Ib &= \frac{e^{-\beta\hbar\omega_\alpha}}{(1-e^{-\beta\hbar\omega_\alpha})}\, u\, e^{-i\omega_\alpha t} \times \underbrace{K(t) \sum_{l=0}^{\infty} \frac{e^{-\beta\hbar\omega_\alpha l}}{(1-e^{-\beta\hbar\omega_\alpha})^l} \frac{(-|u|^2)^l}{l!}}_{F_\alpha(t)} \\ &= N(\omega_\alpha)\, u\, e^{-i\omega_\alpha t} F_\alpha(t) \ . \end{aligned}$$

Putting it all back together, we finally get

$$\left\langle B_\alpha(t)\chi(t)\chi^\dagger \right\rangle \approx -\frac{\lambda_\alpha}{\omega_\alpha}(N(\omega_\alpha)+1)(1-e^{-i\omega_\alpha t}) \left\langle \chi(t)\chi^\dagger \right\rangle \ .$$

The other correlators are calculated similarly.

B.3. Detailed balance relation

using the following representation for the boson correlator:

$$\left\langle \chi(t)\chi^\dagger \right\rangle = \exp\left\{ -\sum_\alpha \left(\frac{\lambda_0}{\omega_\alpha}\right)^2 \frac{\cosh(\omega_\alpha\beta/2) - \cos(\omega_\alpha[t+i\beta/2])}{\sinh(\omega_\alpha\beta/2)} \right\} \tag{B.3}$$

$$\left\langle \chi^\dagger\chi(t) \right\rangle = \exp\left\{ -\sum_\alpha \left(\frac{\lambda_0}{\omega_\alpha}\right)^2 \frac{\cosh(\omega_\alpha\beta/2) - \cos(\omega_\alpha[t-i\beta/2])}{\sinh(\omega_\alpha\beta/2)} \right\} \tag{B.4}$$

$$\tag{B.5}$$

It is easy to show that $P(E)$ follows the details balance relation $P(-E) = e^{-\beta E} P(E)$, where

$$P(E) = \int dt e^{iEt} \left\langle \chi(t)\chi^\dagger \right\rangle \tag{B.6}$$

$$P(-E) = \int dt e^{iEt} \left\langle \chi^\dagger\chi(t) \right\rangle \tag{B.7}$$

We verify this by writing the inverse Fourier transform for $P(-E)$ and $e^{-\beta E}P(E)$:

$$\int \frac{dE}{2\pi} e^{-iEt} P(-E) = \left\langle \chi^\dagger \chi(t) \right\rangle \tag{B.8}$$

$$\int \frac{dE}{2\pi} e^{-iE(t-i\beta)} P(E) \tag{B.9}$$

$$= \exp\left\{ -\sum_\alpha \left(\frac{\lambda_0}{\omega_\alpha}\right)^2 \frac{\cosh\left(\omega_\alpha \beta/2\right) - \cos\left(\omega_\alpha \left[t - i\beta + i\beta/2\right]\right)}{\sinh\left(\omega_\alpha \beta/2\right)} \right\} \tag{B.10}$$

$$= \exp\left\{ -\sum_\alpha \left(\frac{\lambda_0}{\omega_\alpha}\right)^2 \frac{\cosh\left(\omega_\alpha \beta/2\right) - \cos\left(\omega_\alpha \left[t - i\beta/2\right]\right)}{\sinh\left(\omega_\alpha \beta/2\right)} \right\} \tag{B.11}$$

$$= \left\langle \chi^\dagger \chi(t) \right\rangle \tag{B.12}$$

Since the first and last line are identical, also the details balance relation is true.

Appendix C. Electrode self-energy

We define $\mathcal{G}^1_{\nu lr}(t) = -i\theta(t)\left\langle c^r_\nu(t) a^\dagger_l \chi^\dagger \right\rangle$ and $\mathcal{G}^2_{\nu lr}(t) = -i\theta(t)\left\langle a^\dagger_l \chi^\dagger c^r_\nu(t) \right\rangle$ and calculate the according EOMs with the Hamiltonian from Eq. 4.4.

$$
\begin{aligned}
\underbrace{\left(i\frac{d}{dt} - \epsilon_\nu\right)}_{[g^{\mathrm{ret}}(t)]^{-1}} \mathcal{G}^1_{\nu lr}(t) &= \delta(t)\left\langle c^r_\nu a^\dagger_l \chi^\dagger \right\rangle + \sum_j t^r_j \underbrace{\left[-i\theta(t)\left\langle a_j(t)\chi(t) a^\dagger_l \chi^\dagger \right\rangle\right]}_{G^1_{jl}(t)} \\
\underbrace{\left(i\frac{d}{dt} - \epsilon_\nu\right)}_{[g^{\mathrm{ret}}(t)]^{-1}} \mathcal{G}^2_{\nu lr}(t) &= \delta(t)\left\langle a^\dagger_l \chi^\dagger c^r_\nu \right\rangle + \sum_j t^r_j \underbrace{\left[-i\theta(t)\left\langle a^\dagger_l \chi^\dagger a_j(t)\chi(t) \right\rangle\right]}_{G^2_{jl}(t)} \\
&\downarrow \\
\mathcal{G}^1_{\nu lr}(t) &= g^{\mathrm{ret}}_{\nu r}(t)\left\langle c^r_\nu a^\dagger_l \chi^\dagger \right\rangle + \int dt' \sum_j t^r_j g^{\mathrm{ret}}_{\nu r}(t-t') G^1_{jl}(t') \\
\mathcal{G}^2_{\nu lr}(t) &= g^{\mathrm{ret}}_{\nu r}(t)\left\langle a^\dagger_l \chi^\dagger c^r_\nu \right\rangle + \int dt' \sum_j t^r_j g^{\mathrm{ret}}_{\nu r}(t-t') G^2_{jl}(t')
\end{aligned}
$$

where t^r_j is the coupling of the left, $r = L$ (right, $r = R$) electrode to the first, $j = 1$ (last, $j = N$) base pair and $g^{\mathrm{ret}}_{\nu r}(E) =$ is the non-interacting retarded green functions of the left or right electrode. For the wide band limit, this simplifies to $g^{\mathrm{ret}}_{\nu r}(E) = -i2\pi\rho^r_e$.

The so far unspecified equal time correlator of the first equation reads

$$
\left\langle c^r_\nu a^\dagger_l \chi^\dagger \right\rangle = -\int \frac{dE}{2\pi i} \sum_i t^r_i \left[g^{\mathrm{ret}}_{\nu r}(E)\, G^>_{il}(E) + g^>_{\nu r}(E)\, G^{\mathrm{adv}}_{il}(E) \right]. \tag{C.1}
$$

The second unspecified correlator has the same magnitude, but with opposite sign, since the relation

$$
\left\langle c^r_n a^\dagger_l \chi^\dagger \right\rangle + \left\langle a^\dagger_l \chi^\dagger c^r_n \right\rangle = \left\langle \left\{ c^r_n, a^\dagger_l \right\} \chi^\dagger \right\rangle = 0 \tag{C.2}
$$

holds. As one can see from Eq. C.1 this would lead to a coupling between $G^1(t)$ and $G^2(t)$ to other Green functions. To have fully decoupled equations, we set both correlators $\left\langle c^r_n a^\dagger_l \chi^\dagger \right\rangle$ and $\left\langle a^\dagger_l \chi^\dagger c^r_n \right\rangle$ to zero. This approximation is reasonable, since their contribution to Eq. 4.6 and 4.7 is small, at most of the order of Γ^r and adding $G^1(t)$ and $G^2(t)$ in the end results in their cancellation according to Eq. C.2. The validity of this approximation has been checked numerically.

Appendix D. Non-equilibrium Equation of motion

In contrast to the method described in Chapter 4 for determining the transport properties of the molecular system, where the lesser self-energy was approximated by an effective Fermi function, we now want calculate the full non-equilibrium transport of the system. The vibration occupation can still be described by the equilibrium Bose-function, since the coupling to the bath relaxes the vibration fast enough into equilibrium.

In non-equilibrium the distribution-function ($G^<$) and the density of states (G^{ret}) are independent of each other. In contrast, the fluctuation-dissipation relation links these two in equilibrium. To calculate the non-equilibrium properties of the system we calculate the equation of motion for the contour ordered Green function $G_{kl}(\tau,\tau') = -i\left\langle \mathrm{T_C} a_k(\tau)\chi(\tau)a_l^\dagger(\tau')\chi^\dagger(\tau')\right\rangle$ For this we split the Hamiltonian (Eq. 4.3) into a part describing the uncoupled system and a part describing the rest, $\bar{H} = \bar{H}_0 + \bar{H}_1$, with

$$\begin{aligned}\bar{H}_0 =& \sum_i (\epsilon_i - \Delta) a_i^\dagger a_i - \sum_{<ij>} t_{ij} a_i^\dagger a_j \\ \bar{H}_1 =& \sum_{n,r,i}\left[t_{in}^r c_{nr}^\dagger a_i \chi + t_{in}^{r*} a_i^\dagger \chi^\dagger c_{nr}\right] + \bar{H}_{\mathrm{R}} + \bar{H}_{\mathrm{L}} \\ &+ \sum_\alpha \omega_\alpha B_\alpha^\dagger B_\alpha + \sum_\alpha \sum_{<ij>} \lambda_{ij}\, a_i^\dagger a_j (B_\alpha + B_\alpha^\dagger)\,. \end{aligned} \tag{D.1}$$

The equation of motion (EOM) then reads

$$\sum_j \underbrace{\left[\left(i\frac{d}{d\tau} - \epsilon_k + \Delta\right)\delta_{kj} + t_{kj}\right]}_{\left[G_{jl}^0\right]^{-1}} G_{jl}(\tau,\tau') = \delta(\tau-\tau')\delta_{kl} \underbrace{-i\left\langle \mathrm{T_C}\left[a_k(\tau)\chi(\tau), \bar{H}_1\right] a_l^\dagger(\tau')\chi^\dagger(\tau')\right\rangle}_{<<\left[a_k\chi,\bar{H}_1\right]a_l^\dagger\chi^\dagger>>_{(\tau-\tau')}}. \tag{D.2}$$

After rearranging we obtain

$$G_{kl}(\tau,\tau') = G_{kl}^0(\tau,\tau') + \sum_j \int d\tau_1 G_{kj}^0(\tau,\tau_1) << \left[a_j\chi, \bar{H}_1\right] a_l^\dagger\chi^\dagger >>_{(\tau_1-\tau')}\,. \tag{D.3}$$

Applying the Langreth rules we get for the retarded/advanced and lesser/greater Green function in real time

$$G^{\mathrm{ret}}_{kl}(t,t') = G^{\mathrm{ret},0}_{kl}(t,t') + \sum_j \int dt_1 G^{\mathrm{ret},0}_{kj}(t,t_1) << \left[a_j\chi, \bar{H}_1\right] a^\dagger_l \chi^\dagger >>^{\mathrm{ret}}_{(t_1-t')} \tag{D.4}$$

$$G^{\mathrm{adv}}_{kl}(t,t') = G^{\mathrm{adv},0}_{kl}(t,t') + \sum_j \int dt_1 G^{\mathrm{adv},0}_{kj}(t,t_1) << \left[a_j\chi, \bar{H}_1\right] a^\dagger_l \chi^\dagger >>^{\mathrm{adv}}_{(t_1-t')} \tag{D.5}$$

$$\begin{aligned} G^{>/<}_{kl}(t,t') =& G^{>/<,0}_{kl}(t,t') + \sum_j \int dt_1 G^{\mathrm{ret},0}_{kj}(t,t_1) << \left[a_j\chi, \bar{H}_1\right] a^\dagger_l \chi^\dagger >>^{>/<}_{(t_1-t')} \\ &+ \sum_j \int dt_1 G^{>/<,0}_{kj}(t,t_1) << \left[a_j\chi, \bar{H}_1\right] a^\dagger_l \chi^\dagger >>^{\mathrm{adv}}_{(t_1-t')} \end{aligned} \tag{D.6}$$

or in energy space

$$G^{\mathrm{ret}}_{kl}(E) = G^{\mathrm{ret},0}_{kl}(E) + \sum_j G^{\mathrm{ret},0}_{kj}(E) << \left[a_j\chi, \bar{H}_1\right] a^\dagger_l \chi^\dagger >>^{\mathrm{ret}}_{E} \tag{D.7}$$

$$G^{\mathrm{adv}}_{kl}(E) = G^{\mathrm{adv},0}_{kl}(E) + \sum_j G^{\mathrm{adv},0}_{kj}(E) << \left[a_j\chi, \bar{H}_1\right] a^\dagger_l \chi^\dagger >>^{\mathrm{adv}}_{E} \tag{D.8}$$

$$\begin{aligned} G^{>/<}_{kl}(E) =& G^{>/<,0}_{kl}(E) + \sum_j G^{\mathrm{ret},0}_{kj}(E) << \left[a_j\chi, \bar{H}_1\right] a^\dagger_l \chi^\dagger >>^{>/<}_{E} \\ &+ \sum_j G^{>/<,0}_{kj}(E) << \left[a_j\chi, \bar{H}_1\right] a^\dagger_l \chi^\dagger >>^{\mathrm{adv}}_{E} \quad . \end{aligned} \tag{D.9}$$

This is equivalent to the result obtained by the far more complicated method of Niu *et al* [125]. Using the Eq. (D.8) one can rewrite Eq. (D.9) to (in matrix notation)

$$\begin{aligned} G^{>/<}(E) =& G^{>/<,0}(E)\left[\left[G^{\mathrm{adv},0}(E)\right]^{-1} G^{\mathrm{adv}}(E)\right] \\ &+ G^{\mathrm{ret},0}(E) << \left[a\chi, \bar{H}_1\right] a^\dagger \chi^\dagger >>^{>/<}_{E} \quad . \end{aligned} \tag{D.10}$$

The Green function $<< \left[a_j\chi, \bar{H}_1\right] a^\dagger_l\chi^\dagger >>^{\mathrm{ret/adv}}_{E}$ depends on $G^>(E)$ and $G^<(E)$. Therefore we have a set of coupled equations which have to be solved self-consistently. The Green function consisting of the commutator with $\bar{H}_1$ describe the interaction with the leads, the non-local electron-vibration coupling and the influence of the strong local electron-vibration coupling.

The commutator with the electrode-system Hamiltonian $\bar{H}_{\mathrm{T,L}}$ and $\bar{H}_{\mathrm{T,R}}$ give rise to

$$<< \left[a_j\chi, \bar{H}_{\mathrm{T,L/R}}\right] a^\dagger_l \chi^\dagger >>^{\mathrm{ret}}_{t} = -i\theta(t)\left\langle \left\{c^{\mathrm{L/R}}_n(t), a^\dagger_l\chi^\dagger_l\right\} \underbrace{\chi^\dagger(t)\chi(t)}_{=1} \right\rangle \tag{D.11}$$

$$<< \left[a_j\chi, \bar{H}_{\mathrm{T,L/R}}\right] a^\dagger_l \chi^\dagger >>^{<}_{t} = i\left\langle a^\dagger_l\chi^\dagger c^{\mathrm{L/R}}_n(t) \underbrace{\chi^\dagger(t)\chi(t)}_{=1} \right\rangle \ , \tag{D.12}$$

respectively.

To obtain the retarded self-energy due to the electrodes we calculate the EOM for Eq. (D.11). We define $\mathcal{G}^{\rm ret}_{nlr}(t) = -i\theta(t)\left\langle\left\{c^r_n(t), a^\dagger_l\chi^\dagger_l\right\}\right\rangle$ with r =L/R and then we compute the equation of motion for $\mathcal{G}^{\rm ret}_{nlr}(t)$

$$\begin{aligned} i\frac{\partial}{\partial t}\mathcal{G}^{\rm ret}_{nlr}(t) &= \delta(t)\underbrace{\left\langle\left\{c^r_n, a^\dagger_l\chi^\dagger\right\}\right\rangle}_{=0} \\ &\quad +\epsilon_n\mathcal{G}^{\rm ret}_{nlr}(t) \\ &\quad +\sum_j t^r_{nj}\underbrace{\left[-i\theta(t)\left\langle a_j(t)\chi(t)a^\dagger_l\chi^\dagger\right\rangle - i\theta(t)\left\langle a^\dagger_l\chi^\dagger a_j(t)\chi(t)\right\rangle\right]}_{G^{\rm ret}_{jl}(t)} . \end{aligned}$$

After fourier transformation from time to energy-domain, we obtain

$$\begin{aligned} E\,\mathcal{G}^{\rm ret}_{nlr}(E) &= \epsilon_n\mathcal{G}^{\rm ret}_{nlr}(E) + \sum_j t^r_{nj}\,G^{\rm ret}_{jl}(E) \\ \rightarrow \quad \mathcal{G}^{\rm ret}_{nlr}(E) &= g^{\rm ret}_{nr}(E)\sum_i t^r_{nj}\,G^{\rm ret}_{jl}(E) , \end{aligned}$$

where $g^{\rm ret}_{nr}(E)$ is the retarded Green function of electrode $r = R/L$.
With this, the retarded electrode self-energy becomes

$$\Sigma^{\rm ret,r}_{jk} = \left[\sum_n t^{r*}_{nk} g^{\rm ret}_{nr}(E) t^r_{nj}\right] = -i\Gamma^r_{kj} . \tag{D.13}$$

The last equality arises in the so called wide-band limit, where the density of states in the electrodes is assumed to be constant.

To solve Eq. (D.12) we calculate the EOM for $\mathcal{G}^<_{nlr}(t) = i\left\langle a^\dagger_l\chi^\dagger c^r_n(t)\right\rangle$. In analogy to the non-equilibrium derivation in the book of Haug and Jauho [124] (pages 162,163) we get

$$\mathcal{G}^<_{nlr}(E) = \sum_i t^r_{ni}\left[g^{\rm ret}_{nr}(E)\,G^<_{il}(E) + g^<_{nr}(E)\,G^{\rm adv}_{il}(E)\right] ,$$

where we can identify the lesser self-energy due to coupling to left ($r = L$) or right ($r = R$) lead.

$$\Sigma^{<,r}_{jk} = \sum_n t^{r*}_{nk} g^<_{nr}(E) t^r_{nj} = if(E)2\Gamma^r_{kj}$$

Note, that we used the full coupling to leads, i. e. including the χ-terms in $\bar{H}_{\rm T,L}$ and $H_{\rm T,R}$.

In the EOM we encounter the same types of terms which arose in the EOM in section before, e. g. $\left\langle a_k(t)B_\alpha(t)\chi(t)a^\dagger_l\chi^\dagger\right\rangle$. We treat these in the same manner, as in the previous section, see Eq. (4.8) and following. Effectively this is equivalent to factorizing the

electronic and vibrational degrees if freedom. **Is this?** This is the only approximation in this theory.

With these approximations the retarded and lesser correlators read

$$\begin{aligned} << [a_k(t)\chi(t), H_1], a_l^\dagger \chi^\dagger >>^{\mathrm{ret}}(E) = & \sum_j \Lambda_{kj} G_{jl}^{\mathrm{ret}}(E) \\ & + \sum_{j\neq k} \lambda_{kj}\lambda_0 \left[\mathcal{F}_1(G_{jl}^{>r})(E) + \mathcal{F}_2(G_{jl}^{<r})(E)\right] \\ & + \lambda_0^2 \left[\mathcal{F}_1(G_{kl}^{>r})(E) + \mathcal{F}_2(G_{kl}^{<r})(E)\right] \end{aligned} \tag{D.14}$$

and

$$\begin{aligned} << a_l^\dagger \chi^\dagger [a_k(t)\chi(t), H_1] >>^{<}(E) = & \sum_j \Lambda_{kj} G_{jl}^{<}(E) + \sum_j \Sigma_{kj}^{<} G_{jl}^{\mathrm{adv}}(E) \\ & + \sum_{j\neq k} \lambda_{kj}\lambda_0 \mathcal{F}_2\left(G_{jl}^{<}\right)(E) \\ & + \lambda_0^2 \mathcal{F}_2\left(G_{kl}^{<}\right)(E)\,, \end{aligned} \tag{D.15}$$

with the functionals $\mathcal{F}_1(G_{kl}^{\nu})(E)$ and $\mathcal{F}_2(G_{kl}^{\nu})(E)$, that describe the strong interaction with the local vibrations

$$\begin{aligned} \mathcal{F}_1(G_{kl}^{\nu})(E) &= \int dt e^{iEt} \int d\omega \frac{D(\omega)}{\omega} \left[(N(\omega)+1)\, e^{-i\omega t} - N(\omega) e^{i\omega t}\right] G_{kl}^{\nu}(t) \\ &= \int d\omega \frac{D(\omega)}{\omega} \left[(N(\omega)+1)\, G_{kl}^{\nu}(E-\omega) - N(\omega) G_{kl}^{\nu}(E+\omega)\right] \end{aligned} \tag{D.16}$$

$$\begin{aligned} \mathcal{F}_2(G_{kl}^{\nu})(E) &= \int dt e^{iEt} \int d\omega \frac{D(\omega)}{\omega} \left[N(\omega) e^{-i\omega t} - (N(\omega)+1)\, e^{i\omega t}\right] G_{kl}^{\nu}(t) \\ &= \int d\omega \frac{D(\omega)}{\omega} \left[N(\omega) G_{kl}^{\nu}(E-\omega) - (N(\omega)+1)\, G_{kl}^{\nu}(E+\omega)\right] \end{aligned} \tag{D.17}$$

and the definition

$$\begin{aligned} \Lambda_{kj} = & -\Delta\delta_{kj} + \Sigma_{kj}^{\mathrm{ret}} + \int d\omega \frac{D(\omega)}{\omega} \Bigg[2 \sum_{i\neq j} \left\langle a_k a_i^\dagger \right\rangle \lambda_{ij}\lambda_0 \\ & - 2 \sum_{<ij'>} \left\langle a_{j'} a_i^\dagger \right\rangle \lambda_{ij'}\lambda_0 \delta_{kj} - \sum_{j\neq k} \lambda_{kj}\lambda_0 \Bigg]\,. \end{aligned}$$

The uncommon Green functions in Eq. (D.14) are $G_{kl}^{>r}(t) = \theta(t) G_{kl}^{>}(t)$ and $G_{kl}^{<r}(t) = -\theta(t) G_{kl}^{<}(t)$. The variable ν in Eq. (D.16) and Eq. (D.17) stands for the various Green functions in Keldysh space.

Inserting Eq. (D.14) and Eq. (D.15) into the EOM formulas (Eq. (D.7) and Eq. (D.10) respectively) and comparing the result for the lesser Green function (Eq. (D.10)) with the general relation

$$\begin{aligned} G^{<}(E) \;=\; & G_0^{<}(E) + G_0^{\mathrm{ret}}(E)\Sigma^{\mathrm{ret}}(E) G^{\mathrm{adv}}(E) \\ & + G_0^{\mathrm{ret}}(E)\Sigma^{<}(E) G^{\mathrm{adv}}(E) + G_0^{<}(E)\Sigma^{\mathrm{adv}} G^{\mathrm{adv}}(E)\,, \end{aligned}$$

we can identify

$$\mathcal{F}_2(G^<)(E) = \Sigma^{\mathrm{ret}}_{\mathrm{vib}}(E)G^<(E) + \Sigma^<_{\mathrm{vib}}(E)G^{\mathrm{adv}}(E)\ . \tag{D.18}$$

For G^{ret} and $G^<$ self-consistency equations have to be solved numerically. The other Green functions can be derived from the relations given in App. A. The drawback is that the current computed by the Meir and Wingreen formula (Eq. 3.3) is not conserved, i. e. $I_L \neq I_R$. This unphysical result is due to the approximation in calculating the boson correlators. Other authors using similar approaches, but without non-local electron-vibration coupling, do not comment on this problem although they should experience it as well [96, 115].

Appendix E. Vibrational operator products

In the perturbation expansion of the single particle density matrix $\rho_k^l(t) = \left\langle a_k^\dagger(t) a_l(t) \right\rangle_{\tilde{H}}$ to order n in the perturbative Hamiltonian $\tilde{H}'$ (Eq. 6.3), one obtains up to n vibrational operators (equal number of χ and $\chi^\dagger$) at different times which act upon the same vibrational states.

$$\begin{aligned}\left\langle \chi_k(t_1)\chi_k^\dagger(t_2)\chi_k(t_3)\chi_k^\dagger(t_4)\cdots\chi_k(t_{n-1})\chi_k^\dagger(t_n)\right\rangle_{H_0} = \\ \left(\exp\left\{-\frac{1}{2}\sum_\alpha\left(\frac{\lambda_{k\alpha}}{\Omega_{k\alpha}}\right)^2(2N(\Omega_{k\alpha})+1)\right\}\right)^n \\ \times\exp\Big\{\{\zeta_{12}A_k(t_1-t_2)\}+\mathrm{T}_C\{\zeta_{13}A_k(t_1-t_3)\}+\cdots \\ +\mathrm{T}_C\{\zeta_{n-1,n}A_k(t_{n-1}-t_n)\}\Big\},\end{aligned}$$

where

$$\zeta_{ij} = \begin{cases} +1 & \text{when } \chi_k(t_i)\chi_k^\dagger(t_j) \text{ or } \chi_k^\dagger(t_j)\chi_k(t_i), \\ -1 & \text{when } \chi_k(t_i)\chi_k(t_j) \text{ or } \chi_k^\dagger(t_i)\chi_k^\dagger(t_j) \end{cases}.$$

The evaluation of the operator products proceeds similar to the derivation in App. B.2, except that now more functions $\chi_k(t_i)$ are involved. The expression T_C in $\mathrm{T}_C\{\zeta_{12}A_k(t_1-t_2)\}$ ensures, that t_1 is later on the contour than t_2 and $A_k(t_1-t_2)$ is given by

$$\begin{aligned}A_k(t_1-t_2) &= \sum_\alpha\left(\frac{\lambda_{k\alpha}}{\omega_{k\alpha}}\right)^2\left[(N(\omega_{k\alpha})+1)\,e^{-i\omega_{k\alpha}(t_1-t_2)}+N(\omega_{k\alpha})e^{i\omega_{k\alpha}(t_1-t_2)}\right] \\ &= \sum_\alpha\left(\frac{\lambda_{k\alpha}}{\omega_{k\alpha}}\right)^2\frac{\cos\left(\omega_{k\alpha}\left[t_1-t_2+i\hbar\beta/2\right]\right)}{\sinh\left(\hbar\omega_{k\alpha}\beta/2\right)}.\end{aligned}$$

For a correlator with n operators χ_k and $\chi_k^\dagger$ acting on the same state one gets $N = \frac{(n)(n-1)}{2}$ different terms $A_k(t_i - t_j)$ in the exponential function. This is due to the various operator commutations involved in deriving the above expression.

Bibliography

[1] A. Aviram and M. A. Ratner, Molecular rectifiers, Chem. Phys. Lett. **29**, 277 (1975).

[2] C. J. Muller, J. M. van Ruitenbeek, and L. J. de Jongh, Conductance and supercurrent discontinuities in atomic scale metallic constrictions of variable width., Physica C **191**, 485 (1992).

[3] E. Scheer, N. Agrait, J. C. Cuevas, A. L. Yeyati, B. Ludoph, A. Martin-Roderos, G. R. Bollinger, J. M. van Ruitenbeek, and C. Urbina, The signature of chemical valence in the electrical conduction through a single-atom contact, Nature **394**, 154 (1998).

[4] S. Datta, W. D. Tian, S. H. Hong, R. Reifenberger, J. I. Henderson, and C. P. Kubiak, Current-voltage characteristics of self-assembled monolayers by scanning tunneling microscopy, Phys. Rev. Lett. **79**, 2530 (1997).

[5] T. W. Kelley, E. L. Granstrom, and C. D. Frisbie, Conducting Probe Atomic Force Microscopy: A Characterization Tool for Molecular Electronics, Adv. Mater. **11**, 261 (1999).

[6] P. C. Collins, M. S. Arnold, and P. Avouris, Engineering carbon nanotubes and nanotube circuits using electrical breakdown, Science **292**, 706 (2001).

[7] A. Bachtold, P. Hadley, T. Nakanishi, and C. Dekker, Logic circuits with carbon nanotube transistors, Science **294**, 1317 (2001).

[8] H. W. C. Postma, T. Teepen, Z. Yao, M. Grifoni, and C. Dekker, Carbon nanotube single-electron transistors at room temperature, Science **293**, 76 (2001).

[9] L. A. Bumm, J. J. Arnold, M. T. Cygan, T. D. Dunbar, T. P. Burgin, L. Jones, D. L. Allara, J. M. Tour, and P. S. Weiss, Are single molecular wires conducting?, Science **271**, 1705 (1996).

[10] H. Park, J. Park, A. K. L. Lim, E. H. Anderson, A. P. Alivisatos, and P. L. McEuen, Nanomechanical oscillations in a single-C-60 transistor, Nature **407**, 57 (2000).

[11] B. Q. Xu and N. J. J. Tao, Measurement of single-molecule resistance by repeated formation of molecular junctions, Science **301**, 1221 (2003).

[12] E. Lörtscher, J. W. Ciszek, J. Tour, and H. Riel, Reversible and Controllable Switching of a Single-Molecule Junction, Small **2**(8-9), 973 (2006).

[13] L. Cai, H. Tabata, and T. Kawai, Self-assembled DNA networks and their electrical conductivity, Appl. Phys. Lett. **77**, 3105 (2000).

[14] E. Koplin, C. M. Niemeyer, and U. Simon, Formation of electrically conducting DNA-assembled gold nanoparticle monolayers, J. Mater. Chem. **16**, 1338 (2006).

[15] C. A. Mirkin, R. L. Letsinger, R. C. Mucic, and J. J. Storhoff, A DNA-based method for rationally assembling nanoparticles into macroscopic materials, Nature **382**, 607 (1996).

[16] E. Braun, Y. Eichen, U. Sivan, and G. Ben-Yoseph, DNA-templated assembly and electrode attachment of a conducting silver wire, Nature **391**, 775 (1998).

[17] R. G. Endres, D. L. Cox, and R. R. P. Songh, The quest for high-conductance DNA, Rev. Mod. Phys. **76**, 195 (2004).

[18] S. R. Rajski, B. A. Jackson, and J. K. Barton, DNA Repair: Models for Damage and Mismatch Recognition, Mutation Res. **447**, 49 (2000).

[19] M. Zwolak and M. Di Ventra, *Introdcution to Nanoscale Science and Technology*, chapter 3, Kluwer Academic/Plenum Publishers, 2004.

[20] M. Zwolak and M. Di Ventra, Physical approaches to DNA sequencing and detection, Rev. Mod. Phys. **80**, 141 (2008).

[21] S. Datta, *Electronic Transport in Mesoscopic Systems*, Cambridge University Press, 1997.

[22] K. Hansen, E. Lægsgaard, I. Stensgaard, and F. Besenbacher, Quantized conductance in relays, Phys. Rev. B **56**(4), 2208–2220 (Jul 1997).

[23] F. Pauly, J. K. Viljas, J. C. Cuevas, and G. Schön, Density-functional study of tilt-angle and temperature-dependent conductance in biphenyl-dithiol single-molecule contacts, Phys. Rev. B **77**, 155312 (2008).

[24] M. Di Ventra, S. T. Pantelides, and N. D. Lang, First-Principles Calculation of Transport Properties of a Molecular Device, Phys. Rev. Lett. **84**(5), 979 (Jan 2000).

[25] A. Nitzan and M. A. Ratner, Electron Transport in Molecular Wire Junctions, Science **300**, 1384 (2003).

[26] M. A. Young, G. Ravishanker, and D. L. Beveridge, A 5-nanosecond molecular dynamics trajectory for B-DNA: analysis of structure, motions, and solvation, Biophys. J. **73**, 2313 (1997).

[27] B. Giese and M. Spichty, Long distance charge transport through DNA: quantification and extension of the hopping model, chemphyschem **1**, 195 (2000).

[28] *http:// www.contexo.info/ DNA_ Basics/ deoxyribose.htm.*

[29] D. D. Eley and D. I. Spivey, Semiconductivity of organic substances. Part 9.-Nucleic acid in the dry state, Trans. Faraday Soc. **58**, 411 (1962).

[30] E. Artacho, M. Machado, D. Sanchez-Portal, P. Ordejon, and J. Soler, Electrons in dry DNA from density functional calculations, Mol. Phys. **101**(11), 1587 (2003).

[31] M. Hjort and S. Stafström, Band Resonant Tunneling in DNA Molecules, Phys. Rev. Lett. **87**(22), 228101 (2001).

[32] J. P. Lewis, T. E. Cheatham, E. B. Starikov, H. Wang, and O. F. Sankey, Dynamically amorphous character of electronic states in poly(dA)-poly(dT) DNA, J. Phys. Chem. B **107**, 2581 (2003).

[33] H. Wang, J. P. Lewis, and O. F. Sankey, Band-gap Tunneling States in DNA, Phys. Rev. Lett. **93**(1), 016401 (2004).

[34] I. Buchvarov, Q. Wang, M. Raytchev, A. Trifonov, and T. Fiebig, Electronic delocalization and dissipation in single- and double-stranded DNA, Proc. Natl. Acad. Sci. USA **104**, 4794 (2007).

[35] K. Senthilkumar, F. C. Grozema, C. Fonseca Guerra, F. M. Bickelhaupt, F. D. Lewis, Y. A. Berlin, M. A. Ratner, and L. D. A. Siebbeles, Absolute Rates of Hole Transfer in DNA, J. Am. Chem. Soc. **127**, 14894 (2005).

[36] C. J. Murphy, M. R. Arkin, Y. Jenkins, N. D. Ghatliaa, S. H. Bossmann, N. J. Turro, and J. K. Barton, Long-range photoinduced electron transfer through a DNA helix, Science **262**, 1025 (1993).

[37] B. Giese, J. Amaudrut, A. Köhler, M. Spormann, and S. Wessely, Direct observation of hole transfer through DNA by hopping between adenine bases and by tunnelling, Nature **412**, 318 (2001).

[38] P. Henderson, D. Jones, G. Hampikian, Y. Kan, and G. Schuster, long-distance charge transport in duplex DNA: The phonon-assisted polaron-like hopping mechanism, Proc. Natl. Acad. Sci. USA **96**, 8353 (1999).

[39] C. Wan, T. Fiebig, S. O. Kelley, C. R. Treadway, J. K. Barton, and A. H. Zewail, Femtosecond dynamics of DNA-mediated electron transfer, Proc. Natl. Acad. Sci. USA **96**, 6014 (1999).

[40] G. Schuster, Long-range charge transfer in DNA: transient structural distortions control the distance dependence, Acc. Chem. Res. **33**, 253 (2000).

[41] C. Behrens, L. Burgdorf, A. Schwögler, and T. Carell, Weak distance dependence of excess electron transfer in DNA, Angew. Chem. Int. Ed. **41**, 1763 (2002).

[42] A. Joy and G. B. Schuster, Long-range radical cation migration in DNA: Investigation of the mechanism, Chem. Commun. , 2778 (2005).

[43] A. Joy, G. Guler, S. Ahmed, L. W. McLaughlin, and G. B. Schuster, Polaronic semiconductor behavior of long-range charge transfer in DNA oligomers in solution: controlling barriers to long-distance radical cation migration in DNA with thymine analogs, Faraday Discuss. **131**, 357 (2006).

[44] A. A. Voityuk, Charge transfer in DNA: Hole charge is confined to a single base pair due to solvation effects, J. Chem. Phys. **122**, 204904 (2005).

[45] D. B. Uskov and A. L. Burin, Strong localization of positive charge in DNA induced by its interaction with environment, arXiv:0803.2266v1.

[46] J. Olofsson and S. Larsson, Electron Hole Transport in DNA, J. Phys. Chem. B **105**, 10398 (2001).

[47] S. S. Alexandre, E. Artacho, J. M. Soler, and H. Chacham, Small polarons in dry DNA, Phys. Rev. Lett. **91**(10), 108105 (2003).

[48] R. Bruinsma, G. Grüner, M. R. D'Orsogna, and J. Rudnick, Fluctuation-facilitated charge migration along DNA, Phys. Rev. Lett. **85**(20), 4393 (2000).

[49] M. O'Neill and J. Barton, DNA Charge transport: conformationally gated hopping through stacked domains, J. Am. Chem. Soc. **126**(126), 11471 (2004).

[50] E. B. Starikov, Electron-phonon coupling in DNA: a systematic study, Phil. Mag. **85**, 3435 (2005).

[51] A. A. Voityuk, Conformations of poly{G}–poly{C} π stacks with high hole mobility, J. Chem. Phys. **128**, 045104 (2008).

[52] E. M. Conwell and S. Rakhmanova, Polarons in DNA, Proc. Natl. Acad. Sci. USA **97**(9), 4556 (2000).

[53] Y. Asai, Theory of Electric Conductance of DNA Molecule, J. Phys. Chem. B **107**, 4647 (2003).

[54] J. A. Berashevich, V. Apalkov, and T. Chakraborty, Polaron tunneling dynamics of a linear polymer of nucleotides, J. Phys.: Condens. Matter **20**, 075104 (2008), cond-mat 0709.0954.

[55] F. C. Grozema, Y. A. Berlin, and L. D. A. Siebbeles, Machanism of charge migration through DNA: molecular wire behavior, single-step tunneling or hopping, J. Am. Chem. Soc. **122**, 10903 (2000).

[56] Y. A. Berlin, A. L. Burin, and M. A. Ratner, Charge Hopping in DNA, J. Am. Chem. Soc. **123**, 260 (2001).

[57] Y. A. Berlin, A. L. Burin, and M. A. Ratner, Elementary steps for charge transport in DNA: thermal activation vs tunneling, Chem. Phys. **275**(275), 61 (2002).

[58] D. Porath, G. Cuniberti, and R. Di Felice, Charge Transport in DNA-Based Devices, TOP. Curr. Chem. **237**, 183 (2004).

[59] H. Fink and C. Schönenberger, Electrical conduction through DNA molecules, Nature **398**, 407 (1999).

[60] D. Porath, A. Bezryadin, S. de Vries, and C. Dekker, Direct measurement of electrical transport through DNA molecules, Nature **403**, 635 (2000).

[61] A. Kasumov, M. Kociak, S. Gueron, B. Reulet, V. Volkov, D. Klinov, and H. Bouchiat, Proximity-induced superconductivity in DNA, Science **291**, 280 (2001).

[62] K. H. Yoo, D. H. Ha, J. O. Lee, J. W. Park, J. Kim, J. J. Kim, H. Y. Lee, T. Kawai, and H. Y. Choi, Electrical conduction through Poly(dA)-Poly(dT) and Poly(dG)-Poly(dC) DNA Molecules, Phys. Rev. Lett. **87**(19), 198102 (2001).

[63] H. Zhang, X. Li, P. Han, X. Yu, and Y. Yan, A partially incohenrent rate theory of long-range charge transfer in deoxyribose nucleic acid, J. Chem. Phys. **117**(9), 4578 (2002).

[64] B. Xu, P. Zhang, X. Li, and N. Tao, Direct Conductance measurement of single DNA molecules in aqueous solution, Nano Lett. **4**(6), 1105 (2004).

[65] H. Cohen, C. Nogues, R. Naaman, and D. Porath, Direct measurement of electrical transport through single DNA molecules of complex sequence, Proc. Natl. Acad. Sci. USA **102**(33), 11589 (2005).

[66] S. K. Mandal, Direct electrical conduction in DNA molecules confined in nanoporous membrane, Appl. Phys. Lett. **89**, 193102 (2006).

[67] H. van Zalinge, D. J. Schiffrin, A. D. Bates, E. B. Starikov, W. Wenzel, and R. J. Nichols, Variable-Temperature Measurements of the Single-Molecule Conductance of Double-Stranded DNA, Angew. Chem. Int. Ed. **45**, 5499 (2006).

[68] S. Roy, H. Vedala, A. D. Roy, D. H. Kim, M. Doud, K. Mathee, H. K. Shin, N. Shimamoto, V. Prasad, and W. Choi, Direct Electrical Measurements on Single-Molecule Genomic DNA Using Single-Walled Carbon Nanotubes, Nano Lett. **8**, 26 (2008).

[69] C. Nogues, S. Cohen, S. Daube, N. Apter, and R. Naaman, Sequence dependence of charge transport properties of DNA, J. Phys. Chem. B **110**, 8910 (2006).

[70] S. M. Iqbal, G. Balasundaram, and S. Ghosh, Direct current electrical characterization of ds-DNA in nanogap junctions, Appl. Phys. Lett. **86**, 153901 (2005).

[71] P. J. de Pablo, F. Moreno-Herrero, J. Colchero, J. G. Herrero, P. Herrero, A. M. Baró, P. Ordejón, J. M. Soler, and E. Artacho, Absence of dc-Conductivity in λ-DNA, Phys. Rev. Lett. **84**(23), 4992 (2000).

[72] Y. Zhang, R. Austin, J. Kraeft, E. Cox, and N. Ong, Insulating behavior of λ-DNA on the micron scale, Phys. Rev. Lett. **89**(19), 198102 (2002).

[73] A. J. Storm, J. van Noort, S. de Vries, and C. Dekker, Insulating behavior for DNA molecules between nanoelectrodes at the 100 nm length scale, Appl. Phys. Lett. **79**, 3881 (2001).

[74] H. Watanabe, C. Manabe, T. Shigematsu, K. Shimotani, and M. Shimizu, Single molecule DNA device measured with triple-probe atomic force microscope, Appl. Phys. Lett. **79**, 2462 (2001).

[75] T. Shigematsu, K. Shimotani, C. Manabe, H. Watanabe, and M. Shimizu, Transport properties of carrier-injected DNA, J. Chem. Phys. **118**, 4245 (2003).

[76] H. Boettger and V. V. Bryksin, *Hopping conduction in Solids*, Akademie Verlag Berlin, 1985.

[77] L. D. Landau, Electron motion in crystal lattices, Sow. Phys. **3**, 664 (1933).

[78] S. I. Pekar, Autolocalization of the electron in a dielectric inertially polarizing medium, Zh. Eksp. Teor. Fiz **16**, 341 (1946).

[79] G. D. Mahan, *Many-Particle Physics*, Kluwer Academic/Plenum Publishers, 2000.

[80] A. S. Alexandrov and N. Mott, *Polarons and Bipolarons*, World Scientific, 1995.

[81] H. Fröhlich, H. Pelzer, and S. Zeinau, Phil. Mag. **41**, 221 (1950).

[82] R. P. Feynman, Slow Electrons in a Polar Crystal, Phys. Rev. **97**, 660 (1955).

[83] Y. A. Firsov, Small Polarons: Transport Phenomena, in *Polarons in Advanced Materials*, edited by A. S. Alexandrov, Springer Series in Material Science 103, Springer, 2007.

[84] R. R. Heikes and W. D. Johnston, Mechanism of Conduction in Li-Substituted Transition Metal Oxides, J. Chem. Phys. **26**, 582 (1957).

[85] T. Holstein, Studies of Polaron motion, Ann. Phys. **8**, 325 (1959).

[86] I. G. Lang and Y. A. Firsov, Sov. Phys. JETP **16**, 1301 (1962).

[87] R. Marcus, Electron transfer reactions in chemistry. Theory and experiment, Rev. Mod. Phys. **65**(3), 599 (1993).

[88] M. Galperin, M. A. Ratner, and A. Nitzan, Molecular Transport Junctions: Vibrational Effects, J. Phys.: Condens. Matter **19**, 103201 (2007).

[89] A. Nitzan, a relationship between electron-transfer rates and molecular conduction, J. Phys. Chem. A **105**, 2677 (2001).

[90] F. Zahid, M. Paulsson, and S. Datta, Electrical Conduction through Molecules, in *Advanced Semiconductors and Organic Nano-Techniques*, edited by H. Morkoc, Academic Press, 2003.

[91] R. Landauer, Spatial variation of currents and fields due to localized scatterers in metallic conductors, IBM J. Res. Develop. **1**, 223 (1957).

[92] D. S. Fisher and P. A. Lee, Relation between conductivity and transmission matrix, Phys. Rev. B **23**(12), 6851 (1981).

[93] Y. Meir and N. S. Wingreen, Landauer formula for current through an interacting electron region, Phys. Rev. Lett. **68**(16), 2512 (1992).

[94] J. Rammer and H. Smith, Quantum field-theoretical methods in transport theory of metals, Rev. Mod. Phys. **58**(2), 323 (1986).

[95] R. Gutierrez, S. Mandal, and G. Cuniberti, Dissipative Effects in the electronic transport through DNA molecular wires, Phys. Rev. B **71**, 235116 (2005).

[96] R. Gutierrez, S. Mohapatra, H. Cohen, D. Porath, and G. Cuniberti, Inelastic quantum transport in a ladder model: Implications for DNA conduction and comparison to experiments on suspended DNA oligomers, Phys. Rev. B **74**, 235105 (2006).

[97] X. Li and Y. Yan, Electrical transport through individual DNA molecules, Appl. Phys. Lett. **79**(14), 2190 (2001).

[98] M. Bixon and J. Jortner, Incoherent charge hopping and conduction in DNA and long molecular chains, Chem. Phys. **319**, 173 (2005).

[99] Y. J. Yan and H. Zhang, Toward the mechanism of long-range charge transfer in DNA: theories and models, Journal of Theoretical and Computational Chemistry **1**, 225 (2002).

[100] J. König, J. Schmid, H. Schoeller, and G. Schön, Resonant tunneling through ultrasmall quantum dots: Zero-bias anomalies, magnetic-field dependence, and boson-assisted transport, Phys. Rev. B **54**(23), 16820–16837 (Dec 1996).

[101] F. Bloch, Über die Quantenmechanik der Elektronen in Kristallgittern, Z. Physik **52**, 555 (1929).

[102] J. C. Slater and G. F. Koster, Simplified LCAO Method for the Periodic Potential Problem, Phys. Rev. **94**(6), 1498 (1954).

[103] A. Troisi and G. Orlandi, Hole migration in DNA: a theoretical analysis of the role of structural fluctuations, J. Phys. Chem. B **106**(8), 2093 (2002).

[104] G. Cuniberti, L. Craco, D. Porath, and C. Dekker, Backbone-induced semiconductiong behavior in short DNA wires, Phys. Rev. B **65**, 241314(R) (2002).

[105] M. Zwolak and M. Di Ventra, DNA spintronics, Appl. Phys. Lett **81**, 925 (2002).

[106] S. Roche, Sequence Dependent DNA-Mediated Conduction, Phys. Rev. Lett. **91**(10), 108101 (2003).

[107] E. B. Starikov, S. Tanaka, N. Kurita, Y. Sengoku, T. Natsume, and W. Wenzel, Investigation of a Kubo-formula-based approach to estimate DNA conductance in an atomistic model, Eur. Phys. J. E **18**, 437 (2005).

[108] D. Klotsa, R. A. Römer, and M. S. Turner, Electronic Transport in DNA, Biophys. J. **89**, 2187 (2005).

[109] E. Macia, Electronic structure and transport properties of double-stranded Fibonacci DNA, Phys. Rev. B **74**, 245106 (2006).

[110] H. Yamada, E. B. Starikov, and D. Hennig, Quantum diffusion in polaron model of poly(dG)-poly(dC) and poly(dA)-poly(dT) DNA polymers, Eur. Phys. J. B **59**, 185 (2007).

[111] A. Voityuk, J. Jortner, M. Bixon, and N. Rösch, Energetics of hole transfer in DNA, Chem. Phys. Lett. **324**, 430 (2000).

[112] W. K. Purves, G. H. Orians, H. C. Heller, and D. Sadava, *Life: The Science of Biology*, W .H. Freeman & Company, 4th edition, 1998.

[113] U. Weiss, *Quantum Dissipative Systems*, World Scientific, 1999.

[114] M. Galperin, A. Nitzan, and M. A. Ratner, Resonant inelastic tunneling in molecular junctions, Phys. Rev. B **73**, 045314 (2006).

[115] M. Galperin, M. A. Ratner, and A. Nitzan, Inelastic electron tunneling spectroscopy in molecular junctions: Peaks and dips, J. Chem. Phys. **121**(23), 11965 (2004).

[116] J. Viljas, J. Cuevas, F. Pauly, and M. Häfner, Electron-vibration interaction in transport through atomic gold wires, Phys. Rev. B **72**, 245415 (2005).

[117] A. A. Odintsov, Effect of dissipation on the characteristics of small-area tunnel junctions: Application of the polaron model, Sov. Phys. JETP **67**, 1265 (1988).

[118] M. H. Devoret, D. Esteve, H. Grabert, G.-L. Ingold, H. Pothier, and C. Urbina, Effect of the electromagnetic environment on the Coulomb blockade in ultrasmall tunnel junctions, Phys. Rev. Lett. **64**(15), 1824–1827 (Apr 1990).

[119] A. A. Odintsov, G. Falci, and G. Schön, Single-electron tunneling in systems of small junctions coupled to an electromagnetic environment, Phys. Rev. B **44**(23), 13089–13092 (Dec 1991).

[120] H. Böttger, V. V. Bryksin, and F. Schulz, Hopping transport in the three-site model in the presence of electric and magnetic fields: Rate equation and transport phenomena for small polarons, Phys. Rev. B **48**(1), 161–171 (Jul 1993).

[121] O. V. Konstantinov and V. I. Perel, A diagram technique for evaluating transport quantities, Sov. Phys. JETP **12**, 142 (1961).

[122] R. Gutierrez, S. Mandal, and G. Cuniberti, Quantum transport through a DNA wire in a dissipative environment, Nano Lett. **5**, 1093 (2005).

[123] B. B. Schmidt, M. H. Hettler, and G. Schön, Influence of vibrational modes on the electronic properties of DNA, Phys. Rev. B **75**(115125), 115125 (2007).

[124] H. Haug and A. Jauho, *Quantum Kinetics in Transport and Optics of Semiconductors*, Springer-Verlag Berlin, 1996.

[125] C. Niu, D. L. Lin, and T.-H. Lin, Equation of motion for nonequilibrium Green function, J. Phys.: Condens. Matter **11**, 1511 (1999).

Acknowledgements

This thesis would not have been written, without the help of so many people, which I would like to thank wholeheartedly.
First of all, I would like to give my sincere thanks to Gerd Schön who took me into his group and offered me the opportunity to write this thesis. He gave me all possible freedom, two workplaces and all the advice I could ever ask for.
I wish to thank Juan Carlos Cuevas for refereeing this thesis.
I owe many thanks to Matthias Hettler, who had the idea for this thesis. I spend many hours with Matthias, discussing every aspect of this work, and he always offered an open ear and help for all of the problems that I ran into.
I also would like to thank Verena Körting, Janne Viljas and Dima Golubev for their support. They explained to me many technical details of the calculations for this thesis and always were eager to discuss with me.
I would like to thank Poeni, who was a perfect office mate at the TFP and my source of help for all computer related questions and beyond.
Likewise I want to thank Aina and Julia with whom I shared the office at the INT. I enjoyed very much discussing all physical and not so physical topics with them.
It was great to work with all the people from the INT and TFP and I like to thank Robert, Verena, Erika, Ines, Christine, Lothar, Olaf, Christoph and everybody else in those institutes for the great working atmosphere.
Special thanks go to Matthias Hettler and Verena Körting for proofreading this thesis.
I send all my thanks to my family (which has miraculously doubled in the last part of this thesis...) for giving me all their support and love throughout the years. This was invaluable to me.
Although she is named last, she is always first in my thoughts — Sabine.